STABILITY-DEPENDENT MASS ISOLATION FOR STEEL BUILDINGS

A Dissertation

by

LUIS EDUARDO PETERNELL ALTAMIRA

Submitted to the Office of Graduate Studies of
Texas A&M University
in partial fulfillment of the requirements for the degree of

DOCTOR OF PHILOSOPHY

Approved by:

Chair of Committee,	Gary T. Fry
Committee Members,	Mary Beth D. Hueste
	David C. Hyland
	Harry L. Jones
Head of Department,	John M. Niedzwecki

December 2012

Major Subject: Civil Engineering

ABSTRACT

A new seismic isolation system for steel building structures based on the principle of mass isolation is introduced. In this system, isolating interfaces are placed between the lateral-load-resisting sub-system and the gravity-load-resisting sub-system. Because of the virtual de-coupling existing between the two structural sub-systems, the gravity-load resisting one is susceptible to instability. Due to the fact that the provided level of isolation from the ground is constrained by the stability requirements of the gravity-load resisting structure, the system is named stability-dependent mass isolation (SDMI).

Lyapunov stability and its association with energy principles are used to assess the stable limits of the SDMI system, its equilibrium positions, the stability of the equilibrium positions, and to propose a series of design guidelines and equations that allow the optimal seismic performance of the system while guaranteeing the restoration of its undistorted position. It is mathematically shown that the use of soft elastic interfaces, between the lateral- and gravity-load-resisting sub-systems, can serve the dual role of stability braces and isolators well.

The second part of the document is concerned with the analytical evaluation of the seismic performance of the SDMI method. First, a genetic algorithm is used to find optimized SDMI building prototypes and, later, these prototypes are subjected to a series of earthquake records having different hazard levels. This analytical testing program shows that, with the use of SDMI, not only can structural failure be avoided, but a damage-free structural performance can also be achieved, accompanied by average reduc-

tions in the floor accelerations of ca. 70% when compared to those developed by typical braced-frame structures.

Since the SDMI system is to be used in conjunction with viscous energy dissipaters, the analytical testing program is also used to determine the best places to place the dampers so that they are most effective in minimizing the floor accelerations and controlling the floors' drift-ratios. Finally, recommendations on continuing research are made.

DEDICATION

To my grandmother María Bertha Peláez Valdés

ACKNOWLEDGEMENTS

Multiple people and circumstances made the completion of this dissertation possible. Although I gratefully acknowledge all of them, I unfortunately have no option, but to limit myself in the allusion of people in the expression of my gratitude. It is my pleasure, and a minimal form of recognition to use this space to give special thanks and credit to the people at Texas A&M University that helped me in many different ways and contributed objectively and subjectively to the elaboration of this document.

First of all, I would like to express my thanks to my Academic Advisor Dr. Gary T. Fry. Dr. Fry's ingenuity and ability to solve problems were always an extraordinary example of how engineering should be applied in many aspects of life, and not only in the solution of academically-designed engineering problems or research projects. It was also thanks to Dr. Fry and his arrangements through the Texas Transportation Institute and the Texas Engineering Experiment Station that my graduate studies at Texas A&M University were funded since the very first moment I required assistance. His preparation and enthusiasm for his work also resulted in an outstanding mentorship, without which, my academic development would not have been the same.

In terms of funding, I would also like to thank the Mexican National Council of Science and Technology for providing the economic resources that initially brought me to Texas A&M, and which constituted a first link in the chain of events that led me to this point of my academic career.

The technical and moral contributions of many professors and friends have been no less important than the material resources. It happened commonly that “small” ideas and input from fellow students transformed into major advancements of my project. Of all the students that I interacted with, my friend Ramesh Kumar deserves a special mention for having shared with me academic knowledge, life experiences, and recharging and morally-supporting moments.

The quality of the redaction of this manuscript would not be the same without the comments made by Amy White of the Center for Railway research of the Texas Transportation Institute. In the same way, the technical contents and organization of this dissertation were improved by observations and comments made by the members of my research group.

Finally, this section would not be complete without the just mention of my parents. I have been blessed with ones that have always oriented their daily efforts in supporting every aspect of my personal development. They are, above all, a true example of love.

NOMENCLATURE

AISC	American Institute of Steel Construction
BRB	Buckling-restrained brace
DoA	Domain of attraction
DoF	Degree of freedom
$(DR)_{y,i}$	Interstory drift ratio at the onset of yield for the lateral structural system used at the i^{th} story
EoM	Equation of motion
EP	Equilibrium point
$F_{\delta,i}$	Allowable interstory drift ratio reduction factor for the i^{th} story
F_k	Factor of safety for the minimum equivalent stiffness needed for continuous stability and restoration of the system
FS	Factor of safety
$F_{s,i}$(t)	Total force induced by the earthquake on the i^{th}-story time histories
GA	Genetic algorithm
IC	Initial condition
IDR	Interstory drift ratio
$\boldsymbol{K}_{des}$	Reduced design stiffness matrix
$\boldsymbol{K}_G$	Gravity sub-system's stiffness matrix
KJMA	Kobe Japanese Meteorological Agency
$\boldsymbol{K}_L$	Lateral sub-system's stiffness matrix

MCE	Maximum considered earthquake
MDF	Multi-degree of freedom
MRF	Moment-resisting frame
MS-	Multi-story
ODE	Ordinary differential equation
SS-	Single-story
SDF	Single degree of freedom
SDMI	Stability-dependent mass isolation
W_i	Weight of the i^{th}-floor
c_{eq}	Total equivalent lateral damping coefficient
c_{ij}	Damping coefficient of equivalent damper i,j in the condensed model
$c_{g,i}$	Total lateral damping device coefficient at the i^{th}-level in the gravity sub-system
$c_{l,i}$	Total lateral damping device coefficient at the i^{th}-level in the lateral sub-system
$c_{s,i}$	Total lateral damping device coefficient at the i^{th}-level
g	Standard acceleration of gravity
h_i	Height of the i^{th}-story
k_{eq}	Total equivalent stiffness
$k_{eq,cr}$	Critical total equivalent stiffness
k_{ij}	Stiffness of equivalent spring i,j in the condensed model
$k_{l,i}$	Total lateral stiffness of the lateral sub-system at the i^{th}-level

$k_{s,i}$	Total stiffness of the stability springs at the i^{th}-level
k_u	Total vertical stiffness of the gravity sub-system
l_s	Undeformed stability spring length
m_i	Mass of the i^{th}-floor
u	Generalized deformation of the column spring
$\boldsymbol{x}_G(t)$	Displacement-response time-histories to a particular ground motion
θ	Generalized rotation of the gravity sub-system

TABLE OF CONTENTS

Page

Page

Page

LIST OF FIGURES

Page

Page

Page

Page

LIST OF TABLES

Page

1. INTRODUCTION

Despite the continuous efforts of governments and the scientific community to preserve the integrity of society and its assets during and after earthquakes, major seismic events continue to expose the vulnerability of our infrastructure. A recent example is the 2011 Tohoku Pacific earthquake and tsunami that resulted in catastrophic infrastructure damage in the north-east of Japan and an estimated death toll of about 16,000 people (NPA 2012).

After more than forty years of development, earthquake engineering has diversified and specialized its efforts to include as many infrastructure elements as possible in its objectives of protection. Of all the elements that conform infrastructure, of primary value are buildings, since their protection may signify safeguarding extremely valuable resources and human lives. Consequently, a large focus of the research in earthquake engineering has been oriented at increasing the seismic resilience of building structures. The results of these scientific investigations have been materialized in the form of building code provisions, control systems, and seismic isolation.

The project that is presented in the following sections constitutes one more of the efforts that have been developed to improve the seismic resilience of building structures. This effort takes the form of a structural system that makes an alternative application of the seismic isolation concept, although it also makes use of actuators whose type belongs to the sub-category of passive control.

In the context of simultaneous global population growth and global decrease of resources, modern engineering practices require or should require engineering systems to be not only technically efficient but also as sustainable as possible, if not fully sustainable. Buildings are complex systems that have impacts on economy, environment, and society. Therefore, to achieve sustainability, the relationships between these impacts have to be well balanced.

The focus of this project is the development of a new structural system for buildings that shows improved seismic performance. Within this area of focus, it is important that the structural system contributes as much as possible to the sustainability of the greater system, which is the whole building. The structural system not only serves to control the seismic response, but in the long and short term, it results in a more cost-effective product, compared to conventional or alternative earthquake-resisting systems.

A recent trend in earthquake engineering research focuses on the aftershocks that follow a main seismic event. Aftershocks may represent a significant ground motion hazard, since they may cause additional weakening and/or the collapse of structures that have already been damaged by previous main- and aftershocks. After a mainshock, the life-safety threat that an occupant is exposed to could be even higher than before the occurrence of the mainshock because of the potential number, magnitude, etc. of subsequent aftershocks and/or because of already existing building damage.

Buildings that have been structurally damaged by a mainshock require inspections and analyses to assess the level of damage and determine if repairs are required to recover the original structural capacities. In some cases, downtimes due to structural re-

pairs could last several years. The non-functionality of the building during these down-times adds to financial losses.

The performance of a mainshock-damaged building during aftershocks may have a significant impact on its post-earthquake functionality and economy; therefore, after-shock considerations should influence design criteria and earthquake-engineering re-search. Nevertheless, the development of seismic-resistant knowledge and technologies has generally been carried out with the sole consideration of mainshocks. Some re-searchers (ATC 1999) have provided guidelines on the safety evaluation of earthquake-damaged buildings as well as conditions for permitting the re-occupancy of buildings that might have become structurally unsound to resist future ground motions.

In support of the short and long term objective of structural cost-efficiency, and in consideration of potential aftershocks and subsequent ground motions, a damage-free earthquake-resisting system is proposed. Depending on the results of further studies, the system might not need inspections or component replacements. In technical terms, if practical experience is faithful to the theoretical aspects and analytical results given in this document, stability-dependent mass isolation could become a powerful and cost-effective strategy for achieving improved and reliable seismic performance of buildings under a broad range of earthquakes (in terms of hazard levels), when compared to other structural systems. The new form of seismic isolation that is introduced, which is en-hanced with passive structural control actuators, should also motivate new research on alternative earthquake-resisting systems that incorporate the hybrid seismic isolation and control concepts that are presented in this document.

2. LITERATURE REVIEW

2.1 Background

Historically, earthquakes have caused the deaths of millions of people as well as significant economic losses (USGS 2009). For more than 50 years, engineers and governments have been formally developing knowledge, technologies, and programs to mitigate the devastating effects of earthquakes (NIST 2008). As a result, current seismic design philosophies favor ductile deformations of the structural elements in buildings as a means to provide damping and limit the input of energy into the structure. By obeying ductility standards, primary structural components dissipate energy through incursions into their material's nonlinear (plastic) range; however, the implied inelastic strains signify structural damage, which may eventually result in non-structural damage as well. Therefore it is important that design provisions establish limits to the allowed levels of plastic behavior.

In order to relieve the primary structural members from their seismic energy dissipation assignment, alternative concepts have been engineered to take over this responsibility. These ideas incorporate into buildings special structural components and/or mechanisms, energy dissipating devices, or modify the inherent dynamic properties of the structure in question so that less energy is transferred from the ground.

One example of an energy dissipating device is the so-called buckling-restrained brace (BRB). This brace uses the hysteretic behavior of steel as a dissipating mechanism. Instead of the structural members, the BRB undergoes plastic deformations and suffers

damage as it dissipates energy (Fig. 2.1). This damage, however, requires that the brace be periodically inspected and/or replaced, especially after it has served during a major earthquake. In fact, several types of energy dissipating devices require regular inspections and replacements, which are expensive and time consuming (PDL 2009).

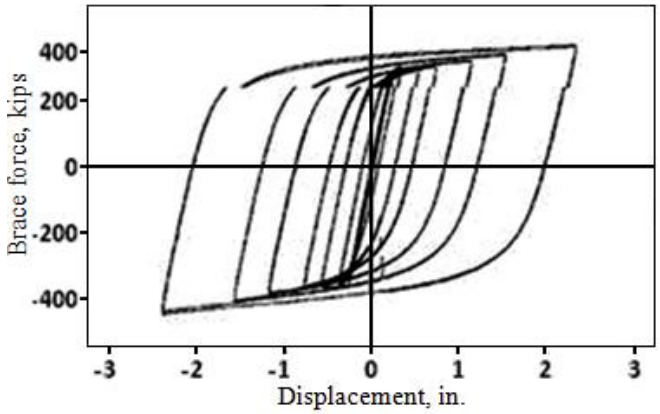

Fig. 2.1. Force-displacement plot of buckling-restrained braces (Sabelli et al. 2003)

On the other hand, a popular technique belonging to those that modify the inherent structural properties and that has proven to be simple and effective in the protection of superstructures against earthquakes is *Base Isolation* (Naeim and Kelly 1999). This method consists in providing a relatively flexible interface in the form of isolating devices (isolators) between the superstructure and its foundations. This is done with the intention of "detaching" the building from the ground so that the former becomes immune to the accelerations of the latter (Fig. 2.2). The working principle of Base Isolation is that of increasing the fundamental period of vibration of the structure so that it does not fall in the most energetic region of response spectra. Also, it aims at achieving a greater fre-

quency-wise separation of the vibration modes so that the first mode of vibration is predominant. By doing this, the seismic demands on the superstructure are reduced.

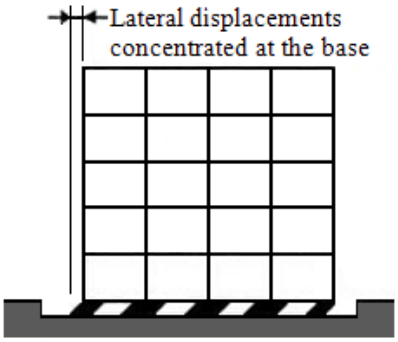

Fig. 2.2. Base isolation (ASCE 2004)

The provision of a soft isolating layer is advantageous for the reduction of structural demands; however, it also induces problems. These problems involve a higher chance of resonance and a considerable increase of the lateral displacements during earthquake and wind excitations (Komodromos et al. 2007). These increased displacements result from the flexibility at the base level.

The problem with large lateral deflections is that they present the risk of pounding of the building against other structures and, especially, against the walls of the seismic moat that is built around the base of base-isolated buildings to accommodate the translations. Pounding signifies a sudden modification in the vibration pattern, which translates into unexpected behavior (participation of higher response modes) and a dangerous increase of the dynamic response for which the structure might not have been designed (Komodromos et al. 2007). Because the risk of pounding represents safety con-

cerns, Base Isolation design code provisions are conservative, which is detrimental to the possible system's effectiveness (Kelly 1999; Pan and Cui 1998).

Technical measures like the addition of energy dissipaters at the isolation level have been proposed to reduce the base's displacements and, thus, avoid pounding and/or mitigate its effects. However, similar to conservative code provisions, this measure negatively affects the virtues of Base Isolation, mainly because it reduces the level of isolation provided to the building (ASCE 2004; Kelly 1999).

In a more radical manner, researchers have proposed modifications and/or adaptations to the concept of Base Isolation to help with the management of the lateral displacements (Earl and Ryan 2006; Komodromos et al. 2007; Pan and Cui 1998; Pan et al. 1995). As an example, Pan et al. (1998; 1995) proposed to place intermediate isolation layers at various levels of the building, not just the base (Fig. 2.3). By doing so, the lateral displacements are reduced while the level of seismic protection is similar to the one provided by typical Base Isolation.

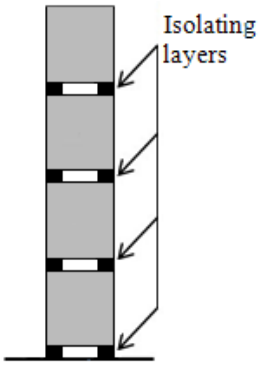

Fig. 2.3. Segmental building (Pan and Cui 1998)

On the other hand, the relatively low vertical-load capacity of the isolators has also limited the application of Base Isolation. Although new isolating devices are able to resist larger vertical forces, the development of higher capacity isolators means challenges that have to do with the large gravity forces imposed by the building on the isolators that are difficult to simulate at the developing premises (ASCE 2004).

The simultaneous action of large displacements and high vertical forces that takes place in the isolating devices results in stability issues (Fig. 2.4). The p-delta effects on the isolators have been the subject of several research studies (Gent 1964; Gent and Lindley 1959; Haringx 1948; Kircher et al. 1979) and represents a problem in the design of base isolated structures.

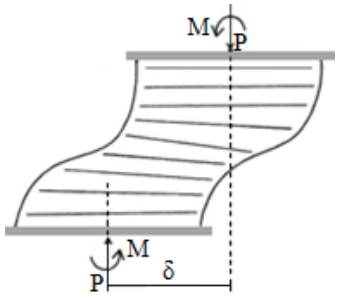

Fig. 2.4. P-delta effect in rubber isolator (Naeim and Kelly 1999)

Recently, there has been a trend to reinvent seismic structural systems. As a result, several innovating earthquake resisting structural systems or structural additions for the current ones have been introduced. Although most of them may not have found practical applications yet, they all promise to perform better that the conventional systems that have been used for years. A few examples of these systems are rocking frames

(Eatherton et al. 2010; Ma et al. 2010), post-tensioned steel frames (Ricles et al. 2001), braced frames that use smart materials (McCormick et al. 2007), zipper frames (Yang et al. 2008; Yang et al. 2010), and also systems that incorporate active control devices (Chen and Chen 2004; Sakamoto et al. 2000; Singh and Matheu 1997; Spencer et al. 1998a; Spencer et al. 1998b). One of the alternative seismic isolation techniques that have been recently proposed for application in buildings is that of mass isolation, which is the subject of the following sub-section.

2.2 Mass isolation

2.2.1 Principles of mass isolation

The superstructures of conventional buildings are rigidly linked to their foundations which, in turn, are "bonded" to the ground. Because of this bonding, typical buildings experience the full magnitude of ground accelerations during earthquakes. In recognition of this phenomenon and as a technique to prevent or, at least, minimize the transmission of vibration waves from the ground throughout the building, a means to detach the structure from its base is sought. The isolation of a building from the ground can be achieved through Base-Isolation, or in a different way, i.e., in the ground-spring-mass system that a building represents, isolating interfaces can be placed between the springs and the masses with, theoretically, the same result as placing a single isolating interface at the base level. This implies that the isolation of the building can be achieved by discretely isolating the mass concentrations instead of attempting to separate the whole bulky superstructure from its foundations.

A typical building is designed to resist vertical (gravity) and horizontal (earthquake, wind, blast, etc.) forces. This requires a structural system capable of simultaneously resisting both types of loads. It is common to differentiate an "independent" subsystem that takes care of the gravity loads [gravity (-load-resisting) sub-system] from another sub-system that is responsible for the lateral forces [lateral (-load-resisting) subsystem]. Although the two are designed in a relatively independent way, they are constructed forming a monolithic system, which enables a coupled behavior between the two. This coupling may sometimes be intentional, particularly in the case of steel buildings where the linkage between the two systems is used to provide stability to the gravity sub-system.

On the other hand, it is common to consider that the total mass of a building is discretely lumped at the floor slabs, which are part of the gravity sub-system. Because the gravity sub-system is coupled to the lateral sub-system, a direct linkage exists between the building's masses and the ground; hence, the vibrations of the building are possible.

The concept of mass isolation is based on the introduction of isolating interfaces between the masses (gravity sub-system) and the springs (lateral sub-system) (Fig. 2.5). By placing isolating gaps between the two sub-systems, their physical coupling is automatically eliminated and, likewise, that of the masses with the ground. A complete removal of the physical links existing between the two structural sub-systems would theoretically preclude the vibrations of the building, while a partial reduction of the coupling translates into a proportional reduction of the structure's susceptibility to ground mo-

tions. A detailed description of the mass isolation concept is given in (Ziyaeifar 2000; Ziyaeifar 2002; Ziyaeifar and Noguchi 1998).

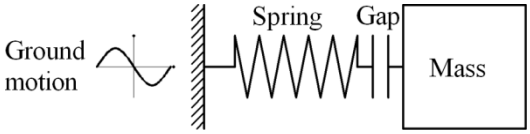

Fig. 2.5. Mass isolation (Ziyaeifar 2002)

2.2.2 Current state of the concept of mass isolation

A number of researchers have already worked in direct or indirect forms with the concept of mass isolation. In Japan, for example, Niiya et al. (1992) and Sakamoto et al. (2000) proposed the placement of low-stiffness links between auxiliary masses and the rest of the superstructure at the roof level of a building to create a vibration absorber (Fig. 2.6). Pan and his co-researchers (Pan and Cui 1998; Pan et al. 1995) have proposed an extension of the Base Isolation concept that consists in segmenting a building by placing isolating layers at various levels of the building, not only the base (Fig. 2.3). Through these insertions, the magnitudes of the lateral displacements are reduced while a level of seismic protection comparable to that provided by Base Isolation is achieved. Earl and Ryan (2006) did a more in-depth study of the segmental isolation concept with one of the outcomes being that placing isolation layers at various levels except the base presented the technical benefit of pounding avoidance while achieving a level of protection comparable to that provided by Base Isolation.

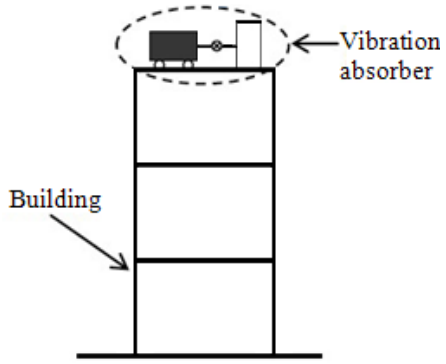

Fig. 2.6. Building with active vibration absorber (Sakamoto et al. 2000)

In a slightly different way, Villaverde and his co-researchers (Villaverde 1998; Villaverde et al. 2005; Villaverde and Mosqueda 1999) studied the effect of isolating the building's roof using the same type of isolators used in Base Isolation. By implementing this technique, the roof becomes a sort of vibration absorber (Fig. 2.7). It was recognized that a relatively large roof mass is required to achieve an effective absorption of the building's vibrations and that the resulting large drifts of the roof require special care. However, it was shown that a reduction in structural demands can be achieved by isolating portions of the building's mass. An important point is that, in cases of retrofit, isolating the roof is less disruptive to the service of the building than the isolation of its base. As an extension of Villaverde's work, Pourmohammad and his colleagues (2006) proposed the placement of isolators between the floor slabs and their supporting beams (Fig. 2.8a).

A more detailed description of the mass isolation concept was given by Ziyaeifar (Ziyaeifar 2000; Ziyaeifar 2002; Ziyaeifar and Noguchi 1998). Besides explaining the concept, he also proposed several mass isolated structural systems that are consistent

with the definition of mass isolation given in sub-section 2.2.1. His systems achieve the isolation of the floor slabs in different ways (Fig. 2.8) and their effectiveness was backed up positively through limited analytical testing.

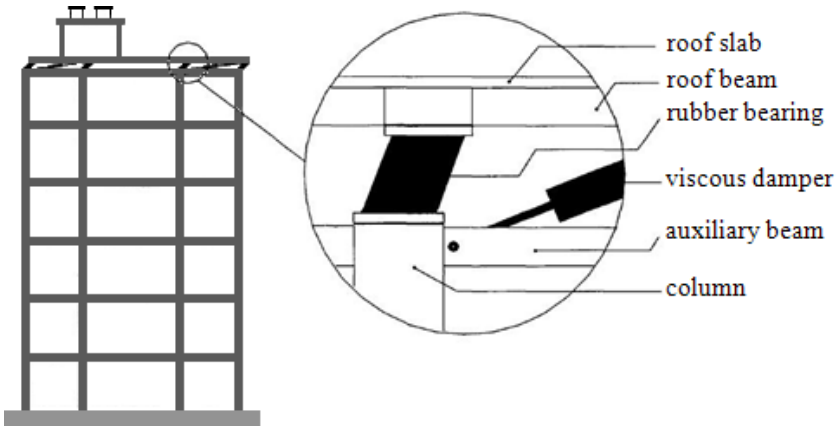

Fig. 2.7. Building with roof isolation (Villaverde 1998)

Mass isolation is a simple concept with proved potential; however, to date, a small amount of research associated with it has been done. The technical, architectural, and economic benefits (or disadvantages) that could be drawn from this concept are still far from being determined. The studies that have been carried out to date have served as an introduction to the idea.

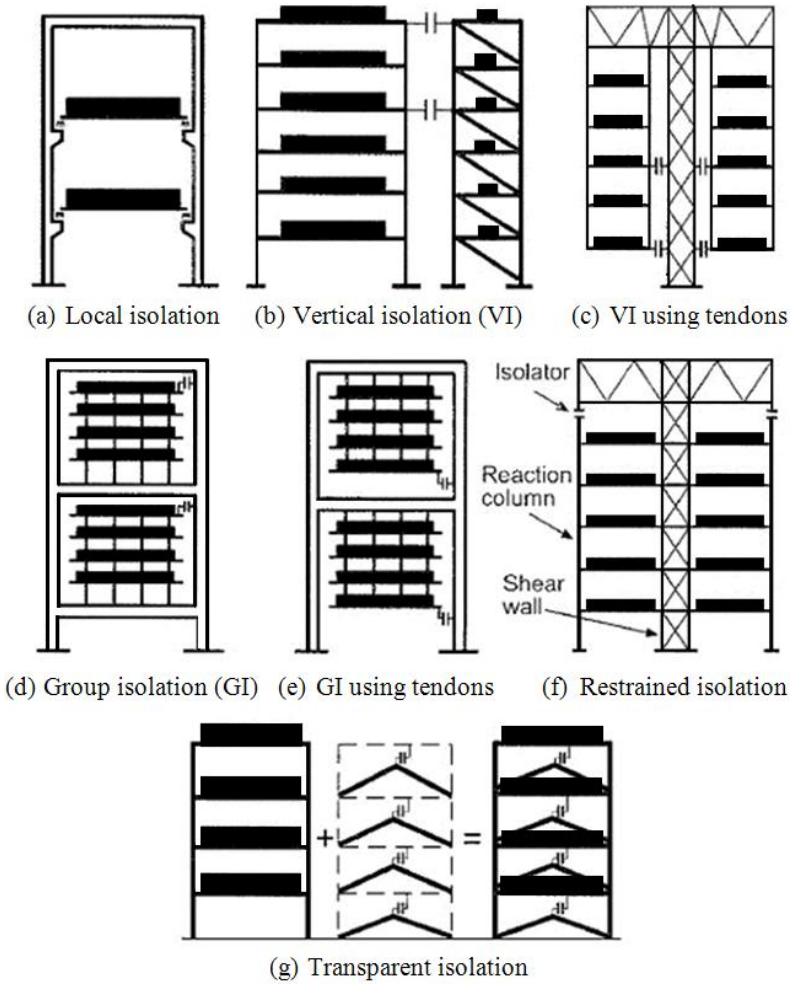

Fig. 2.8. Different methods of mass isolation (Ziyaeifar 2002)

3. OBJECTIVES

As was mentioned in the introduction and literature review sections above, there are still concerns about the resilience of our infrastructure, not only to major main events, but to all the potential ground motions that may follow a *'design earthquake'* throughout the service life. Therefore, it is sought to develop a new earthquake-resisting structural system for buildings that provides sufficient seismic resilience to the structure every time it is subjected to ground motions, even if the latter reach magnitudes of the order of the design maximum considered earthquake(s) (MCE) more than once. Continuous seismic resilience would imply that any concerns about the residual capacity of the system following every time it resists an earthquake would be eliminated, and the life-cycle cost of the structure would be maximized. To preserve the earthquake capacity of the system without structural and/or component maintenance and retrofit, seismic structural degradation must be avoided. Another objective is for the system to perform inducing minimal or no structural damage.

While resilience might be the most desired quality in a structure, at least in terms of post-earthquake economy, new seismic-resistant systems should also technically outperform the ones that are currently available. It is intended to achieve a level of seismic performance in terms of the dynamic response that permits a safer operation of the system, not only at the structural level as was proposed in the previous paragraph through minimal structural damage, but also for the occupants of the building. If the seismic structural degradation is minimal or zero, the collapse of the building would be avoided

so that any increase in the level of safety for the occupants resulting from a reduced seismic response should come from reduced floor accelerations. Most earthquake-related injuries and deaths result from collapsing walls, flying glass, and falling objects, which are caused by the accelerations of the floors (FEMA 2006). The system should, therefore, be able to work displaying a reduced acceleration response.

In the literature review section, technical disadvantages of the Base Isolation method are highlighted. Seismic isolation alternatives that have been proposed by other researchers to counteract the technical deficiencies inherent to Base Isolation were presented; one of which, the so-called mass isolation, has shown to deliver good seismic performance. The mass isolation concept is applied to overcome the applicability limitations of Base Isolation and some of its undesired performance byproducts like the large rigid-body-like displacements of the building, its base, and the associated risks of pounding and resonance.

Finally, the system's design has to contribute to the sustainability of the building. This is accomplished by requiring less building material and/or less maintenance, which represent the use of different forms of resources. As previously noted, minimum maintenance costs can be achieved by implementing a design that does not result in structural degradation; the proposed design should also incorporate components that require little to no inspection and/or replacements throughout the service life of the building. By achieving an outstanding seismic performance and reduced seismic response, the system will be able to be constructed using lighter structural designs.

4. PROTOTYPE DESCRIPTION

4.1 Stability-dependent mass isolation

Stability-dependent mass isolation (SDMI) is an earthquake-resisting system based on the concept of seismic isolation and, particularly, that of mass isolation. Fig. 4.1 shows how the isolation of the gravity sub-system is achieved by this method. On the sides, the gravity sub-system is isolated from the lateral sub-system by the use of elastic isolators. "True" pins are used at the columns ends to achieve isolation from the ground. From a theoretical point of view, it would be more effective not to have the isolators between the two structural sub-systems; however, doing so would result in the instability of the gravity sub-system. Since instability is unacceptable, the intended "full" detachment between the two sub-systems cannot be accomplished, and some level of linkage has to be provided. SDMI gets its name because the system's level of isolation is directly dependent upon the stability requirements.

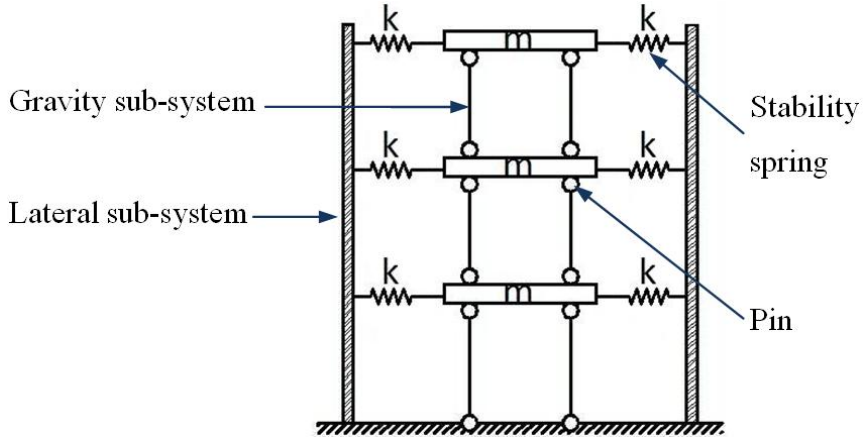

Fig. 4.1. Stability-dependent mass isolation

The SDMI characteristic features are as follows:

- The columns in the gravity load sub-system are pinned at both ends permitting "isolated" translations of the floor slabs (masses). Therefore, SDMI is well suited for steel building construction where hinged end-conditions can be approximated well.
- Rather than having the gravity and lateral sub-systems form a monolithic system, the two sub-systems are constructed independently.
- In order to provide stability to the inherently unstable gravity sub-system, springs are placed at each level joining the slabs to the lateral sub-system. The stiffness of these springs can be tuned to minimize the seismic response of the structure.
- The lateral sub-system can be of any type.
- Damping devices are used to dissipate seismic energy and control the response. These can be placed in different parts of the building in order to maximize their effectiveness and/or to minimize the architectural disruptions they may cause. Their damping properties can also be tuned to minimize the response of the structure.
- The resistance to wind is provided as in typical buildings where the wind-induced forces are resisted directly by the lateral system.

Due to their structural function, the springs linking the gravity and lateral sub-systems are referred to as stability springs. Their provision couples the mass and lateral sub-systems to some extent, which implies that the isolation of the mass lumps cannot be perfected. However, this necessary coupling can be used favorably if a combination of

stability spring stiffnesses can be found that reduces one or more seismic response parameters.

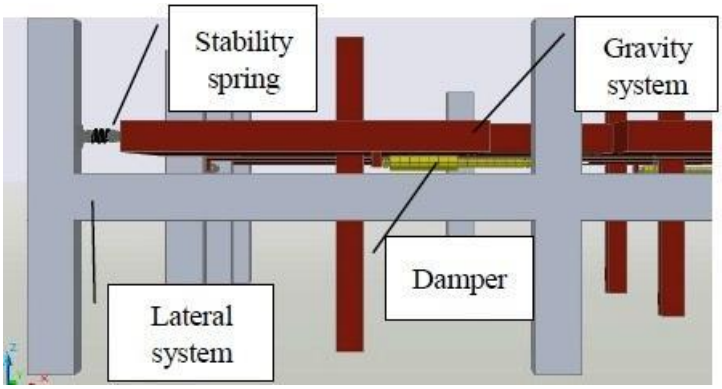

Fig. 4.2. SDMI with energy-dissipating devices

The stability springs are a key component in SDMI because the efficiency of the system relies on the appropriate determination of their properties. An adequate choice of spring properties guarantees the restoration of the system while minimizing one or more seismic response quantities. To optimize the performance of the system, the stiffness of the stability springs needs to be relatively low. During earthquake excitations, the required flexibility of these springs favors large displacements and velocities of the floor slabs. While this condition may be regarded as inconvenient at first, these velocities and displacements can be exploited to dissipate the seismic input energy through the use of velocity-dependent dampers. Moreover, these dampers can be tuned and strategically placed in different locations of the building to minimize the structural response. Fig. 4.2 shows dampers located between the two structural sub-systems as a viable option. The inclusion of energy dissipaters helps further improve the performance of a system that

has already been made less susceptible to seismic-induced vibrations through the isolation of the masses (gravity sub-system).

4.2 Requirements for the stability springs

The stability of the gravity sub-system is a fundamental requirement. However, for the SDMI system to work as intended, there are aspects that have to be accounted for in the selection and design of the characteristics of the stability springs so that stability requirements are met without compromising the seismic effectiveness of the system.

First, the desired "free and independent" motion of the floor slabs in the building is a three-dimensional phenomenon that involves all six Cartesian degrees of freedom; however, this free motion is interfered by the presence of the stability springs. In order to minimize the interference with such freedom of motion, the stability springs should not provide larger restoring forces than required in any of the directions of motion of the slabs.

Second, the continuous provision of the stabilizing forces is a delicate requirement. Since the factor of safety against buckling and system restoration is low in optimized SDMI designs, any loss of stiffness in any structural element could be unaffordable. This condition implies that all the springs in the system (lateral sub-system's beams and columns, and stability springs) have to remain elastic.

Finally, a third issue concerns the necessity of system restoration after the seismic motions have ceased. This situation implies two requirements: 1. the restoration forces must be adequate in magnitude, point of application, and direction, and 2. residual

displacements cannot be permitted. The former requirement can be met with the provision of adequate levels of stiffness and an appropriate stability spring mechanism, which is addressed in the next paragraph. The latter requirement implies, again, that the stability springs have to remain elastic.

The kinematic requirements of the springs can be met if supports are used that are conceptually like the seismic isolation support invented by Yaghoubian (1988) (Fig. 4.3). This support consists of a coil spring that is mounted around a telescopic mast having a roller bearing at one end. Another option would be that of using spring devices having pinned ends in conjunction with specialized connections that allow free three-dimensional movements of the slabs (Fig. 4.4). Devices like these, if located between the lateral- and gravity sub-systems, would be able to provide restoring forces without interfering with the freedom of motion of the floor slabs.

At this point, however, the stability spring is rather a generic concept that does not necessarily have to be materialized in the form of a device. As long as stability is provided to the gravity sub-system and the slabs' freedom of motion is allowed, the stability springs simply suppose an elastic interface that could, be provided in the form of a continuous elastic material interface. If a material interface is chosen to act as a stability spring, apart from providing the necessary restoring forces, it would also have to possess enough deformation capacity to accommodate the expected relatively large displacements of the floor slabs.

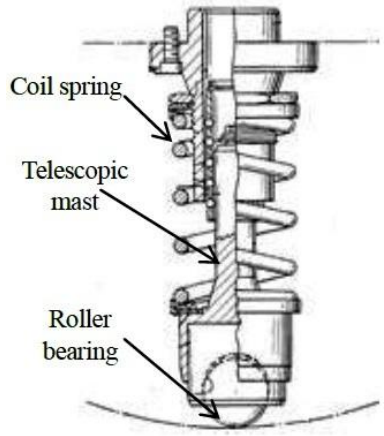

Fig. 4.3. Earthquake isolating support (Yaghoubian 1988)

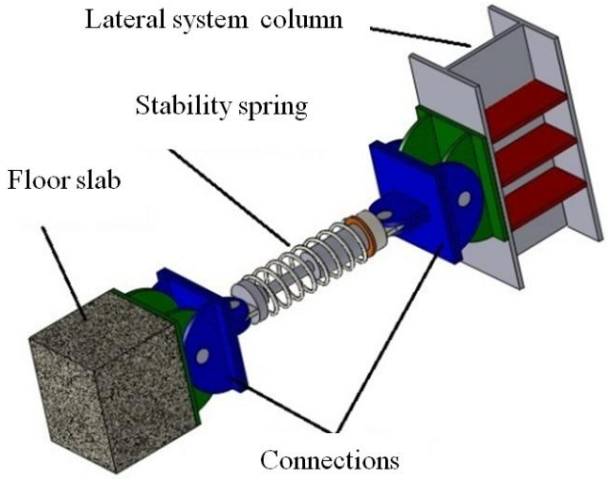

Fig. 4.4 Stability spring alternative design

4.3 Requirements for the energy dissipaters

As in the case of the stability springs, the energy dissipaters have to also permit the "isolated" motion of the floor slabs and not interfere with the full restoration of the system. Of the many types of energy dissipaters available commercially, fluid viscous dampers seem most appropriate for compliance with these requirements. Metallic or friction dampers, for example, would not allow the building to recover its original undistorted position after an earthquake because residual deformations are a byproduct of their functioning. The use of fluid viscous dampers would not interfere with the restoration tasks of the stability springs, and the allowance of the "isolated" motion of the gravity subsystem would be granted if devices with pinned ends and appropriate connections are used.

4.4 Anticipated advantages of SDMI

Some of the expected advantages of SDMI compared to typical fixed-base, base-isolated and other types of controlled structures are:

- Reduced floor accelerations and interstory drift-ratios in the lateral sub-system,
- Lateral displacements of the floor slabs distributed throughout the height of the building instead of concentrating them at the base as in Base Isolation,
- Non-cumulative lateral displacements with height of the floor slabs, since the displacements at each floor level are "independent" from each other and fitted inside the region limited by the lateral sub-system,

- Predominant participation of the first mode of vibration in the seismic response of the building due to the virtually inexistent coupling between the floor masses, achieving the same effect as Base Isolation in the response of the structure,
- Greater energy dissipation and controlled seismic response through the use of energy dissipating devices,
- Applicability to heavier structures, since vertical isolators are not used,
- Low cost derived from the use of simple mechanisms and already available response-control devices,
- Lighter lateral and gravity sub-systems that compensate for the costs of incorporating energy dissipaters, stability springs, and column pins,
- Reduced system life-cycle cost and continuous availability of the structure for occupancy due to the better and damage-proof performance of the system even after major seismic events (related to the continuous elasticity of the system), and
- Virtually no disturbances resulting from wind loads.

5. THE SINGLE-STORY SDMI BUILDING

The special case of the single-story (SS-) SDMI building serves to introduce, explain, and understand the mathematical concepts, modeling assumptions, and logic behind the analytical and design philosophies applicable to the more general case of a multi-story SDMI building in a simple and graphical way.

5.1 Analytical modeling

Fig. 4.1 reveals that the gravity sub-system in a SDMI building consists of a stack of inverted pendulums and it can, as such, be idealized. To simplify the mathematical model of the system, the "mass-less" degrees-of-freedom (DoFs) can be condensed to yield a reduced set of DoFs linked by equivalent stiffness springs and equivalent damping elements. In order to obtain an accurate dynamic model, if energy dissipating devices are incorporated into the system, these have to be translated into equivalent dampers using an appropriate dynamic condensation scheme such as the exact dynamic condensation of non-classically damped systems of reference (Qu 2004). A condensed idealization of the SS-SDMI building is shown in Fig. 5.1.

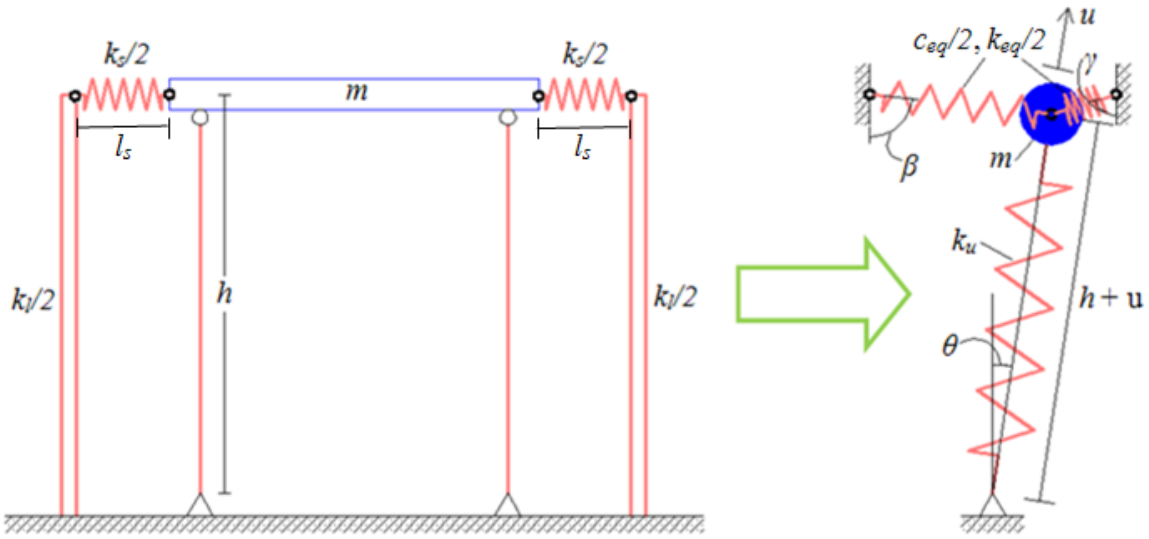

m = floor mass

h = story height

l_s = undeformed length of the stability springs

k_l = lateral stiffness of the lateral sub-system

k_s = total stiffness of the stability springs

k_{eq} = total equivalent lateral stiffness

k_u = total vertical stiffness of the gravity sub-system

c_{eq} = total equivalent lateral damping coefficient

θ = generalized rotation of the gravity sub-system

u = generalized deformation of the column spring

β, γ = rotations of the stability springs

Fig. 5.1. Discretization of the single-story SDMI building

The equations governing the motion of the two DoF system model can be obtained using principles of *Planar Motion* or *Lagrangian Mechanics*. The application of either formulations results in the following coupled ordinary differential equations (ODEs), which constitute the mathematical model of the single-story system:

$$\ddot{u} = \omega^2(u+h) - g\cos\theta - \frac{k_u}{m}u + \frac{k_{eq}}{4m}\left\{\frac{I\left[l_s-(A+L^2)^{1/2}\right]}{(A+L^2)^{1/2}} + \frac{J\left[l_s-(A+B^2)^{1/2}\right]}{(A+B^2)^{1/2}}\right\} + \frac{c_{eq}}{4m}\left[\frac{I(C-2KL)}{2(A+L^2)} - \frac{J(2BK-C)}{2(A+B^2)}\right] \quad (5.1)$$

and

$$\ddot{\theta} = \frac{\left\langle mg\sin\theta - 2m\omega\dot{u} - \frac{Fk_{eq}}{4(u+h)}\left[\frac{D(l_s-G^{1/2})}{G^{1/2}} - \frac{E(l_s-H)}{H}\right] - \frac{c_{eq}}{4}\left\{\begin{array}{l}\frac{E\left[B(2\dot{u}\sin\theta+2u\omega\cos\theta+2h\omega\cos\theta)-C\right]}{A+B^2} \\ +\frac{D\left[C-(2u\sin\theta-2l_s+2h\sin\theta)(\dot{u}\sin\theta+u\omega\cos\theta+h\omega\cos\theta)\right]}{G}\end{array}\right\}\right\rangle}{m(u+h)} \quad (5.2)$$

where

$$A = (u\cos\theta - h + h\cos\theta)^2$$

$$B = l_s + u\sin\theta + h\sin\theta$$

$$C = (2u\cos\theta - 2h + 2h\cos\theta)(h\omega\sin\theta - \dot{u}\cos\theta + u\omega\sin\theta)$$

$$D = l_s\cos\theta - h\sin\theta$$

$$E = l_s\cos\theta + h\sin\theta$$

$$F = 2(u + h)$$

$$G = A + (u\sin\theta - ls + h\sin\theta)^2$$

$$H = (B^2 + A)^{1/2}$$

$$I = 2u + 2h - 2h\cos\theta - 2l_s\sin\theta$$

$$J = 2u + 2h - 2h\cos\theta + 2l_s\sin\theta$$

$$K = \dot{u}\sin\theta + u\omega\cos\theta + h\omega\cos\theta$$

$$L = u\sin\theta - l_s + h\sin\theta$$

5.1.1 Validation of the mathematical model

In order to verify the correctness of the equations of motion (EoMs), a computer model of the SS-SDMI building is created and analyzed using the computer program SAP2000 (CSI 2010). Later, the structural parameters specified in the computer model are used in the time-history solution of Eqs. (5.1) and (5.2) to carry out a subsequent comparison of the results obtained by the two methods of analysis. The structure selected for the validation purposes of this sub-section corresponds to a one story, four bay moment-resisting frame (MRF) surrounding a mass-isolated gravity sub-system. This SDMI building has the same weight, material, and geometric properties as the first story of the 3-story benchmark building of Ohtori et al. (2004) (Fig. 5.2).

Only one MRF is modeled, which is assigned with half of the total seismic mass; this results in a structure having the properties given in Table 5.1. The corresponding equivalent stiffness (k_{eq}) for the analytical model is calculated as:

$$k_{eq} = \frac{k_l k_s}{k_l + k_s} \tag{5.3}$$

Table 5.1. Structural properties of the frame used for the SDMI model validation

W (kips)	*h (ft)*	k_u *(kips/in.)*	k_l *(kips/in.)*	k_s *(kips/in.)*	l_s *(in.)*
1,055	13	27, 885 (est.)	757.9	30	20

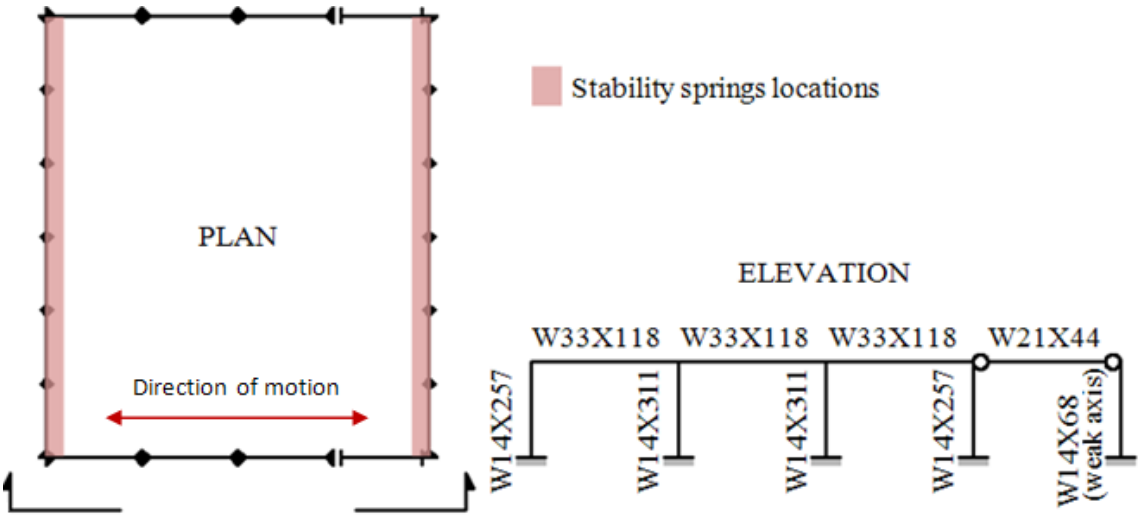

Fig. 5.2. Structure used for the validation of the SDMI mathematical model

The dynamic simulations of the two models are carried out subjecting them to both the vertical and horizontal components of the Kobe (KJMA000) earthquake record, simultaneously for 20 seconds (Fig. 5.3). The choice of earthquake record does not obey any particular reason with regards to the system's evaluation the only intention is that of validating the mathematical equations of motion (EoMs). However, a strong ground motion was selected in order to magnify any possible differences existing between the two models. With the same purpose, no damping was specified in the analyses.

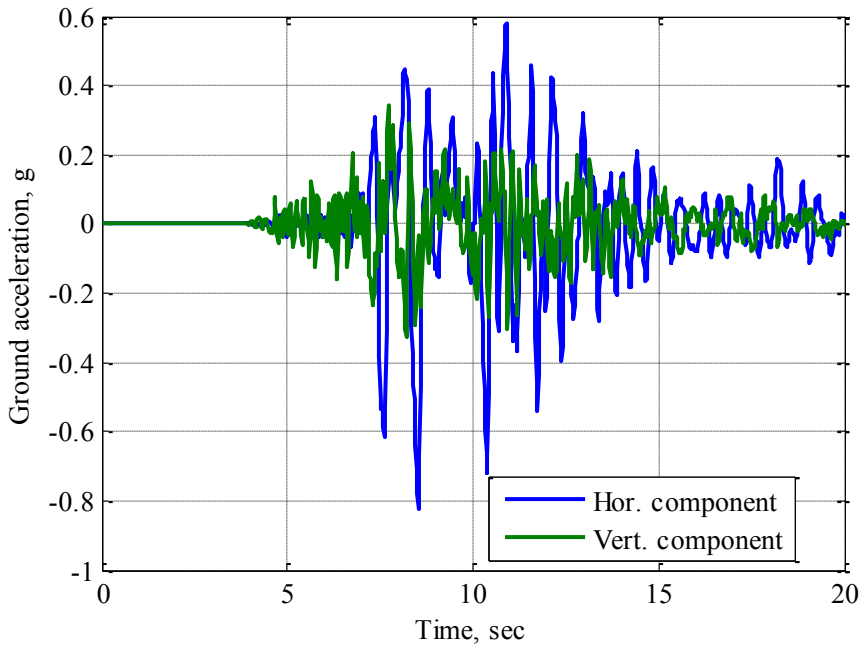

Fig. 5.3. The Kobe (KJMA000) earthquake record

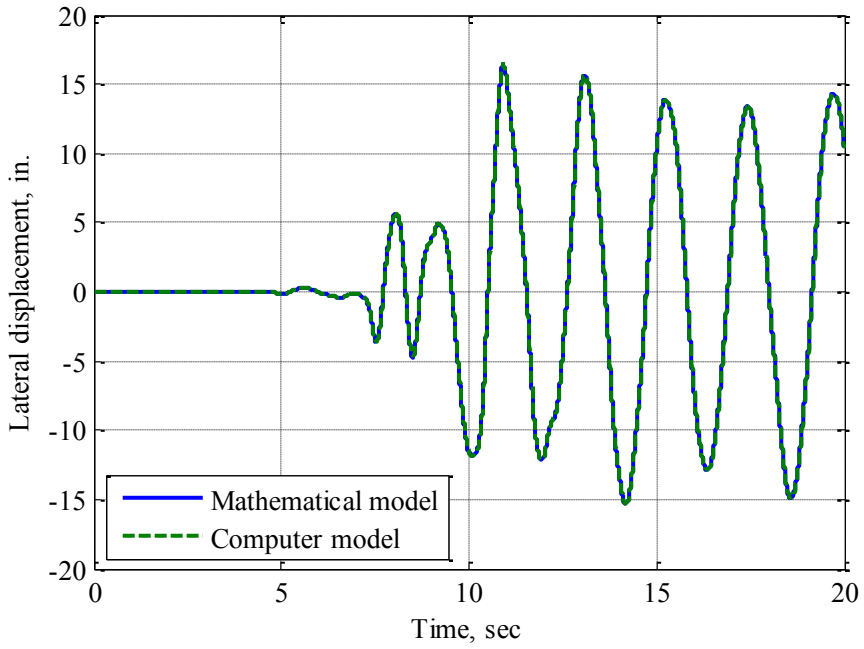

Fig. 5.4. Validation of the mathematical model

The numerical integration of the EoMs is carried out with the computer program MATLAB (TheMathWorks 2009), and the simulation of the computer model is made using the full nonlinear (geometric) capabilities of SAP2000 (p-delta and large displacements). The results of these simulations are given in Fig. 5.4 where the horizontal displacement of the floor mass is plotted against time. The perfect agreement between the results given by the simulations of the two models allows the conclusion of the correctness of the mathematical equations.

5.2 The effect of considering the axial stiffness of the gravity sub-system in the mathematical SDMI model

In order to follow the approach that has been chosen for the dynamic study of the SDMI system, which will be described later, the differential EoMs of the physical idealization of the system have to be at hand. Obtaining the continuous-time EoMs can be a very demanding task in the case of multi-story SDMI buildings. The large number of simulations that are carried out as part of the optimization process performed later in section 7.2 would benefit from a faster-to-analyze model. Therefore, any justifiable simplification of the physical model of the system that leads to lower computational efforts is advantageous.

In view of the aforementioned, the importance of including the radial DoF u in the mathematical model was evaluated having in mind that, if u did not contribute significantly to the lateral response of the building, which is the variable of interest, it could be eliminated without compromising the accuracy in the estimation of the seismic response while reducing the computational resources needed to analyze the model. Moreover, the reduction of DoFs from two to one turns out to be excellent for the purposes of this section, which aims to provide a relatively simple and graphical introduction to the theory and philosophy behind the analysis and design of the SDMI system.

To study the magnitude of the contribution of the radial DoF to the overall seismic response, the same structure as in the previous sub-section was used and subjected to the same Kobe horizontal and vertical ground acceleration time-histories. In this case, two different mathematical models were simulated: one having a flexible spring with the

same stiffness k_u as the structure used in the last sub-section, and one having a rigid rod. The results of the simulations are given in Fig. 5.5, which shows that practically no difference is made by the use of either of the two models. Due to the aforementioned conveniences of reducing the number of DoFs of the model's discretization, a decision was made to work with the single-degree-of-freedom (SDF), rigid-rod model for the study of the SDMI dynamics.

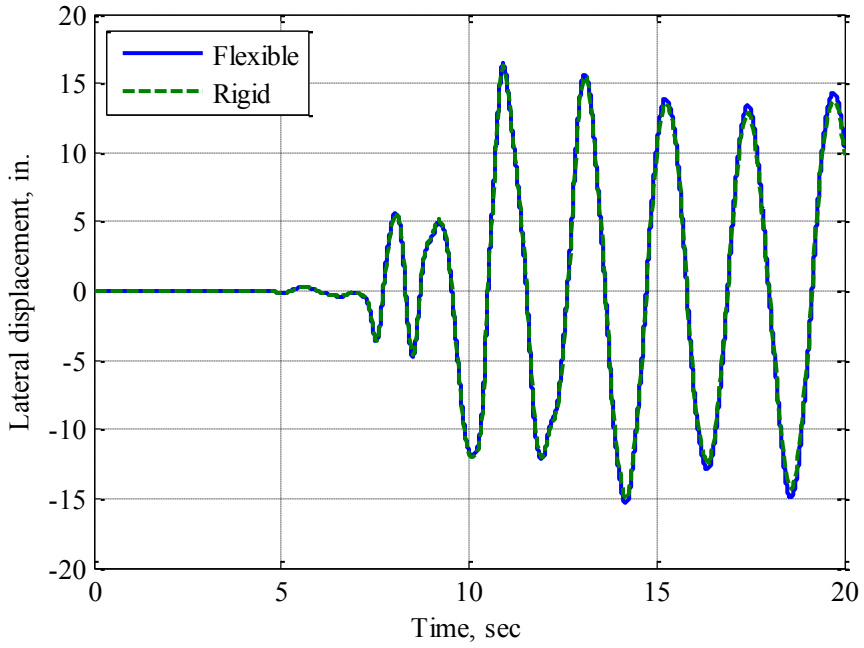

Fig. 5.5. Comparison between the consideration of axially flexible and axially rigid columns in the gravity sub-system

5.3 Stability analysis of the single-story SDMI building

Due to the inherent "looseness" of the SDMI system, its motion involves large rotations at the base of the pendulums that make up the gravity sub-system. As a result, the use of small-displacement theory for modeling results in erroneous predictions of the dynamic response of the system and is useless in the determination and characterization of the nature of its equilibrium states. Nonlinear models and methods of dynamic (stability) analysis are more appropriate.

Consequently, the approach that is followed for the stability analysis of the SS-SDMI building uses Lyapunov's second method for stability (Jordan and Smith 2007). This method performs the study of a (nonlinear) dynamic system's stability based on the dynamic progression of the system's response on a phase plane. Based on whether the system converges to or diverges from one of the different possible equilibrium states following its perturbation from these states, their full characterization can be realized. The first step required for this characterization is the determination of the dynamic system's ODEs governing its motion, which are afterwards used to find the system's equilibrium points (EPs) or limit cycles (steady-state orbitals). Both the EPs and limit cycles are defined by time-invariant sets of states. By time-invariance it is implied that if the system finds itself in one of these sets, it will remain there as time tends to infinity, unless the system is perturbed.

To study the stability and restoration capacities of the SDMI system, one is concerned with the characterization of its EPs rather than with that of the limit cycles that could arise from subjecting the system to (periodic) excitations or from starting it from

non-zero initial conditions (ICs). The reason is, first, earthquake excitations are not periodic and occur during a finite period of time, which does not lead to a steady-state response. Second, damping eventually stops the motion of the structure once the ground motion is over.

5.3.1 Equilibrium points of the SS-SDMI building

For the formal study of the dynamic stability of the SS-SDMI system, Lyapunov stability and asymptotic stability concepts are evoked. According to these concepts, if a dynamic system $\dot{\boldsymbol{x}} = \boldsymbol{X}(\boldsymbol{x})$ is regular and $\boldsymbol{X}(\mathbf{0}) = \mathbf{0}$, to study the stability of the zero solution (the EP at the origin of the phase plane), a test function $V(\boldsymbol{x}): \mathbb{R}^n \to \mathbb{R}$ needs to be determined, such that $V(\boldsymbol{x}) \geq 0$ in some neighborhood N_μ of the origin with equality if and only if $\boldsymbol{x} = \mathbf{0}$. If, in the same neighborhood of the origin, the time-derivative $\dot{V}(\boldsymbol{x})$ is negative semi-definite, then the EP at the origin is said to be stable in the sense of Lyapunov; if $\dot{V}(\boldsymbol{x})$ is negative definite, the EP is said to be asymptotically stable.

Although this theorem is stated for the EP at the origin, it can be applied to the study of other EPs if the origin of the phase plane is translated to the location of the EP that one desires to investigate. The concept of asymptotic stability is of particular importance. If an EP is asymptotically stable, it means that it is both stable and attractive (Vidyasagar 2002), which, if applied to the SS-SDMI system, implies that the motion of the system will eventually stop at an asymptotically stable EP if, after the ground excitation stops, the system is or enters the neighborhood N_μ surrounding that particular EP. As a particular case, if the EP at the origin (the originally undistorted position of the sys-

tem) is asymptotically stable, it means that the undistorted configuration of the SS-SDMI system will always be restored, provided that the system continuously oscillates inside the region surrounding the origin where both V and $-\dot{V}$ are positive definite or if it enters such region after the ground motion has stopped.

Since the SS-SDMI system constitutes a mechanical system and its energy function can be established, the classical association of the Lyapunov function with the system's energy can be used. Therefore, the "natural" use of the mechanical energy of the system as Lyapunov test-function V is carried out. This function is given by:

$$V(\theta,\omega)=\frac{k_{eq}}{4}\left\{l_s-\left[\left(h-h\cos\theta\right)^2+\left(l_s+h\sin\theta\right)^2\right]^{\frac{1}{2}}\right\}^2+ \\ +\frac{k_{eq}}{4}\left\{l_s-\left[\left(h-h\cos\theta\right)^2+\left(l_s-h\sin\theta\right)^2\right]^{\frac{1}{2}}\right\}^2+\frac{1}{2}mh^2\omega^2+mgh\cos\theta+Z \tag{5.4}$$

which can easily be made zero at any EP of interest by applying to the function the appropriate shift Z. The time-derivative of the energy function is calculated as:

$$\dot{V}(\theta,\omega)=\omega\frac{\partial V}{\partial\theta}+\alpha(\theta,\omega)\frac{\partial V}{\partial\omega} \tag{5.5}$$

where α = angular acceleration at the base of the pendulum.

ω = angular velocity at the base of the pendulum

θ = rotation at the base of the pendulum

To illustrate the application of the above mathematical theory to a SS-SDMI system, consider a condensed plane model of a one-story building in which the lateral subsystem in the direction of shaking consists of the four-bay moment-resisting frames (MRFs) shown in Fig. 5.6. The MRFs contain a stability-dependent mass-isolated gravity sub-system as shown. The structure has the mass, material, and geometric properties of the first story of the 3-story benchmark building of Ohtori et al. (2004) but with the lateral and gravity sub-systems detached from each other and linked together by stability springs at the interfaces shown. Here, only one MRF is modeled and assigned with half of the total seismic mass, which results in a structure having the properties given in Table 5.2. The stiffness assigned here to the stability springs corresponds to only about 40% of what would be the *American Institute of Steel Construction* (AISC) (AISC 2011) requirement for a nodal brace.

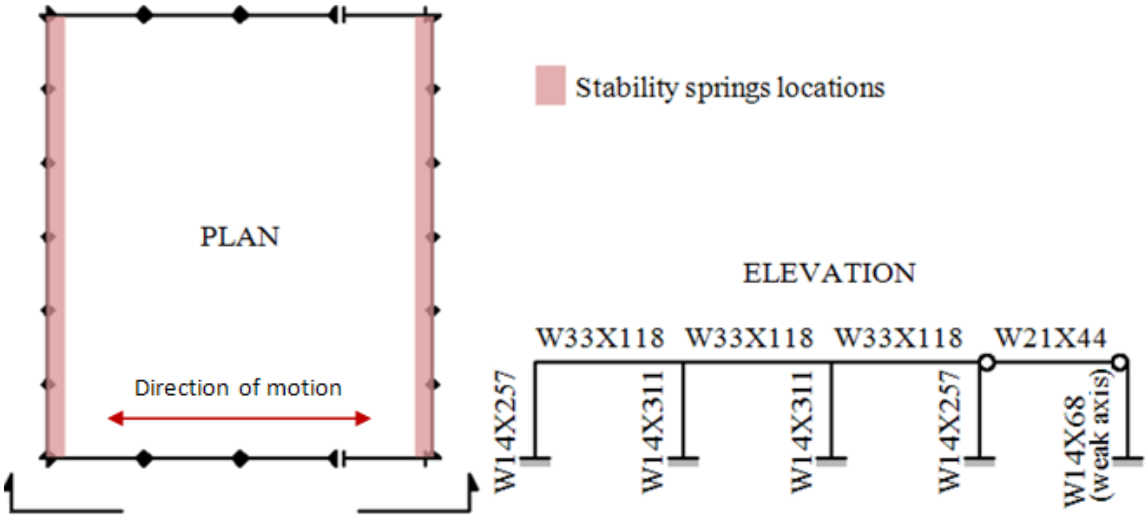

Fig. 5.6. Example SDMI building

Table 5.2. Structural properties of the frame used for the SDMI model validation

W (kips)	*h (ft)*	k_u *(kips/in)*	k_l *(kips/in)*	k_s *(kips/in)*	l_s *(in.)*
1,055	13	27,885 (est.)	757.9	30	20

The mechanical energy of this example system as a function of the system's states (lateral displacement and lateral velocity) is determined and graphically shown in Fig. 5.7. Its time-derivative is given in Fig. 5.8. As said before, the negative definiteness of the test function's time-derivative in a neighborhood of the phase plane surrounding the EP under study is required to diagnose that particular EP with asymptotic stability inside that region. However, as can be seen in Fig. 5.8, the power function $\dot{V}$ is only negative semi-definite and, therefore, at this point, only stability in the sense of Lyapunov can be concluded.

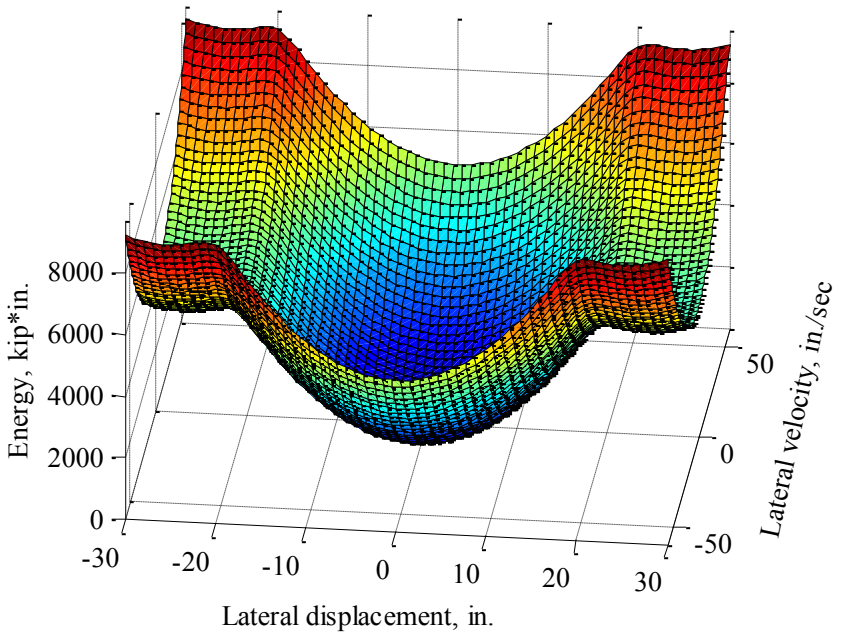

Fig. 5.7. Energy correspondence of the motion

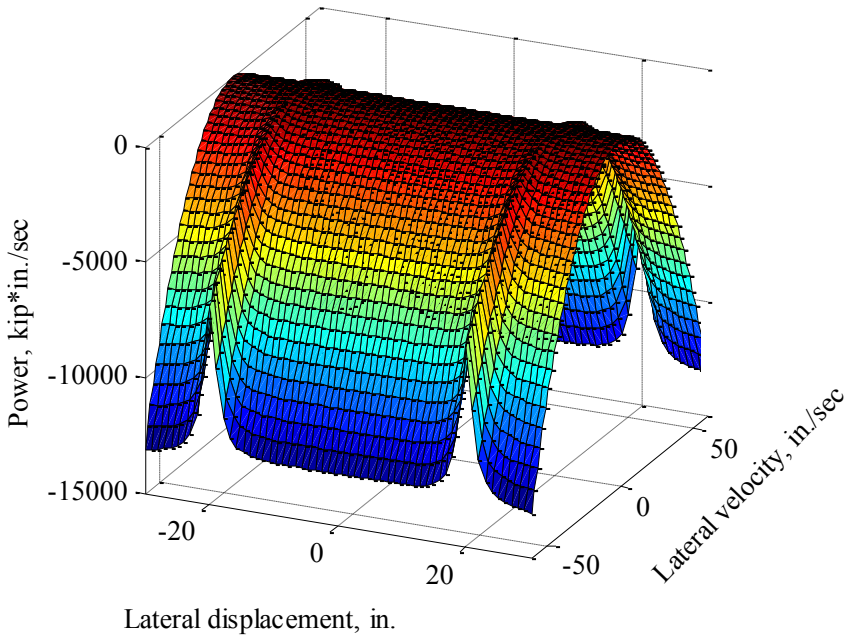

Fig. 5.8. Energy change time rate

There are, however, two ways of asserting the asymptotic stability of the EP at the origin; a mathematical method and a physical method. In the former method, LaSalle's invariance theorem (LaSalle 1976) is used. According to LaSalle's principle, given a regular dynamic system $\dot{\boldsymbol{x}} = \boldsymbol{X}(\boldsymbol{x})$ with $\boldsymbol{X}(\mathbf{0}) = \mathbf{0}$, and a function $V(\boldsymbol{x}) : \mathbb{R}^n \to \mathbb{R}$ such that $V(\boldsymbol{x}) \geq 0$ in some neighborhood N_μ of the origin with equality if and only if $\boldsymbol{x} = \mathbf{0}$. If, in the same neighborhood of the origin, the time-derivative $\dot{V}(\boldsymbol{x})$ is negative semi-definite and the set $\left\{\dot{V}(\boldsymbol{x}) = 0\right\} \cap N_\mu$ does not contain any trajectories besides the trivial trajectory (the EP under study), then the asymptotic stability of that EP can be established. In this case, in Fig. 5.7 and Fig. 5.8, it can be appreciated that there is a neighbor-

hood N_μ of the EP at the origin where V is positive definite and $\dot{V}$ is negative semi-definite. The set $\left\{\dot{V}(\boldsymbol{x})=0\right\}\bigcap N_\mu$ is given by the x- (lateral-displacement-) axis and the trajectories of the system are given in Fig. 5.11; as can be seen, none of the trajectories coincides with the lateral-displacement-axis (which has the logic explained in the next paragraph), so the asymptotic stability of the EP at the origin can be asserted.

From a more physical point of view, it is possible to deduct the asymptotic stability of this EP, first, by seeing in Fig. 5.7 that the origin constitutes a minimum of the energy function, which is associated to a stable EP. Second, the fact that the power function (Fig. 5.8) is negative everywhere except at the displacement-axis means that energy is "continuously" dissipated as the system vibrates, except when the system has zero velocity (which is obvious since viscous damping is being considered). Because it is impossible that the system vibrates with zero velocity, if it vibrates, it will definitely dissipate energy. If energy is dissipated and it is not continuously restored, then the system will eventually reach a state of rest; therefore, the EP has to be asymptotically stable.

5.3.2 The SS-SDMI system characteristic equilibrium points

The stability analysis of the autonomous ODEs governing the motion of the SS-SDMI system on the phase plane results in that, depending on the amount of equivalent stiffness k_{eq} available, the gravity sub-system pendulum can possess either two or six EPs. However, because one of these EPs always corresponds to the vertically-down position of the pendulum, which is senseless in practice, only either one or five EPs are of interest.

Consider a SS-SDMI structure with the same mass and geometric properties as the one used before (m = 2.73 slugs, h = 13 ft), and with a damping coefficient c_{eq} = 3.551 kips-sec/in. The number of EPs depends on the structural properties of the system except for the damping; namely, the mass, height, undistorted length of the stability springs, and equivalent stiffness. A parametric analysis where all the values of the mentioned structural variables are fixed except for the equivalent stiffness, yields the following conclusions: if the equivalent stiffness is below the critical (lower-bound) value given by

$$k_{eq,cr} = \frac{mg}{h} \tag{5.6}$$

(case 1), the system displays only one (meaningful in practice) unstable EP at the origin, (the originally undistorted position) (Fig. 5.9). The physical interpretation of this case is that, if the total stiffness of the stability springs is less than $k_{eq,cr}$, at the smallest perturbation of the undistorted system the mass will hit the ground or the lateral sub-system and not return to its original position.

A second case (case 2) occurs when the equivalent stiffness is higher than some "upper-bound" value. In this case, the up-right position of the pendulum is again the only (meaningful) EP of the system, only that, here, this position is stable. If the stiffness value corresponds to case 2, the motion of the pendulum mass occurs about the original position without hitting the ground, provided that the energy equivalence of the motion corresponds to θ-values that are smaller than $\pi/2$ rad at all times (Fig. 5.10).

An intermediate case occurs if the stiffness in the system is larger than the critical value given by Eq. (5.6), but smaller than the denominated upper-bound value. If this is the case (case 3), then five (meaningful) symmetrically about the origin EPs are generated (Fig. 5.11). The EP at the origin as well as the two extreme EPs are stable, while the two intermediate EPs are (unstable) saddles. In this case, the system will not hit the ground provided that the energy equivalence of the motion of the system implies θ-values that are smaller than $\pi/2$ rad at all times.

With respect to the types of EPs that are generated, these are dependent on all the structural properties of the system. However, when taking into account the fact that damping will always be present in real structures, regardless of whether special energy dissipating devices are installed or not, the result is that the nature of the system's EPs depends on the exact same parameters affecting their number and stability.

Fixing all variables except for the stiffness, as was done before, allows the following conclusions regarding the types of the possible EPs: if the equivalent stiffness is less than the value given by Eq. (5.6) (case 1) (Fig. 5.9), then the EP at the origin becomes a saddle (saddles are always unstable). If the equivalent stiffness provided is sufficiently high so that only a single meaningful stable EP is generated (case 2) (Fig. 5.10), the EP at the origin will always be a stable spiral whose domain of attraction covers the whole phase plane. The implication of this is that the system will always end up in the undistorted upward position after its excitation stops.

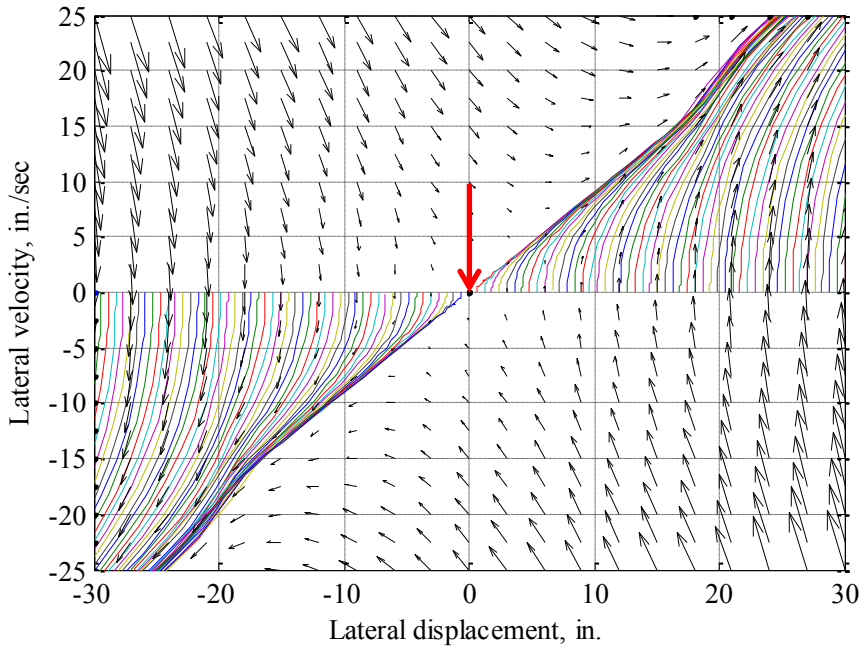

Fig. 5.9. Unstable SS-SDMI system started from different positions (case 1)

Finally, if the equivalent stiffness belongs to the intermediate case 3 (Fig. 5.11), then three attractors in the form of stable spirals separated by two saddles are generated. The existence of the two saddles is associated with the snap-through behavior that occurs when the pendulum mass is in the close vicinity of the lateral sub-system. The sizes of the domains of attraction (DoAs) of the spirals and the actual locations of the five (meaningful) EPs in this case depend on the amount of stiffness provided and the location of the lateral sub-system. Because of the damping presence, the existence of these saddles is not of major relevance, since the system will never be started at them in a situation of zero excitation, nor will they ever interfere with the eventual convergence of the system to any of its EPs. The saddles are, however, useful in the determination of the limits of the DoAs of the spirals, which is of great importance for the safe design of the

system. In this case number 3, although the eventual asymptotic convergence to a (stable) EP is a fact, it is not certain whether the undistorted position of the system will be restored after the excitation stops.

The discussion regarding the number and types of EPs facilitates a shortcut to their characterization, i.e., to determine what case a particular combination of structural properties corresponds to, the equivalent stiffness of the system has to be compared with the one given by Eq. (5.6) first. If the stiffness is below the critical value, then the system belongs to case 1, else, the sole determination of the number of EPs will tell whether a particular SDMI structure belongs to case 2 or 3. This determination is done by determining θ-ω (rotation-angular velocity) pairs that make the autonomous system's state equations equal to zero, simultaneously. Table 5.3 provides the locations and types of the EPs of the example system presented in the previous sub-section. As can be seen, it corresponds to a case 3 system and the dynamic evolution on the phase plane of its autonomous ODEs is given in Fig. 5.11. Notice also that the saddles are located outside of the lateral sub-system, which implies that, with these structural properties, the restoration of the undistorted position is guaranteed.

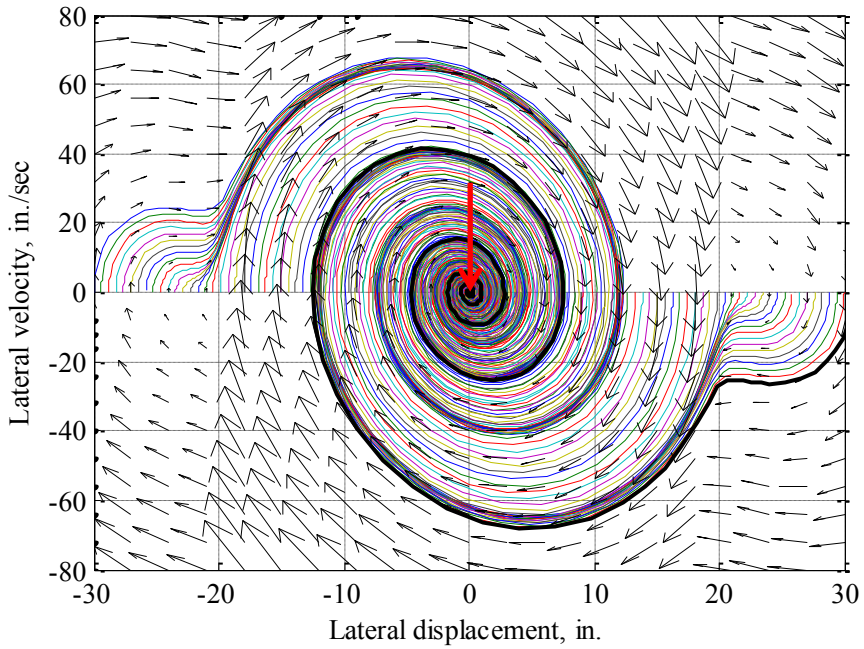

Fig. 5.10. Stable SS-SDMI system started from different positions (case 2)

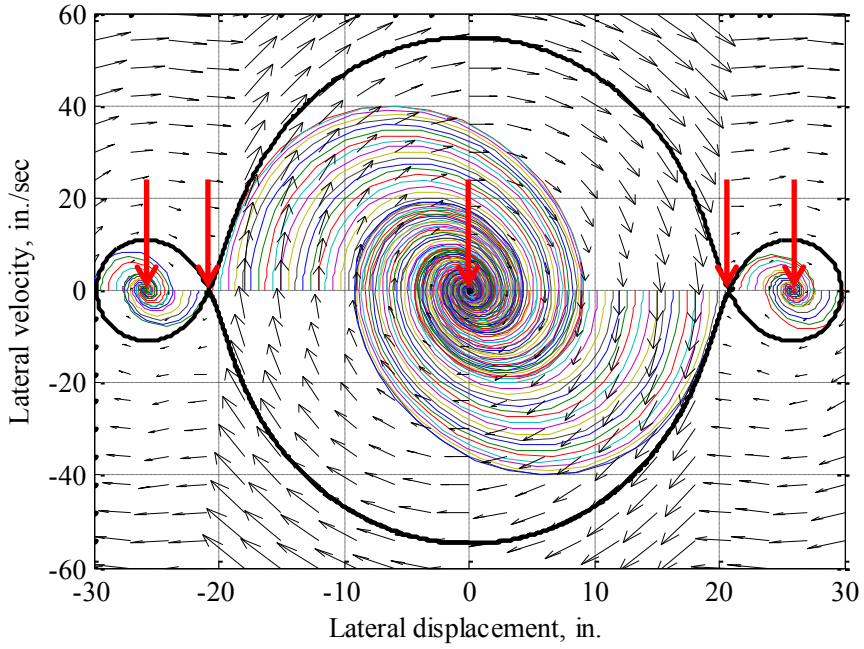

Fig. 5.11. Stable SS-SDMI system started from different positions (case 3)

Table 5.3. Types and locations on the phase diagram of the different EPs existing in a typical SS-SDMI building

EP #	*Lateral displacement (in.)*	*Lateral velocity (in./sec)*	*Type*
1	-25.80	0	Stable spiral
2	-20.76	0	Saddle
3	0	0	Stable spiral
4	20.76	0	Saddle
5	25.80	0	Stable spiral
6	0 ($\theta = \pi$ rad)	0	Saddle

5.4 Design of the single-story stability-dependent mass isolated building

In order to provide the highest level of isolation from the ground, the stiffness k_{eq} and damping c_{eq} of the condensed system have to be minimal. A provision of a "minimal" amount of stiffness favors large displacements of the floor slabs, which may result in, among other things, pounding of the gravity sub-system against the lateral sub-system. Pounding, in turn, can result in structural and non-structural damage as well as increased dynamic response (Komodromos et al. 2007).

To avoid pounding, displacement-response envelopes have to be estimated first with time-history analyses. Due to the large magnitude of the displacement-response of the mass that results from the low levels of stiffness, the envelopes of the displacement-response need to be determined through nonlinear methods of dynamic analysis; the number and requirements for these analyses are dictated by building codes (ASCE 2003;

ASCE 2007; ASCE 2010). To minimize the chances of pounding, the lateral sub-system should be located farther away from the expected extreme displacements multiplied by a factor of safety.

The potential for instability of the undistorted position is associated with the performance-related necessity of low levels of stiffness. The stability of the undistorted position of the system is achieved if more (equivalent) stiffness than the critical value given by Eq. (5.6) is provided. The provision of a greater value than $k_{eq,cr}$ converts the origin of the phase plane into a stable spiral.

To guarantee the restoration of the undistorted position of the pendulum, it is necessary to make sure that the system either enters or finds itself in the DoA of the EP at the origin after its excitation stops. Due to the randomness of earthquake excitations and actual structural properties of the system, it is impossible to make absolutely sure that the system enters the DoA of the EP at the origin after the ground motion is over. Therefore, the only way to guarantee the restoration of the undistorted position is that of making sure that the system finds itself in the DoA surrounding the origin at the moment the ground ceases to shake. The simplest and safest way to achieve this is by actually never letting the system abandon this region or, in other words, by making sure that the dynamic response envelope of the system is contained in the DoA of the EP at the origin. In fact, doing this also precludes pounding.

Because it is assumed that the level of isolation is to be maximized, the equivalent stiffness of the springs needs to be low. In a (stable) low-stiffness system, the system has three asymptotically stable EPs and their associated DoAs (Fig. 5.11). The resto-

ration requirement can be met, by design, if the saddles limiting the DoA of the EP at the origin are located at or outside the lateral sub-system.

A mathematical expression for the equivalent stiffness value that puts the saddles exactly at the location of the lateral sub-system can be determined based on the energy (Lyapunov) function of the system (Fig. 5.7). Since the saddles (and all the EPs) are located along the *X*- (rotation-/lateral-displacement-) axis of the phase plane, setting $\omega = 0$ (or lateral velocity equal to zero) in the energy function *V* yields a potential energy curve whose extrema are located at the locations of to the system's EPs. Taking the first derivative of the potential energy curve with respect to θ, equating it to zero, and solving for the $\theta_{max/min}$ values that satisfy the equation, yields the locations of the system's EPs. In a low stiffness system, the $\theta_{max/min}$ that is closest to $\theta = 0$ corresponds to the location of a saddle. If that $\theta_{max/min}$ is equated to the point corresponding to the location of the lateral sub-system, the associated stiffness k_{lb} can be solved to obtain Eq. (5.7):

$$k_{lb} = \frac{-2mgl_s\left(-d-l_s^2\right)^{0.5}\left(3l_s^2-d\right)^{0.5}}{h\left(-d-l_s^2\right)^{0.5}\left[l_s\left(l_s+f\right)-2l_s\left(3l_s^2-d\right)^{0.5}\right]+hl_s\left(l_s-f\right)\left(3l_s^2-d\right)^{0.5}} \tag{5.7}$$

where

$$d = 2h^2\left[\left(1-\frac{l_s^2}{h^2}\right)^{0.5}-1\right]$$

$$f = l_s\left(1-\frac{l_s^2}{h^2}\right)^{0.5}$$

The provision of an equivalent stiffness equal or greater than the lower-bound stiffness k_{lb} guarantees the restoration of the undistorted position of the pendulum after the ground excitation stops. Therefore, k_{lb} should be treated as a minimum design stiffness value. Once the pounding-safe distance l_s and the minimum stiffness required for stability and restoration k_{lb} are at hand, the design procedure proceeds with the determination, from the k_{lb} value, of the stiffnesses k_l and k_s that the lateral sub-system and the stability springs must have. These stiffnesses have to be proportioned in such a way that ensures that all the springs remain elastic. This is because the plasticization of any structural element would represent a loss in stiffness, which, due to the already low factor of safety against instability, could compromise the safety of the system.

Consider the simplified model given in Fig. 5.12, which is sufficient for the purpose of stiffness proportioning, and the next algebraic derivation. Also, define the following quantities:

F_δ = reduction factor for the allowed drift of the lateral sub-system ($F_\delta \leq 1$)

F_k = factor of safety for the minimum equivalent stiffness needed for continuous stability and restoration of the system ($F_k \geq 1$)

$(DR)_y$ = the lateral sub-system's drift ratio at the onset of yield

$|x_G(t)|_{\max}$ = peak absolute lateral displacement of the floor mass

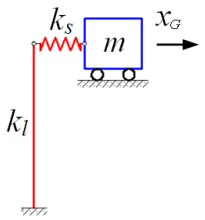

Fig. 5.12. Physical model used in the derivation of the SS-SDMI design equations

The peak absolute force experienced by the equivalent springs is $F_k k_{lb} |x_G(t)|_{\max}$. In the full SDMI model, the lateral and stability springs are in series, so the lateral force resisted by the lateral sub-system will also be $F_k k_{lb} |x_G(t)|_{\max}$. In order to limit the drift-ratio of the lateral sub-system to its allowed value, its stiffness has to be at least

$$k_l = \frac{F_k k_{lb} \left| x_G(t) \right|_{\max}}{F_\delta h (DR)_y} \tag{5.8}$$

The equivalent stiffness of the system is given by

$$k_{eq} = F_k k_{lb} = \frac{k_l k_s}{k_l + k_s} \tag{5.9}$$

Solving for k_s gives

$$k_s = \frac{F_k k_{lb} k_l}{k_l - F_k k_{lb}} \tag{5.10}$$

The substitution of Eq. (5.8) into Eq. (5.10) yields

$$k_s = \frac{F_k k_{lb} \left| x_G(t) \right|_{\max}}{\left| x_G(t) \right|_{\max} - F_\delta h (DR)_y} \tag{5.11}$$

Equations (5.7), (5.8), and (5.11) constitute the design equations for a SS-SDMI building.

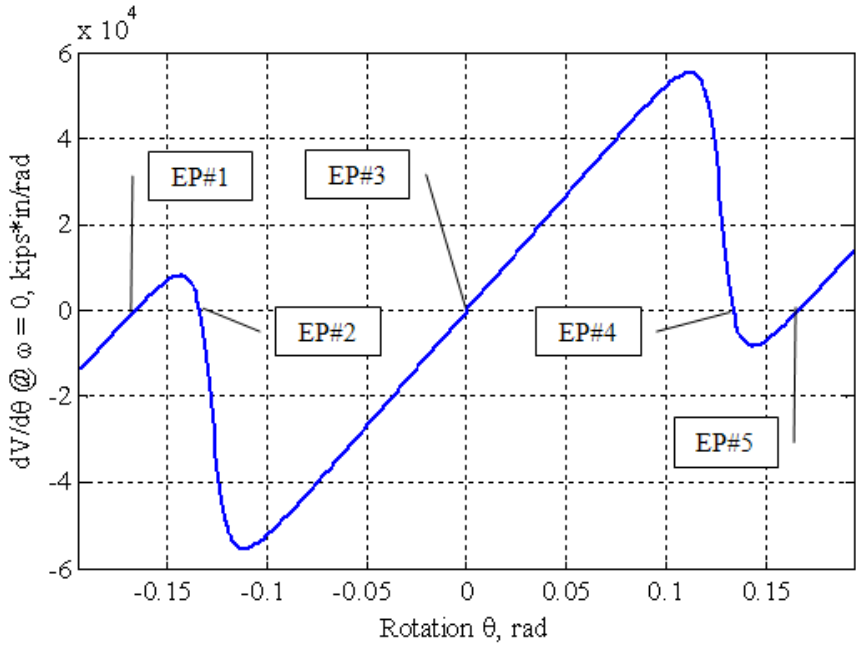

Fig. 5.13. Location of equilibrium points

5.5 Design example

Assume that it is desired to design a one-story SDMI building having a floor weight equal to 1,055 kips, a story height of 13 ft, that is capable of withstanding the Kobe (KJMA000) earthquake. A lateral sub-system based on MRFs is proposed for which a $(DR)_y = 0.01$ is assumed. A stability factor $F_k = 1.87$ and a drift factor $F_\delta = 0.4$ are specified and stability springs having $l_s = 20$ in. are used as a first trial.

Solution:

Assuming that no special structural optimization is made, to maximize the level of isolation, just the minimum stiffness for system restoration as well as no supplemental damping is to be provided. The equivalent stiffness is then determined by the use of Eq. (5.7).

$$d = 2h^2\left[\left(1-\frac{l_s^2}{h^2}\right)^{0.5}-1\right] = 2(156)^2\left[\left(1-\frac{20^2}{156^2}\right)^{0.5}-1\right] = -401.7 \text{ in.}^2$$

$$f = l_s\left(1-\frac{l_s^2}{h^2}\right)^{0.5} = 20\left(1-\frac{20^2}{156^2}\right)^{0.5} = 19.83 \text{ in.}$$

$$\left(3l_s^2-d\right)^{0.5} = \left[3(20)^2+401.7\right]^{0.5} = 40.02 \text{ in.}$$

$$k_{lb} = \frac{-2mgl_s\left(-d-l_s^2\right)^{0.5}\left(3l_s^2-d\right)^{0.5}}{h\left(-d-l_s^2\right)^{0.5}\left[l_s\left(l_s+f\right)-2l_s\left(3l_s^2-d\right)^{0.5}\right]+hl_s\left(l_s-f\right)\left(3l_s^2-d\right)^{0.5}}$$

$$= \frac{-2(1055)(20)\left(401.7-20^2\right)^{0.5}(40.02)}{156\left(401.7-20^2\right)^{0.5}\left[20(20+19.83)-2(20)(40.02)\right]+156(20)(20-19.83)(40.02)}$$

$$= 15.43 \text{ kips/in.}$$

For reference, this stiffness value corresponds to about 20% of what would be the stiffness requirement for a nodal brace according to the AISC provision. With k_{lb} at hand, a time-history analysis of the condensed system having $k_{eq} = F_k k_{lb} = 1.87(15.43) = 28.86$ kips/in. subjected to the horizontal and vertical components of the Kobe (KJMA000) record is carried out (Fig. 5.16). If zero inherent damping is specified, the peak absolute lateral displacement as given by the analysis is $|x_G(t)|_{\max} = 16.36$ in. Because this value is less than 20 in., it is decided to keep the originally proposed $l_s = 20$ in.

The process now continues with the determination of stiffness for the lateral subsystem and stability springs. For this, Eqs. (5.8) and (5.11) are used.

$$F_k k_{lb} = 1.87(15.43) = 28.86 \text{ kips/in.}$$

$$F_\delta h(DR)_y = 0.4(156)0.01 = 0.624 \text{ in.}$$

$$\left|x_G(t)\right|_{\max} = 16.36 \text{ in.}$$

$$k_l = \frac{F_k k_{lb}\left|x_G(t)\right|_{\max}}{F_\delta h(DR)_y} = \frac{28.86(16.36)}{0.624} = 756.8 \text{ kips/in.}$$

$$k_s = \frac{F_k k_{lb}\left|x_G(t)\right|_{\max}}{\left|x_G(t)\right|_{\max} - F_\delta h(DR)_y} = \frac{28.86(16.36)}{16.36-0.624} = 30.00 \text{ kips/in.}$$

An MRF is designed according to the k_l value obtained and the result is given in Fig. 5.14, which corresponds to an actual k_l = 757.9 kips/in.

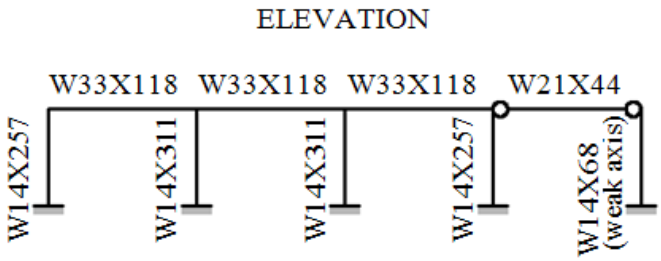

Fig. 5.14. Moment-resisting frame of design example (Ohtori et al. 2004)

5.5.1 Verification of the design

To verify and show that the calculated structural properties meet the design requirements, first, a pushover curve of the lateral sub-system is obtained to check the assumed $(DR)_y$ value. The curve is given in Fig. 5.15 and validates the 1% yield-drift assumption. Later, a dynamic time-history analysis of the designed SDMI system is performed using the design earthquake. The results of the analysis are given in Fig. 5.16; it is possible to verify that the floor slab does not pound against the lateral sub-system and that the maximum lateral sub-system's drift ratio meets or does not exceed the allowable value $(DR)_{\text{all}} = F_\delta(DR)_y = 0.4(0.01) = 0.004 = 0.4\%$.

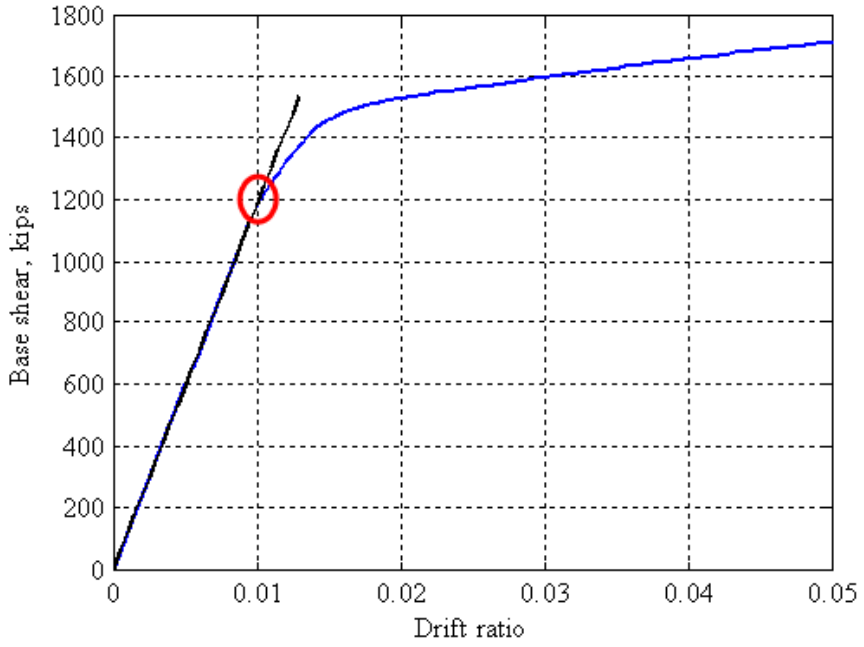

Fig. 5.15. Example structure pushover curve

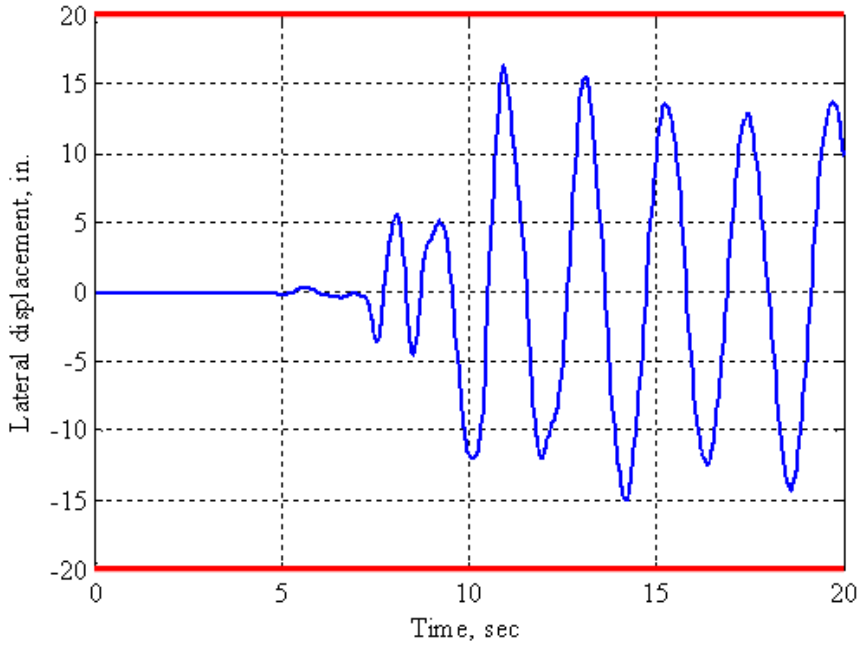

Fig. 5.16. Lateral displacement of the floor mass

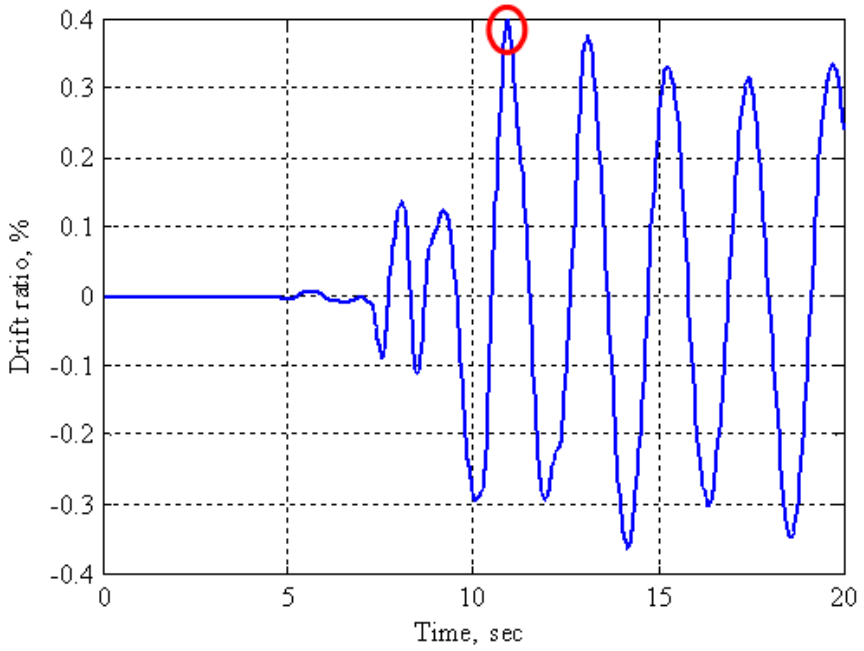

Fig. 5.17. Drift ratio in the lateral sub-system

The present example was designed to yield final results from the first attempt; however, the design procedure is iterative in nature. Nevertheless, the success of the final design should be the same as the one just achieved.

5.6 Design of the gravity sub-system

Because the columns in the gravity sub-system are pinned at both ends, they behave like truss members. The static analysis and design of such a gravity sub-system, when subjected to gravity loads, results in the fact that relatively slender columns are sufficient to resist the axial loads (there is no need to resist end moments). This fact is advantageous because it translates into lighter and more economic designs of the gravity sub-system. However, with a "thinner" design, the factor of safety (FS) against column buckling

might be reduced compared to the FS existing in the case of a more conventional gravity sub-system.

Due to the aforementioned possibility, a more careful assessment of the vertical loads acting on the gravity sub-system is required. The static analysis of the live and dead loads would not suffer any change; however, it is recommended to always include the vertical component of the ground accelerations in the dynamic analyses to dimension any increments in the axial loads imposed on the gravity columns.

For illustration, consider the same pendulum structure that has been used before with a flexible rod (k_u = 27,885 kips/in.) under the action of the Kobe (KJMA000) earthquake. The structure is first subjected only to the horizontal component of the ground accelerations and then simultaneously to both the horizontal and vertical accelerations. The radial acceleration response time-histories are given in Fig. 5.18. As can be seen, the peak axial acceleration response increases from about 0.065g when only the horizontal component is used to 0.4g if both the horizontal and vertical accelerations are considered. If this level of increase in the column forces is disregarded in conjunction with a possibly more compromised gravity sub-system in terms of column buckling, the safety of the system could be put at risk.

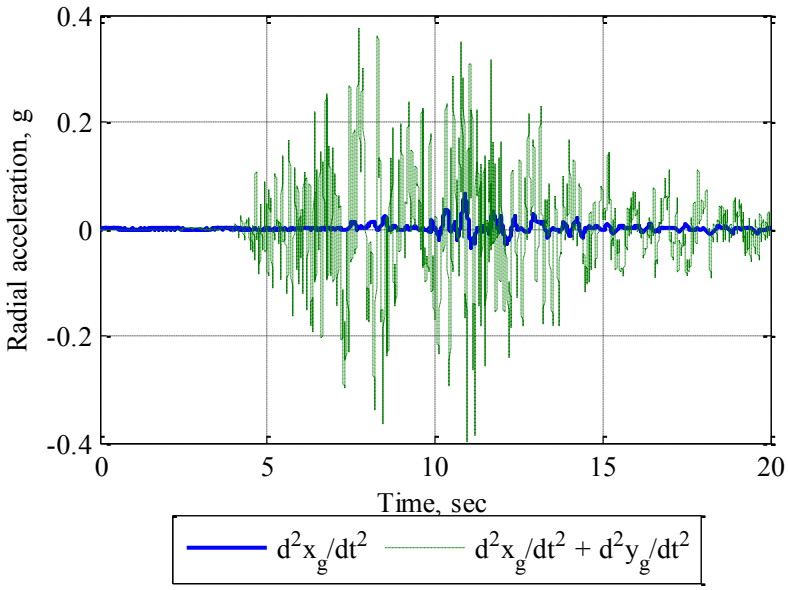

Fig. 5.18. Acceleration of the floor mass in the radial direction

6. THE MULTI-STORY SDMI BUILDING

This section is devoted to the analytical modeling, stability analysis, and design of the stack of inverted pendulums representing a gravity sub-system in the more general case of the multi-story (MS-) SDMI building. The same mathematical concepts and criteria that were applied in the study of the single-story case will be used with appropriate adaptations.

6.1 Analytical modeling

The MS-SDMI building can be idealized as a multiple stack of inverted pendulums, each with a pin at its base. The stack is linked to the lateral system through axial-force-only resisting springs that behave as linear elastic truss elements. As in the single-story case, Lyapunov's second method for stability is used in the dynamic stability study of the MS-SDMI system.

In order to apply Lyapunov's second theorem for stability, the availability of the ODEs governing the motion of the dynamic system under study is required. Obtaining the nonlinear semi-discrete EoMs of a multi-degree-of-freedom (MDF) system can be challenging, and their stability analysis can be even more complicated. For this reason, the condensation of MDF analytical models is sought.

Several static and dynamic model condensation techniques exist in the state-space and the displacement-space (Qu 2004). Each of these methods has particular advantages and disadvantages. Some may work sufficiently well in some cases, but unsat-

isfactorily in others. The SDMI system is nonlinear, dynamic, and non-classically damped; therefore, several forms of static and dynamic condensation are not well suited to perform accurate simulations of its dynamic behavior.

A method of dynamic condensation well suited to the SDMI system consists in a truncated series expansion of the full *exact dynamic condensation of nonclassically damped systems* (Qu 2004). This method converges to the exact condensation of the model, provided the norms of the reduced mass and damping matrices, M_R and C_R, are much smaller than that of the reduced stiffness matrix K_R. The reduced system matrices obtained by the use of this technique are given by:

$$\boldsymbol{K}_R = \boldsymbol{K}_{mm} + \boldsymbol{K}_{ms}\boldsymbol{R}_G \tag{6.1}$$

$$\boldsymbol{C}_R = \boldsymbol{C}_{mm} + \boldsymbol{C}_{ms}\boldsymbol{R}_G + \boldsymbol{R}_G^T\boldsymbol{C}_{sm} + \boldsymbol{R}_G^T\boldsymbol{C}_{ss}\boldsymbol{R}_G \tag{6.2}$$

$$\begin{aligned}\boldsymbol{M}_R = {} & \boldsymbol{M}_{mm} + \boldsymbol{M}_{ms}\boldsymbol{R}_G + \boldsymbol{R}_G^T\boldsymbol{M}_{sm} + \boldsymbol{R}_G^T\boldsymbol{M}_{ss}\boldsymbol{R}_G \\ & -\boldsymbol{R}_G^T\boldsymbol{C}_{ss}\boldsymbol{K}_{ss}^{-1}\boldsymbol{C}_{ss}\boldsymbol{R}_G - \boldsymbol{R}_G^T\boldsymbol{C}_{ss}\boldsymbol{K}_{ss}^{-1}\boldsymbol{C}_{sm} - \boldsymbol{C}_{ms}\boldsymbol{K}_{ss}^{-1}\boldsymbol{C}_{ss}\boldsymbol{R}_G - \boldsymbol{C}_{ms}\boldsymbol{K}_{ss}^{-1}\boldsymbol{C}_{sm}\end{aligned} \tag{6.3}$$

where

$\boldsymbol{R}_G = -\boldsymbol{K}_{ss}^{-1}\boldsymbol{K}_{sm}$

$\boldsymbol{K}$ = model stiffness matrix

$\boldsymbol{C}$ = model damping matrix

$\boldsymbol{M}$ = model mass matrix

m, s = master/slave nodes

It is common to perform narrow bandwidth matrix discretizations of structural systems; however, when applied to the SDMI system, Eqs.(6.1), (6.2), and (6.3) yield reduced matrices that are fully populated. This implies the existence of multiple couplings between the master DoFs at the mass, damping, and stiffness levels (Fig. 6.1). This coupling makes sense from a physical point of view, since the effects of displacing a particular DoF in an SDMI system has repercussions on all other DoFs, even if the latter are fixed.

The application of the mentioned condensation scheme to a 3-story building results in the reduced system of Fig. 6.1, which can be considered as a general MS-SDMI system model. The EoMs of motion of such a system can be obtained using Lagrangian mechanics. Because of the intended generality of the concepts given in this section with regard to the number of DoFs, a particular set of EoMs cannot be given.

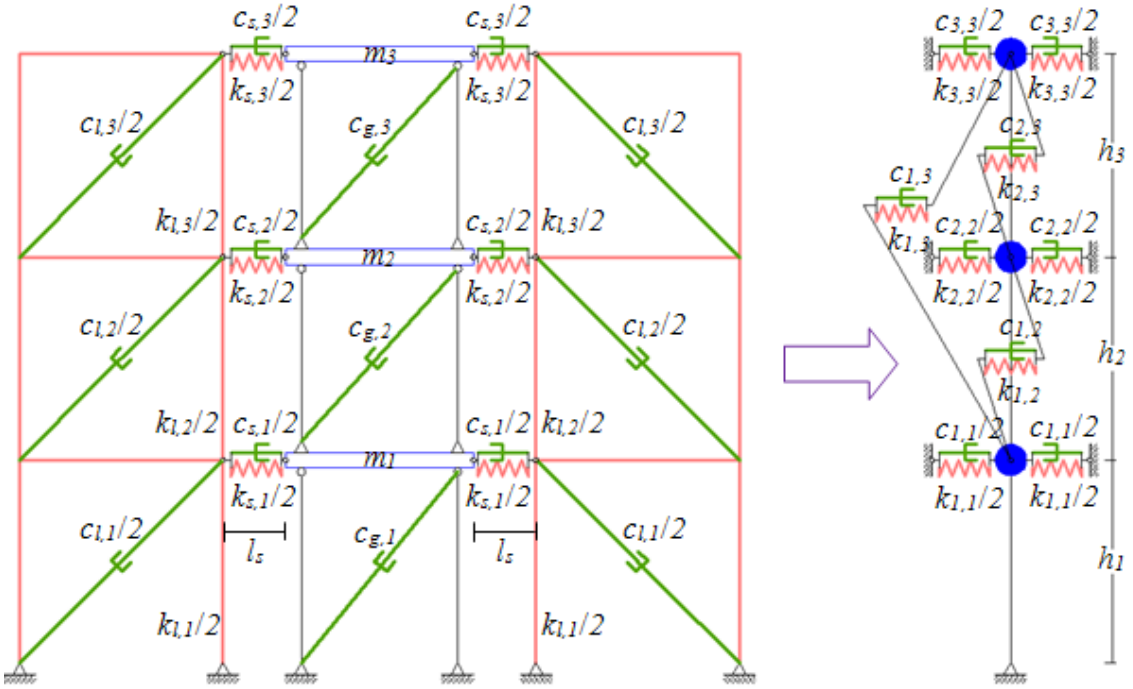

m_n = mass of the n^{th}-floor

h_n = height of the n^{th}-story

l_s = undeformed length of the stability springs

$k_{l,n}$ = total lateral stiffness of the lateral sub-system at the n^{th}-level

$k_{s,n}$ = total stiffness of the stability springs at the n^{th}-level

$c_{l,n}$ = total lateral damping device coefficient at the n^{th}-level in lateral sub-system

$c_{g,n}$ = total lateral damping device coefficient at the n^{th}-level in gravity sub-system

$c_{s,n}$ = total damping device coefficient at the n^{th}-level

$k_{i,j}$ = stiffness of equivalent spring i,j in the condensed model

$c_{i,j}$ = damping coefficient of equivalent damper i,j in the condensed model

Fig. 6.1. Analytical condensation of the MS-SDMI building

6.1.1 Validation of the mathematical model

A building like the one shown in Fig. 6.2 is condensed using Eqs. (6.1) to (6.3), and its EoMs are obtained using Lagrange's equations. The inertial coupling terms of the reduced mass matrix M_R can be incorporated into the EoMs as externally acting forces or can be neglected without concern because of their minimal magnitude when compared to that of the diagonal terms of the reduced mass matrix. A verification of the condensation technique's functionality and the correctness of the obtained EoMs is carried out by comparing the condensed SDMI system's dynamic response with that of a computer model created and analyzed with the computer program SAP2000 (CSI 2010).

The structural properties of the system used in this verification/validation are given in Table 6.1 and correspond to those of the three-story benchmark building of Ohtori et al. (2004). The computer model is analyzed under the simultaneous action of the horizontal and vertical components of the Kobe (KJMA000) earthquake, considering p-delta effects as well as large displacements; the condensed EoMs are solved with the *ode45* solver of Matlab (TheMathWorks 2009), and the results of the analyses of the two models are given in Fig. 6.3. An excellent agreement is achieved between the results given by the two methods of analysis, concluding that the condensation technique utilized works well and that the obtained mathematical equations of motion for the reduced model that will be used throughout this section are correct.

Table 6.1. Structural properties of the SDMI building used for verification purposes

Story #	*W (kips)*	*h (in.)*	*k_l (kips/in.)*	*k_s (kips/in.)*	*l_s (in.)*	*c_s (kips*sec/in.)*
1	1,055	156	744.3	90	100	10
2	1,055	156	439.0	60	100	10
3	1,142	156	318.0	30	100	10

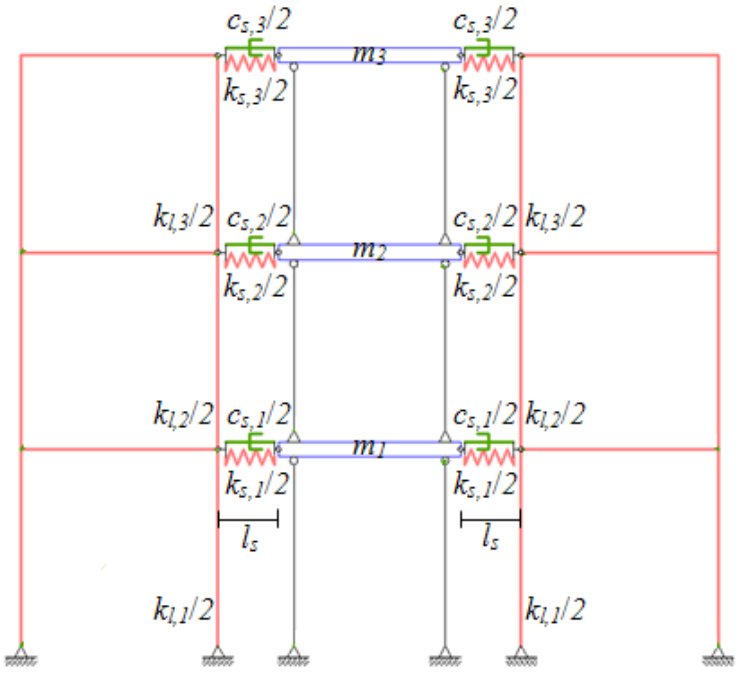

Fig. 6.2. SDMI structure used in the verification of the analytical model

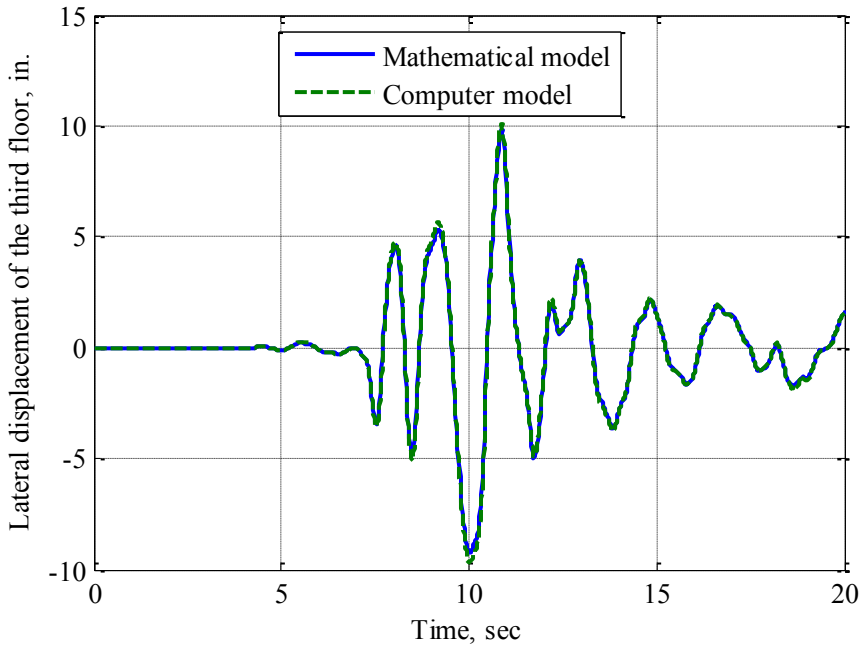

Fig. 6.3. Verification of the modeling procedures

6.2 Stability analysis of the multi-story SDMI building

Because of the looseness of the system required for proper isolation of the masses, the generalized rotations at the bases of the individual pendulums conforming an MS-SDMI building are too large to be analyzed using small-displacements assumptions. If small displacements are considered, the effects of the pendulum rods on the masses are overlooked and the simulation of the dynamic behavior is inaccurate. Furthermore, the use of linearized equations is not useful in identifying all the EPs of the system; particularly, the EPs that are critical in determining the restoration capacities of a particular SDMI system. Therefore, the analysis of the motion of the system and its stability has to consider the system's full kinematics.

6.2.1 Stability of the MS-SDMI building

The classical Lyapunov theory for the study of the stability of the zero solution of an *n-dimensional* regular nonlinear system $\dot{\boldsymbol{x}} = \boldsymbol{A}\boldsymbol{x} + \boldsymbol{h}(\boldsymbol{x})$, with $\boldsymbol{A}$ constant, requires determining the function given by (Jordan and Smith 2007)

$$V(\boldsymbol{x}) = \boldsymbol{x}^T \boldsymbol{K}\boldsymbol{x} \tag{6.4}$$

where

$$\boldsymbol{K} = \int_0^\infty e^{\boldsymbol{A}^T t} e^{\boldsymbol{A}t} dt$$

The matrix $\boldsymbol{K}$ is positive definite if the linear part of the system equation $\dot{\boldsymbol{x}} = \boldsymbol{A}\boldsymbol{x}$ is asymptotically stable. If the linearized system is asymptotically stable, Eq. (6.4) becomes a positive definite Lyapunov function. Then, as required by Lyapunov's second theorem, the time derivative of the function is determined as

$$\dot{V}(\boldsymbol{x}) = -\boldsymbol{x}^T \boldsymbol{x} + 2\boldsymbol{h}^T(\boldsymbol{x})\boldsymbol{K}\boldsymbol{x} \tag{6.5}$$

The zero solution is then asymptotically stable in the neighborhood of the origin where Eq. (6.5) is negative definite, i.e., the region where the norm of the negative term in Eq. (6.5) is larger than that of the positive term.

The use of Eq. (6.5) to estimate DoAs usually gives very conservative results (Vidyasagar 2002), and its application to the SDMI system is no exception. An important amount of research has been done in control theory to develop approximate schemes to determine DoAs more accurately (with less conservatism). Some of the techniques that have been developed use Lyapunov-type methods, trajectory-reversing, neural networks, optimization algorithms, and other numerical methods (Ferreira and Krogh 1997; Genesio et al. 1985; Noldus and Loccufier 1995; Topcu et al. 2010), which imply computational efforts.

A rather exact estimation of the DoA of the EP at the origin of the phase (hyper-) plane is of great value in the case of the SDMI system, since the establishment of a well calculated balance between system safety and isolation is determinant for a successful performance of the system, and the establishment of this balance is directly related to the determination of the limits of this EP's DoA.

In SDMI, the DoA of the EP at the origin cannot be enlarged (or shrunken) arbitrarily without affecting the behavior of the system. The size of this DoA has an inverse relation to the seismic performance of system, but, at the same time, the DoA has to be equal to or larger than a certain minimal size so that the stability of the system and the restoration of the original configuration can be guaranteed.

Assuming that the instability of the undistorted position of the system is precluded by design, the provision of a high level of isolation means the use of low-stiffness stability springs. Flexible springs are associated with small DoAs of the EP at the origin. If the size of this DoA is too small, then the chances of the system leaving this region as

it oscillates during a "random" earthquake increase, which implies the probability that the system ends at an EP different from the one at the origin after the ground stops shaking. On the other hand, if an excess of stiffness is provided in order to eliminate any concern for the system's restoration or simply because the DoA of the EP at the origin was conservatively determined, it will interfere with the level of isolation of the gravity sub-system.

The "ideal" size of the DoA around the origin is produced by the structural design that optimizes the seismic performance of the system. However, depending on the optimization criteria, variables, etc., this DoA might not fully contain the region bounded by the lateral system on the displacement/rotation axes of the phase (hyper-) plane so that there would be chances that the system oscillated outside this DoA and, as said before, ended in an EP that is not the one at the origin. Therefore, for safety reasons, even if it results in some detriment to the system's performance, the limits of the DoA should be, at least, located at the physical limits imposed by the lateral sub-system so that the restoration of the system is guaranteed.

In order to correctly verify and/or manipulate the safety level of an optimized set of geometric and structural properties, a method that allows the accurate determination of the DoA around the undistorted configuration is indispensable. Moreover, this method should be simple and accessible for design purposes. In achieving these two objectives, it is fortunate that the SDMI system is mechanical and, as was done in the case of the SS-SDMI building, it is not only possible but appropriate to use the system's energy (hyper-) surface in the analysis of the system's stability.

In the MS-SDMI case, it is more complicated to determine the semi-discrete EoMs and present Lyapunov functions and regions of (asymptotic) stability simply because the increased number of state variables makes it practically impossible for these mathematical expressions to be determined, plotted, and/or even written; however, it is possible to use energy concepts together with Lyapunov's theory to make assertions about the stability of the EPs of a particular SDMI building.

To use Lyapunov's second theorem as was done in the case of the SS-SDMI building, a strong (Lyapunov) function is a requirement. The energy function satisfies all the mathematical requirements of a strong Lyapunov function because, first, in the case of a SDMI system, it is a continuous function as well as its partial derivatives, since the function is made up by a set of linear, polynomial, sine, and cosine terms. Second, the energy function can be made zero at the origin just by subtracting the amount of potential energy that is due to the positions (heights) of the masses in the undistorted configuration, i.e., $\Sigma m_i g h_i$, which is the only contributor to the system's energy at the origin. After subtracting the energy due to the potential of the masses, if the EP at the origin is stable, then it has to constitute a (local) minimum of the energy function; therefore, the energy surface has to be greater than zero in some region surrounding the origin. Finally, the level (hyper-) surfaces of the energy function are concentric (hyper-) ellipses around the origin; therefore, the energy function constitutes a topographic system on some neighborhood of the origin.

The fortunate mechanical nature of the SDMI system allows for a shortcut in identifying its EPs in that these can be established and characterized directly from the

energy function. A further level of simplification in the study of EPs is possible because only the potential energy function is required, since the EPs in mechanical systems imply states with zero velocities, which, at their time, imply states of zero kinetic energy. The equation for the potential energy of the system is given by Eq. (6.6); having to determine only the potential energy function involves less computational efforts.

Once the potential energy (hyper-) surface corresponding to a particular MS-SDMI system has been determined, the search for EPs is reduced to a local extrema problem. The local minima of the potential energy function correspond to stable EPs and the local maxima to unstable EPs.

$$E_P = \sum_{1}^{n} m_i g h_i + \frac{1}{2}\sum_{1}^{n} \frac{k_i}{2}\left\{\begin{array}{l}\left[\sqrt{\left(x_i + l_s\right)^2 + \left(H_i - y_i\right)^2} - l_s\right]^2 + \\ \left[l_s - \sqrt{\left(l_s - x_i\right)^2 + \left(H_i - y_i\right)^2}\right]^2\end{array}\right\} \qquad (6.6)$$
$$+ \frac{1}{2}\sum_{i=1}^{n-1}\sum_{j=i+1}^{n} k_{ij}\left(x_j - x_i\right)^2$$

where

m_i = mass of the i^{th} floor

g = acceleration of gravity

h_i = height of the i^{th} story

k_i = total stiffness at the i^{th} floor

k_{ij} = stiffness of the ij coupling spring

l_s = undeformed length of the stability springs

$$x_i = \sum_1^i h_j \sin\left(\theta_j\right)$$

$$y_i = \sum_1^i h_j \cos\left(\theta_j\right)$$

$$H_i = \sum_1^i h_j$$

If, for convenience, one wishes to have Eq. (6.6) in terms of the lateral position rather than the rotations at the pendulums' bases, one can make the following substitutions into Eq. (6.6) after it has been calculated for a particular system:

$$\theta_i = \sin^{-1}\left(\frac{u_i - u_{i-1}}{h_i}\right) \tag{6.7}$$

where

u_i = lateral/horizontal position of the i^{th} floor mass

As an illustration of the use of the potential energy for the determination of an SDMI system's EPs, consider a two-story SDMI building having the properties given in Table 6.2. The geometric, weight, and lateral load sub-system properties correspond to those of the first two stories of the 3-story benchmark building of Ohtori et al. (2004),

whose plan is shown in Fig. 6.2. The stiffness assigned here to the stability springs corresponds to about 40% of what would be the AISC (AISC 2011) requirement for nodal braces.

Table 6.2. Structural properties of the example two-story SDMI building

Story #	*W (kips)*	*h (in.)*	k_l *(kips/in.)*	k_s *(kips/in.)*	l_s *(in.)*
1	1,055	156	744.3	60	20
2	1,055	156	439.0	30	20

Table 6.3. Locations and types of EPs of the example two-story SDMI system

EP #	*Lat. deflection of 1st floor (in.)*	*Lat. deflection of 2nd floor (in.)*	*Type*
1	0	0	Stable spiral
2	±3.83	∓24.73	Stable spiral
3	±33.31	∓22.49	Stable spiral
4	±19.87	∓24.71	Saddle
5	±3.83	∓21.34	Saddle
6	±20.22	∓5.04	Saddle
7	±19.87	∓21.57	Saddle

The potential energy is determined for this two-DoF system and shown in Fig. 6.7. Then, a numerical method is used to determine the local maxima and minima of the function to locate and characterize the system's EPs. The system EPs, except for those that imply vertically down positions of the individual pendulums, are given in Table 6.3, and some of them can also be identified in Fig. 6.7. As will be explained later, if a particular EP is determined to be a local minimum of the potential energy function, then it corresponds to a stable spiral; otherwise, if it is determined to be a local maximum, then it is a saddle.

6.2.2 The MS-SDMI system equilibrium points

The characteristics of the EPs in the MS-SDMI case are essentially the same as those in the SS-SDMI case. The determination of EPs implies, obtaining the autonomous state EoMs of the n^{th}-order system, equating them to zero, and solving for the combination of states that satisfy them or, in a simpler way, by the determination of the extreme values of the potential energy function of the system. In the SS-SDMI case, three different well defined stiffness scenarios (cases) were characterized. The undefined and potentially large number of DoFs in a MS-SDMI system makes it impossible to make an assessment of all the possible numbers and nature of EPs based on the stiffness of the equivalent springs. However, the same EP characterization made in the SS-SDMI case can be applied to the MS-SDMI case in terms of global or overall stiffness levels.

For a given geometry and mass distribution in a MS-SDMI building, there is a minimum (critical) level of (total) stiffness that is required to qualify the original un-

distorted position as stable. However, the provision of this minimum level of stiffness does not guarantee the restoration of the undistorted configuration after the system has been perturbed, even if the perturbation is small.

It is possible to identify and characterize a case where the stiffness level is below the mentioned critical value (case I). In this case, a saddle-type EP forms at the origin, collapse will occur at the smallest perturbation, and the system is considered as globally unstable for practical purposes. This consideration is made because, although other (stable) EPs are formed, they represent (sense-less) failure states whose study is of no relevance (the vertically-down positions of the pendulums). The critical level of stiffness for the MS-SDMI case is equivalent in meaning to the level of stiffness given by Eq. (5.6) in the SS-SDMI case. Here, however, it is not possible to obtain a mathematical expression that defines a unique set of spring stiffness that makes the system "just" or neutrally stable because the number of spring stiffnesses combinations that would have this effect is infinite. The general appearance of the potential energy function in the vicinity of the origin of a two-story SDMI building that falls in this case is given in Fig. 6.5. A two-story building is chosen so that the concepts being introduced can be graphically illustrated, since it would be impossible to show a potential energy hyper-surface of a SDMI building having three or more stories.

Although it is not possible to determine a unique set of spring stiffnesses that corresponds to the critical case, it is possible to know how close or far a particular set of spring stiffnesses is from the critical case. This can be done by performing an eigenvalue analysis of matrix $\hat{\boldsymbol{K}}$, whose components are given by Eqs. (6.8) and (6.9), and Fig. 6.4.

The smallest eigenvalue of $\hat{\boldsymbol{K}}$ [Eq. (6.10)] corresponds to the factor of safety (FS) against buckling of the SDMI system. Note that the matrix $\hat{\boldsymbol{K}}$ is a specialization of the system's stiffness matrix of the system where the generalized DoFs are the rotations at the base of each pendulum rather than the lateral displacements of the masses, and Eqs. (6.8) and (6.9) are essentially the transpose of each other.

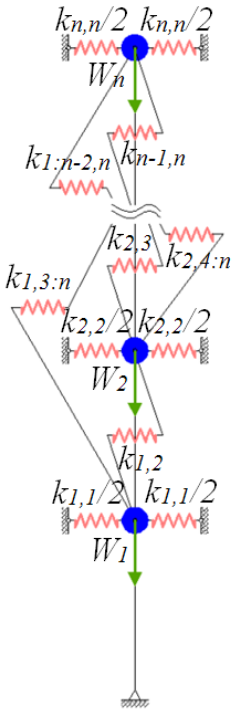

W_i = weight of the ith floor

$k_{i,j}$ = stiffness of equivalent spring i,j in the condensed model

Fig. 6.4. MS-SDMI buckling model

$$\hat{K}_{ij} = \frac{h_j \left(\sum_{k=i}^{n} k_k + \sum_{k=1}^{j-1} \sum_{l=i}^{n} k_{kl} \right)}{\sum_{k=i}^{n} W_k} \text{ (on or below the diagonal)} \tag{6.8}$$

$$\hat{K}_{ij} = \frac{h_j \left(\sum_{k=j}^{n} k_k + \sum_{k=1}^{i-1} \sum_{l=j}^{n} k_{kl} \right)}{\sum_{k=i}^{n} W_k} \text{ (on or above the diagonal)} \tag{6.9}$$

$$FS = \lambda_{\min}(\hat{\boldsymbol{K}}) \tag{6.10}$$

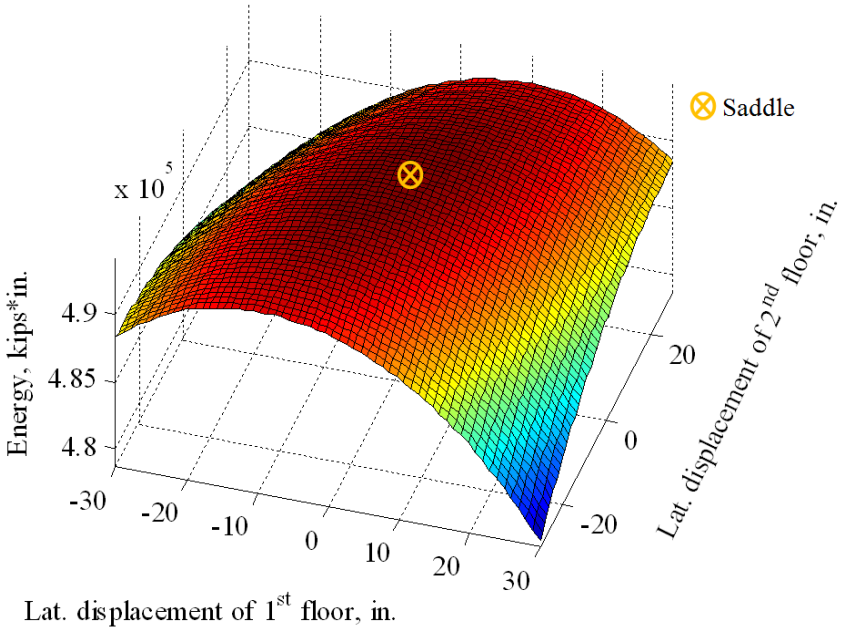

Fig. 6.5. Potential energy surface of an unstable two-story SDMI system (case I)

Another stiffness level case (case II) (Fig. 6.6) occurs if $\lambda_{\min}(\hat{\boldsymbol{K}})$ is greater than one, and the general stiffness level is relatively high. In this case, the EP at the origin is stable and the only one in practical terms, since all other EPs correspond to configurations that include vertically up and down positions of the individual pendulums. The DoA of the EP at the origin encompasses all of the system's states except for those corresponding to the saddles associated to the vertically down positions of the pendulums. As a consequence, the EP at the origin is considered as globally stable.

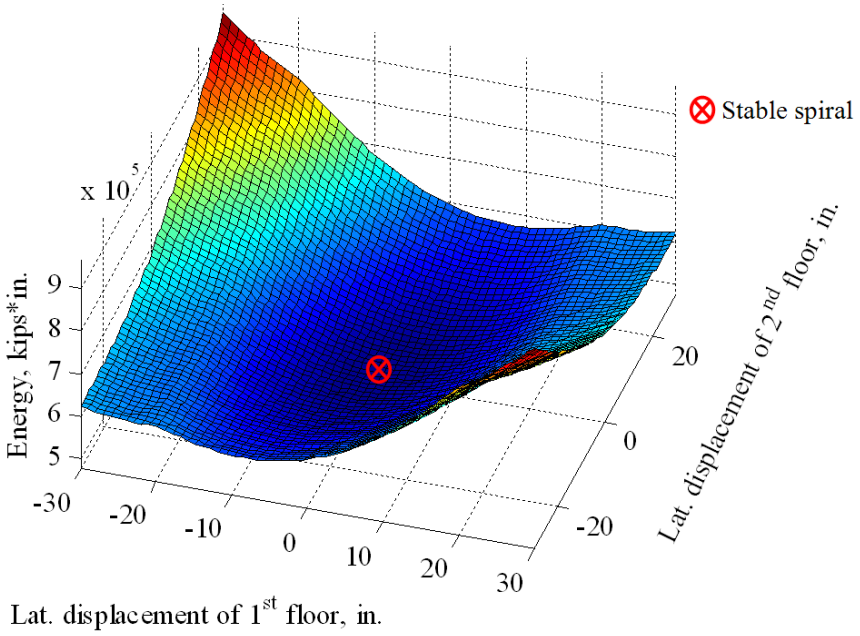

Fig. 6.6. Potential energy surface of a stable two-story SDMI system (case II)

A third and last case (case III) (Fig. 6.7) occurs when $\lambda_{\min}(\hat{\boldsymbol{K}})$ is greater than one, but the general level of stiffness is not high enough to make the EP at the origin globally stable. In this case, both stable and unstable EPs are formed around the origin. The system is considered stable in the sense that it will oscillate around stable EPs and eventually end up at one of them once the ground excitation stops. The generation and location of unstable EPs, which take the form of saddles in the SDMI case, is directly related to the snap-through behavior of the system that occurs close to the location of the lateral sub-system.

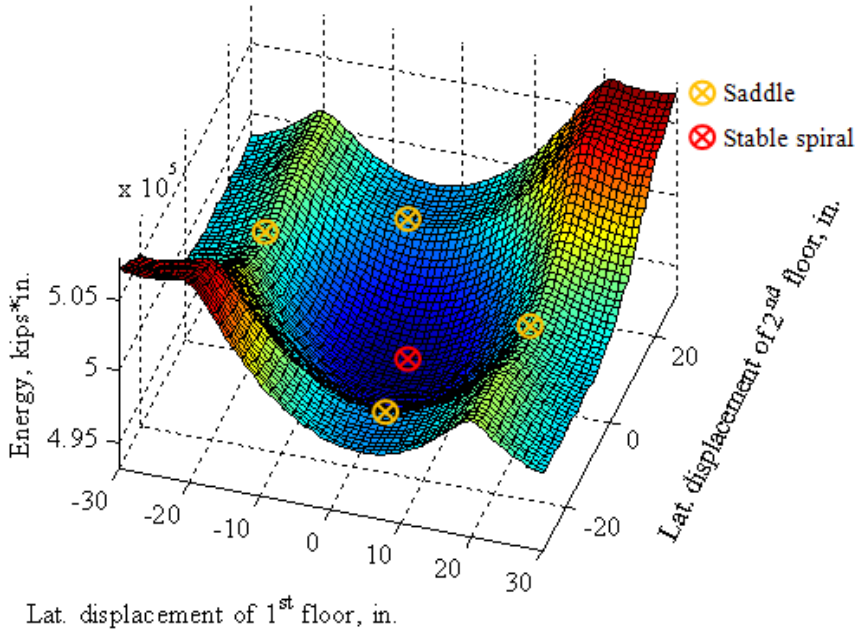

Fig. 6.7. Potential energy surface of a stable two-story SDMI system (case III)

The conceptualization of the nature of the system's EPs follows from the SS-SDMI case. Because damping is present in all structures, energy that is input into them will eventually dissipate. If the dissipated energy is not restored, the total energy has to reach a local minimum as time tends to infinity. If viscous damping is considered, then energy will continuously dissipate, except when all generalized velocities in the system are simultaneously zero. All the system velocities being zero simultaneously implies one of two possibilities: 1) the system is either at an EP or, 2) because the unstable EPs can only be of saddle-type, if the system is not at an EP, then it must be inside a DoA, which, in turn, means that the system has to eventually approach the EP corresponding to that DoA. Therefore, the time-derivative of the energy function has to be negative in the regions included by the DoAs, except at the associated EPs (Fig. 6.8). This dynamic behavior is associated with asymptotic stability and EPs in the form of stable spirals.

The system's unstable EPs always correspond to saddles. Saddles are not associated with regions of instability, which occur around unstable centers, spirals, and nodes. However, these saddles serve to establish the space and energy limits of the DoAs of the stable spirals of the system.

Cases II and III possess stable EPs (stable spirals) that have their own DoAs; of particular interest is the dimension of the DoA around the origin in case III, since it directly relates to the safety a particular system. In case II, where the general level of stiffness is relatively high and there is only a single globally stable EP, asymptotic stability implies that the restoration of the undistorted position of the system is always guaranteed.

In the intermediate general stiffness level case (case III), however, although the EP at the origin is asymptotically stable, the restoration of the undistorted configuration is not certain. If enough energy is input into the system, it could leave the DoA of the EP at the origin and, eventually, finish at a different attractive EP. In practice, this could be represented as the gravity sub-system either being left in an "anti-natural" rest position or bearing against the lateral sub-system after the ground motion has ceased.

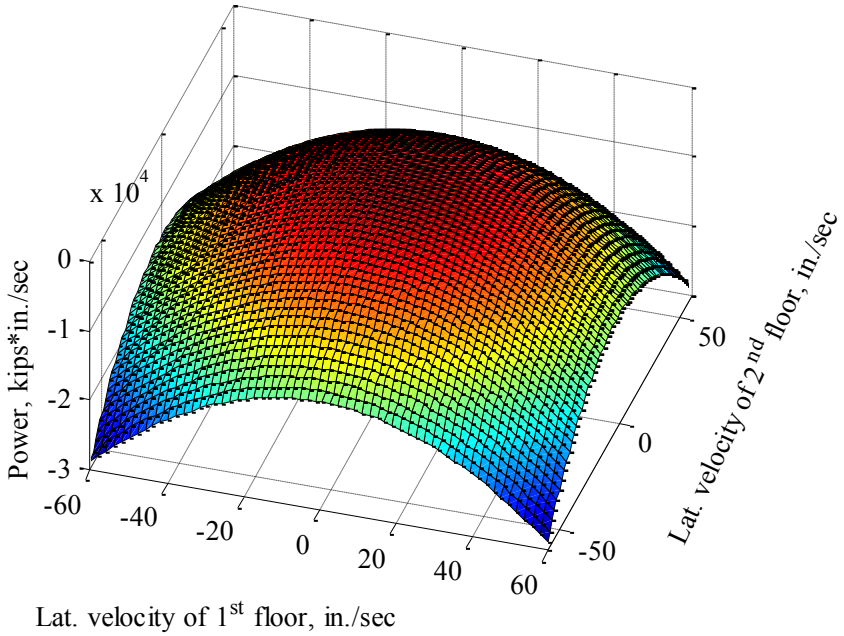

Fig. 6.8. Energy change time-rate of a two-story SDMI system at $\theta_1 = \theta_2 = 0$

6.3 Design of the multi-story stability dependent mass isolated building

An optimal design for a MS-SDMI building achieves two goals: it minimizes the seismic structural response and guarantees the restoration of the original configuration of the system after the ground motion is over. The restoration of the original configuration is associated with the (asymptotic) stability of the EP at the origin. With regard to the design for stability of the undistorted configuration of an SDMI system, given the increased number of variables in MS-SDMI systems, it is not possible to determine a single set of minimum stiffness values for the springs that make the undistorted position of the system "just stable". However, it is possible to know how close or far, above or below, a particular set of spring stiffnesses is from a critical case. This is sufficient, since, in the general MS-SDMI case, the optimal springs design is not the one that makes the vertical position of the building "just stable" for two reasons: 1) First, there is a higher requirement on stiffness, i.e., the spring stiffnesses have to not only provide stability but guarantee the restoration of the system after its excitation finishes, and 2) Although in optimized SDMI designs the stiffness level is close to the critical case, the set of spring stiffnesses that yields the minimum structural response is, in general, not a critical one. The latter results from particular ground-structure interactions that develop depending on the characteristics of the occurring ground motion.

To determine the closeness that the undistorted position of an SDMI structure is from stability/instability, an eigenvalue analysis of the matrix $\hat{\boldsymbol{K}}$ given by Eqs. (6.8), (6.9) and Fig. 6.4 has to be performed. The first criterion to consider or reject a set of structural properties for a (final) design should be Eq. (6.10). In design, a particular min-

imum value for the factor of safety against buckling could be required. If a particular set of structural properties complies with the minimum specified factor of safety against buckling, then that set could be used in the next design filter.

To avoid pounding, a number of time-history analyses need to be performed as per code requirements (ASCE 2003; ASCE 2007; ASCE 2010) to determine a displacements envelope. With the envelope at hand and, probably, a factor of safety, the safe location against pounding of the gravity sub-system can be determined. The existing offset of the lateral sub-system with respect to the gravity one makes it possible for the masses to oscillate within the gap separating them. Therefore, from the system restoration point of view, it is essential to design the system so that the DoA of the EP at the origin encompasses the whole region that is physically bounded by the lateral sub-system. In this way, the system will never abandon this DoA.

Because of the increased number of DoFs in the case of MS-SDMI buildings, it is not feasible to establish closed-form equations to determine spring stiffness levels that set the limits of the DoA of the EP at the origin at those of the lateral sub-system. However, the concepts behind the design of the SS-SDMI building can be used to investigate the adequacy of a set of structural properties to provide sufficient restoring forces inside the region in which they are required.

Different numbers of EPs can be produced by a determinate SDMI system depending on its structural properties. As with the SS-SDMI building, the way of guaranteeing the restoration of a SDMI system is by not letting the system abandon the DoA of the EP at the origin.

If the undistorted position is stable, then the EP at the origin must constitute a local minimum. If the stiffness level falls in case III, described before, there will be saddles limiting the DoAs of all the stable spirals that are generated in the system (assuming that in the process of determination of the spring stiffnesses, case I is precluded by default). Making sure that all the saddles produced by the set of geometric and structural properties of the system are at or outside the limits set by the lateral sub-system means that the DoA of the EP at the origin is equal to or larger than the region bounded by the lateral sub-system, and the possibility of the system reaching or passing any saddle as well as its incursion into other EPs' DoAs as it oscillates is precluded.

If the system does not leave the DoA of the EP at the origin, it will inevitably converge to the undistorted configuration once the energy input by any earthquake has dissipated through damping, as per Lyapunov's theorem. Also, in saying that making sure that the saddles are exactly at the location of the lateral sub-system will guarantee the restoration of the undistorted position, it is assumed that the lateral sub-system is placed farther from the largest expected displacement and/or that the lateral sub-system is stiff enough to preclude significant incursions of the system outside the region bounded by the non-deflected location of the lateral sub-system in any case of pounding, i.e., incursions outside the DoA of the EP at the origin.

The increased number of variables implied in a particular MS-SDMI building makes it impractical to define the limits of the DoA of the EP at the origin using mathematical expressions, as was done in the SS-SDMI case. However, it can be determined whether the undistorted configuration of a particular SDMI system will be restored after

the action of an earthquake. In mechanical systems, the EPs occur at locations where, simultaneously, the kinetic energy is zero, and the potential energy is at a local maximum or minimum. Because the kinetic energy at these locations is zero, it is only necessary to determine the potential energy function of the particular SDMI system and find its local extrema to locate the EPs of the system. The system's potential energy function was given in Eqs. (6.6) and (6.7).

From the point of view of the response, the main response parameter that should be subject to minimization is the lateral acceleration of the floor slabs. The minimization of the lateral accelerations of the floor slabs helps to keep the lateral sub-system elastic by reducing the lateral forces and lowers the possibility of damages, incidents, and accidents associated to floor accelerations. There is no need to minimize displacements anywhere as long as they do not exceed the elastic limits of the springs, and the lateral subsystem is placed farther than the largest expected slab displacements. Naturally, the displacements within the gravity sub-system should not be so large that they signify non-structural damage.

The restoration of the system constitutes a constraint in the process of system properties optimization because there could be a set of properties that yielded the lowest (acceleration-) response; however, these properties might not necessarily guarantee that the system ended in the upright position after the action of all potential earthquakes.

Once an optimized condensed set of structural properties is at hand, it is necessary to translate the reduced design into a full design. At this point, the assignment is that the full SDMI building corresponds to a (reduced) design model and guarantees the

continuous elasticity of the structure. This is achieved by the appropriate distribution of the equivalent stiffnesses among the lateral sub-system's and stability springs.

For the purposes of stiffness proportioning, it is convenient and sufficient to idealize the SDMI system as the shown in Fig. 6.9 specialized to a three-story SDMI building. The lateral stiffness matrix of such a system can be written as

$$\boldsymbol{K} = \begin{bmatrix} k_{s,1} & 0 & 0 & -k_{s,1} & 0 & 0 \\ 0 & k_{s,2} & 0 & 0 & -k_{s,2} & 0 \\ 0 & 0 & k_{s,3} & 0 & 0 & -k_{s,3} \\ -k_{s,1} & 0 & 0 & k_{s,1}+k_{l,1}+k_{l,2} & -k_{l,2} & 0 \\ 0 & -k_{s,2} & 0 & -k_{l,2} & k_{s,2}+k_{l,2}+k_{l,3} & -k_{l,3} \\ 0 & 0 & -k_{s,3} & 0 & -k_{l,3} & k_{s,3}+k_{l,3} \end{bmatrix} \tag{6.11}$$

where

$k_{s,i}$ = total stability springs stiffness at the i^{th} level

$k_{l,i}$ = total lateral sub-system stiffness at the i^{th} story

If the system is discretized in this way and its nodes are numbered as in Fig. 6.9, the system's stiffness matrix may be abbreviated as

$$\boldsymbol{K} = \begin{bmatrix} \boldsymbol{K}_{mm} & \boldsymbol{K}_{ms} \\ \boldsymbol{K}_{sm} & \boldsymbol{K}_{ss} \end{bmatrix} \tag{6.12}$$

where the subscript *m* denotes master nodes/DoFs and *s* stands for slave nodes/DoFs.

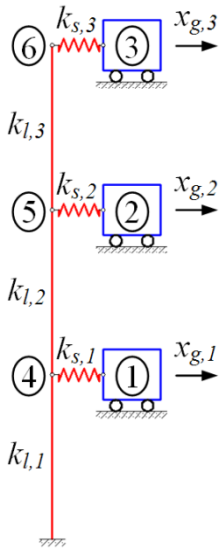

Fig. 6.9. Stiffness proportioning model

The sub-matrix $\boldsymbol{K}_{mm}$ in Eq. (6.12) corresponds to a diagonal matrix having in its diagonal the total stability spring stiffness at each floor level. This sub-matrix will, from now on, be referred to as $\boldsymbol{K}_G$.

$$\boldsymbol{K}_G = \boldsymbol{K}_{mm} = \begin{bmatrix} k_{s,1} & 0 & 0 \\ 0 & k_{s,2} & 0 \\ 0 & 0 & k_{s,3} \end{bmatrix} \tag{6.13}$$

The stiffness matrix of the lateral sub-system alone $\boldsymbol{K}_L$ is given by

$$\boldsymbol{K}_L = \begin{bmatrix} k_{l,1} + k_{l,2} & -k_{l,2} & 0 \\ -k_{l,2} & k_{l,2} + k_{l,3} & -k_{l,3} \\ 0 & -k_{l,3} & k_{l,3} \end{bmatrix} \tag{6.14}$$

so that $\boldsymbol{K}_{ss}$ can be written as

$$\boldsymbol{K}_{ss} = \boldsymbol{K}_G + \boldsymbol{K}_L \tag{6.15}$$

Similarly, the sub-matrices $\boldsymbol{K}_{ms}$ and $\boldsymbol{K}_{sm}$ are given by

$$\boldsymbol{K}_{ms} = \boldsymbol{K}_{sm} = -\boldsymbol{K}_G \tag{6.16}$$

Recall from the dynamic condensation method introduced in sub-section 6.1 that the reduced stiffness matrix of the whole system is given by

$$\boldsymbol{K}_R = \boldsymbol{K}_{mm} - \boldsymbol{K}_{ms}\boldsymbol{K}_{ss}^{-1}\boldsymbol{K}_{sm} \tag{6.17}$$

Substituting Eqs. (6.13), (6.15), and (6.16) into (6.17) gives

$$\boldsymbol{K}_{des} = \boldsymbol{K}_G - \boldsymbol{K}_G \left(\boldsymbol{K}_L + \boldsymbol{K}_G \right)^{-1} \boldsymbol{K}_G \tag{6.18}$$

where the subscript *R* has been changed to *'des'* to denote a reduced design stiffness matrix. The design stiffness matrix should be obtained through an optimization process of the system's properties that minimizes the (acceleration-) response of the system and guarantees the restoration of the undistorted configuration of the system.

Rearranging and multiplying both sides of Eq. twice by $\boldsymbol{K}_G^{-1}$ yields

$$\boldsymbol{K}_G^{-1}(\boldsymbol{K}_L + \boldsymbol{K}_G)\boldsymbol{K}_G^{-1} = (\boldsymbol{K}_G - \boldsymbol{K}_{des})^{-1} \tag{6.19}$$

Expanding the left side of Eq. (6.19) and multiplying both sides by $(\boldsymbol{K}_G - \boldsymbol{K}_{des})$ gives

$$(\boldsymbol{K}_G - \boldsymbol{K}_{des})(\boldsymbol{K}_G^{-1}\boldsymbol{K}_L\boldsymbol{K}_G^{-1} + \boldsymbol{K}_G^{-1}) = \boldsymbol{I} \tag{6.20}$$

Now, expanding and factoring Eq. (6.20) yields

$$(\boldsymbol{K}_L - \boldsymbol{K}_{des}\boldsymbol{K}_G^{-1}\boldsymbol{K}_L - \boldsymbol{K}_{des})\boldsymbol{K}_G^{-1} = \boldsymbol{0} \tag{6.21}$$

which implies that

$$(\boldsymbol{I} - \boldsymbol{K}_{des}\boldsymbol{K}_G^{-1})\boldsymbol{K}_L = \boldsymbol{K}_{des} \tag{6.22}$$

Rearranging and multiplying both sides of Eq. (6.22) results in

$$\boldsymbol{K}_{des}^{-1}(\boldsymbol{K}_L - \boldsymbol{K}_{des})\boldsymbol{K}_L^{-1} = \boldsymbol{K}_G^{-1} \tag{6.23}$$

The expansion and inversion of both sides of Eq. (6.23) gives the design equation for the total stability springs stiffness as

$$\boldsymbol{K}_G = (\boldsymbol{K}_{des}^{-1} - \boldsymbol{K}_L^{-1})^{-1} \tag{6.24}$$

Eq. (6.24) is the design equation for the stability spring stiffnesses. The lateral springs stiffness values contained in $\boldsymbol{K}_L$ can be obtained as

$$k_{l,i} = \frac{\left|F_{s,i}(t)\right|_{\max}}{F_{\delta,i}h_i(DR)_{y,i}} \tag{6.25}$$

where

$F_{s,i}(t) = \sum_{i}^{n} f_{s,k}(t)$ (total force induced by the earthquake on the i^{th}-story)

$\boldsymbol{f}_s(t) = \boldsymbol{K}_{des}\boldsymbol{x}_G(t)$

$\boldsymbol{x}_G(t)$ = displacement-response time-histories to a particular ground motion

$F_{\delta,i}$ = allowable interstory drift ratio reduction factor for the i^{th} story ($F_{\delta,i} \leq 1.0$)

h_i = height of the i^{th} story

$(DR)_{y,i}$ = interstory drift ratio at the onset of yield for the lateral structural system used at the i^{th} story

Eq. (6.25) considers the peak (absolute) value of the force time-histories generated in each of the lateral springs and divides it by the allowable interstory drift ratio to find the value of the required spring stiffness. The number of time-history analyses required to obtain the final design stiffness would be dictated by building codes. Once the lateral sub-system springs' stiffnesses are at hand, the total stiffness of the stability springs at each floor level is obtained as

$$k_{s,i} = K_{G,ii} \tag{6.26}$$

The development of expressions that translate optimized equivalent damping coefficients into the actual full model's coefficients cannot be achieved in the way that was done for the spring stiffnesses. Although general structures for the damping matrices in the full model can be identified as in the case of the stiffness matrices, there are no general design constraints that permit solving for all the variables in the corresponding matrix expression [Eq. (6.2)]. However, the problem can be solved with relative ease by using the mentioned identifiable matrix structures and a priori arbitrarily assigning damping coefficients to all of them except for one. Then, with the use of Eq. (6.2) and

the optimized reduced damping matrix it would be possible to solve for the remaining damping sub-matrix.

A simpler solution to determine the damping coefficients would be to decide in advance the locations where the damping devices will be placed in the building and assign them with optimized damping coefficients directly in the optimization process, avoiding the need for "translation" equations. It will be shown later that there are locations for the placement of the dampers that are advantageous from the architectural and technical points of view.

6.4 Design example

A three-story, four-bay SDMI building frame is designed having the geometric and mass properties given in Table 6.4. The building must be able to resist the vertical and horizontal components of the Kobe earthquake (KJMA000). To reduce the interstory drifts in the gravity sub-system, fluid viscous damping devices are installed at all floor levels joining the lateral and gravity sub-systems as shown schematically in Fig. 6.10. Inherent damping of 2% of the critical is considered.

Assume that the design equivalent spring stiffnesses of the reduced model, as well as the damping coefficients of the energy dissipaters given below, have been determined through a structural optimization process that verifies that, in the designs, the limits of the DoA of the EP at the origin are at or outside the lateral sub-system. Also, the lateral sub-system must consist of MRFs whose yield interstory drift ratios are assumed

to be the ones given below and for which different interstory-drift reduction factors are specified.

$k_{1,1}$ = 73.84 kips/in.	$c_{s,1}$ = 16 kips*sec/in.	$(DR)_{y,1}$ = 0.8 %
$k_{2,2}$ = 41.05 kips/in.	$c_{s,2}$ = 14 kips*sec/in.	$(DR)_{y,2}$ = 1.1 %
$k_{3,3}$ = 18.76 kips/in.	$c_{s,3}$ = 10 kips*sec/in.	$(DR)_{y,3}$ = 1.6 %
$k_{1,2}$ = 4.964 kips/in.		$F_{\delta,1}$ = 1.00
$k_{1,3}$ = 2.268 kips/in.	l_s = 12 in.	$F_{\delta,2}$ = 0.70
$k_{2,3}$ = 4.385 kips/in.		$F_{\delta,3}$ = 0.25

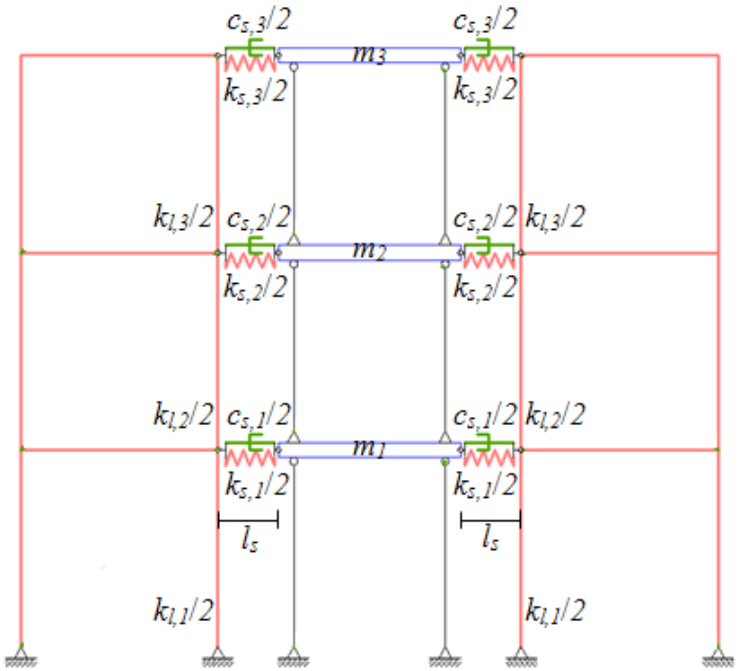

Fig. 6.10. Sketch of SDMI implementation into the design example building

Table 6.4. Geometric and weight properties of the design example structure

Dimensions	
Floor-to-floor heights	156 in.
Bay widths	360 in.
Weight	
1st level	1,055 kips
2nd level	1,055 kips
3rd level	1,142 kips

Solution:

The design stiffness matrix of the reduced model is

$$\boldsymbol{K}_{des} = \begin{bmatrix} 81.07 & -4.964 & -2.268 \\ -4.964 & 50.40 & -4.385 \\ -2.268 & -4.385 & 25.41 \end{bmatrix} \text{ kips/in.}$$

Because the stiffnesses of the lateral sub-system and the stability springs are initially unknown, the reduced damping matrix of the system cannot be established immediately. For its determination, the stiffnesses of the lateral sub-system and the stability springs need to be assumed in an initial iteration. To come up with a first assumption, a time-history analysis of the system is performed without considering the inclusion of the

damping devices. The resulting displacement-response time-histories are used in Eq. (6.25) as the start of the iterative design process that comprises the following steps:

1. Use Eq. (6.25) to determine the stiffness of the lateral sub-system's springs,
2. Determine $\boldsymbol{K}_L$,
3. Use Eq. (6.24) and (6.26) to determine the stability springs stiffnesses,
4. Use the stiffness values obtained in 1. and 3. to determine the reduced damping matrix,
5. Perform a time-history analysis of the model resulting from the structural properties obtained in 1. to 4., and use the displacement-response time-histories in Eq. (6.25) to obtain new lateral spring stiffness values, and
6. Repeat steps 1. to 5. until the results converge to the final structural design values.

For illustration purposes, the results of the last iteration are provided. The displacement-response time-histories of the penultimate iteration are used to calculate the force time-histories $F_{s,i}(t)$ acting on the lateral springs (Fig. 6.11). The peak absolute values of these forces are:

$$\left|F_{s,1}(t)\right|_{\max} = 940.2 \text{ kips}$$

$$\left|F_{s,2}(t)\right|_{\max} = 548.7 \text{ kips}$$

$$\left|F_{s,3}(t)\right|_{\max} = 202.7 \text{ kips}$$

which, upon substitution in Eq. (6.25), become

$$k_{l,1} = \frac{\left|F_{s,1}(t)\right|_{\max}}{F_{\delta,1} h_1 (DR)_y} = \frac{940.2}{1.0(156)0.008} = 753.3 \text{ kips/in.}$$

$$k_{l,2} = \frac{\left|F_{s,2}(t)\right|_{\max}}{F_{\delta,2} h_2 (DR)_y} = \frac{548.7}{0.7(156)0.011} = 456.8 \text{ kips/in.}$$

$$k_{l,3} = \frac{\left|F_{s,3}(t)\right|_{\max}}{F_{\delta,3} h_3 (DR)_y} = \frac{202.7}{0.25(156)0.016} = 324.8 \text{ kips/in.}$$

With these lateral stiffness values at hand, the lateral sub-system's stiffness matrix is computed as:

$$\boldsymbol{K}_L = \begin{bmatrix} k_{l,1}+k_{l,2} & -k_{l,2} & 0 \\ -k_{l,2} & k_{l,2}+k_{l,3} & -k_{l,3} \\ 0 & -k_{l,3} & k_{l,3} \end{bmatrix} = \begin{bmatrix} 1210 & -456.8 & 0 \\ -456.8 & 781.6 & -324.8 \\ 0 & -324.8 & 324.8 \end{bmatrix} \text{ kips/in.}$$

The stiffnesses of the stability springs are calculated using first Eq. (6.24) as:

$$\boldsymbol{K}_G = (\boldsymbol{K}_{des}^{-1} - \boldsymbol{K}_L^{-1})^{-1} = \left(\begin{bmatrix} 81.07 & -4.964 & -2.268 \\ -4.964 & 50.40 & -4.385 \\ -2.268 & -4.385 & 25.41 \end{bmatrix}^{-1} - \begin{bmatrix} 1210 & -456.8 & 0 \\ -456.8 & 781.6 & -324.8 \\ 0 & -324.8 & 324.8 \end{bmatrix}^{-1} \right)^{-1}$$

$$= \begin{bmatrix} 89.87 & -0.09 & -0.04 \\ -0.09 & 59.63 & -0.19 \\ -0.04 & -0.19 & 29.85 \end{bmatrix} \text{ kips/in.}$$

and then Eq. (6.26) to obtain:

$k_{s,1} = K_{G,11} = 89.87$ kips/in.

$k_{s,2} = K_{G,22} = 59.63$ kips/in.

$k_{s,3} = K_{G,33} = 29.85$ kips/in.

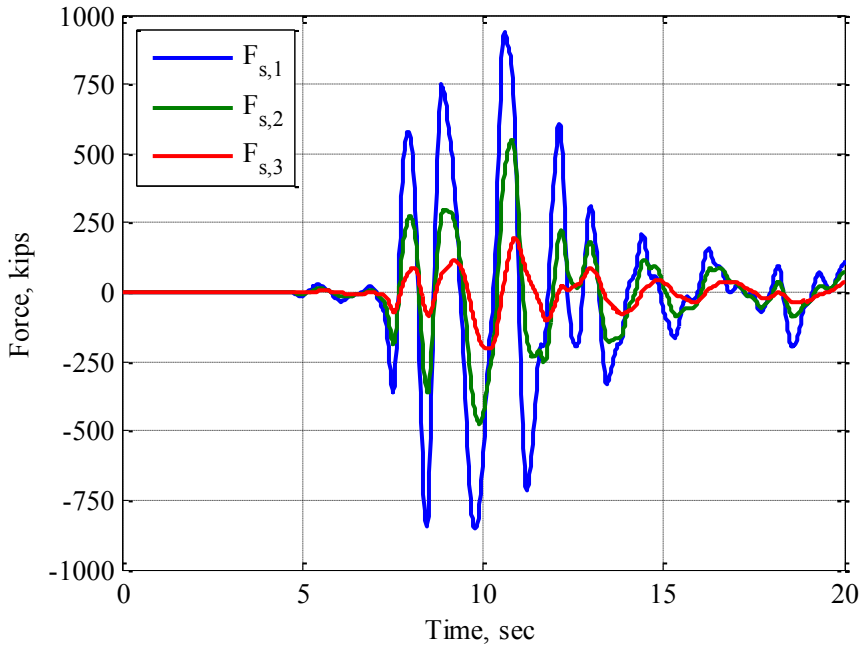

Fig. 6.11. Total lateral forces induced by the ground motion on the lateral sub-system

A proposed MRF design that corresponds very closely to the lateral springs stiffness values is given in Fig. 6.12, which corresponds to $k_{l,i}$ values of:

$k_{l,1}$ = 744.3 kips/in.

$k_{l,2}$ = 439.0 kips/in.

$k_{l,3}$ = 318.0 kips/in.

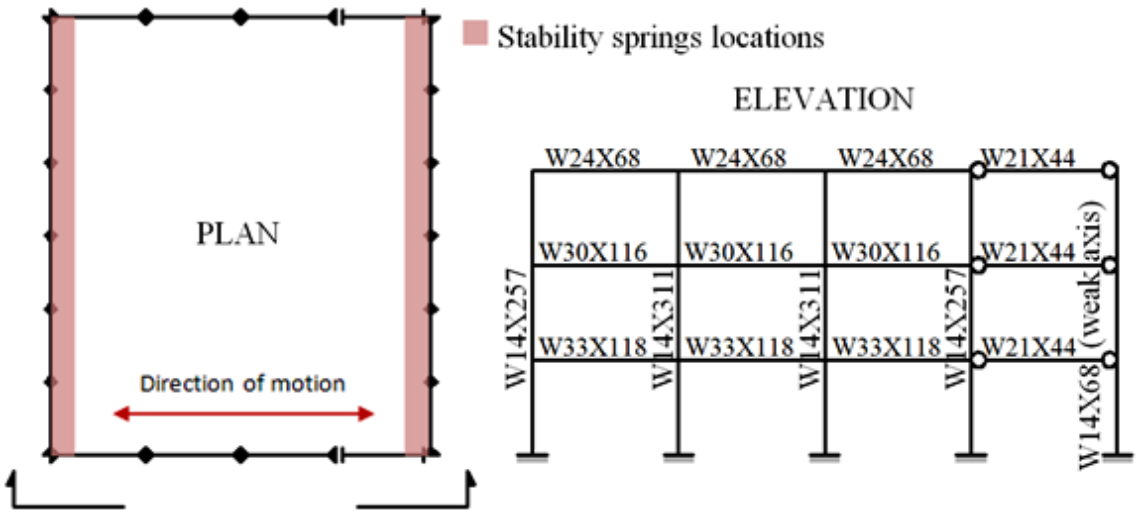

Fig. 6.12. Proposed lateral sub-system design (Ohtori et al. 2004)

These new stiffness values correspond to the following updated lateral sub-system's stiffness matrix:

$$\boldsymbol{K}_L = \begin{bmatrix} k_{l,1}+k_{l,2} & -k_{l,2} & 0 \\ -k_{l,2} & k_{l,2}+k_{l,3} & -k_{l,3} \\ 0 & -k_{l,3} & k_{l,3} \end{bmatrix} = \begin{bmatrix} 1183 & -439.0 & 0 \\ -439.0 & 757.0 & -318.0 \\ 0 & -318.0 & 318.0 \end{bmatrix} \text{ kips/in.}$$

Adjusted values for the stability springs are obtained using Eqs. (6.24) and (6.26) as:

$$\boldsymbol{K}_G = (\boldsymbol{K}_{des}^{-1} - \boldsymbol{K}_L^{-1})^{-1} = \left(\begin{bmatrix} 81.07 & -4.964 & -2.268 \\ -4.964 & 50.40 & -4.385 \\ -2.268 & -4.385 & 25.41 \end{bmatrix}^{-1} - \begin{bmatrix} 1183 & -439.0 & 0 \\ -439.0 & 757.0 & -318.0 \\ 0 & -318.0 & 318.0 \end{bmatrix}^{-1} \right)^{-1}$$

$$= \begin{bmatrix} 90 & 0 & 0 \\ 0 & 60 & 0 \\ 0 & 0 & 30 \end{bmatrix} \text{ kips/in.}$$

and

$$k_{s,1} = K_{G,11} = 90 \text{ kips}$$

$$k_{s,2} = K_{G,22} = 60 \text{ kips}$$

$$k_{s,3} = K_{G,33} = 30 \text{ kips}$$

which show practically no changes with respect to stiffness values obtained previously. This concludes the design of the SDMI structure. Notice that the design values of the damping coefficients of the fluid viscous dampers were determined directly as part of the optimization process.

6.4.1 Verification of the design

A series of checks are performed to make sure that the obtained design complies with the requirements of the problem statement, pounding avoidance, stability, restoration, and elasticity. First, it is necessary to corroborate that the structural design corresponds to the design reduced stiffness matrix. For this, Eq. (6.1) is used in conjunction with $\boldsymbol{K}_L$ and $\boldsymbol{K}_G$ obtained above:

$$\boldsymbol{R}_G = -\boldsymbol{K}_{ss}^{-1}\boldsymbol{K}_{sm} = (\boldsymbol{K}_L + \boldsymbol{K}_G)^{-1}\boldsymbol{K}_G$$

$$= \left(\begin{bmatrix} 1183 & -439.0 & 0 \\ -439.0 & 757.0 & -318.0 \\ 0 & -318.0 & 318.0 \end{bmatrix} + \begin{bmatrix} 90 & 0 & 0 \\ 0 & 60 & 0 \\ 0 & 0 & 30 \end{bmatrix} \right)^{-1} \begin{bmatrix} 90 & 0 & 0 \\ 0 & 60 & 0 \\ 0 & 0 & 30 \end{bmatrix}$$

$$= \begin{bmatrix} 0.0992 & 0.0552 & 0.0252 \\ 0.0827 & 0.1600 & 0.0731 \\ 0.0756 & 0.1462 & 0.1530 \end{bmatrix}$$

$$\boldsymbol{K}_R = \boldsymbol{K}_{mm} + \boldsymbol{K}_{ms}\boldsymbol{R}_G = \boldsymbol{K}_G - \boldsymbol{K}_G\boldsymbol{R}_G$$

$$= \begin{bmatrix} 90 & 0 & 0 \\ 0 & 60 & 0 \\ 0 & 0 & 30 \end{bmatrix} - \begin{bmatrix} 90 & 0 & 0 \\ 0 & 60 & 0 \\ 0 & 0 & 30 \end{bmatrix} \begin{bmatrix} 0.0992 & 0.0552 & 0.0252 \\ 0.0827 & 0.1600 & 0.0731 \\ 0.0756 & 0.1462 & 0.1530 \end{bmatrix}$$

$$= \begin{bmatrix} 81.07 & -4.964 & -2.268 \\ -4.964 & 50.40 & -4.385 \\ -2.268 & -4.385 & 25.41 \end{bmatrix} \text{ kips/in.}$$

The factor of safety against buckling is computed using Eqs. (6.8) to (6.10) as:

$$\hat{\boldsymbol{K}} = \begin{bmatrix} 6.411 & 2.869 & 0.900 \\ 4.247 & 4.760 & 1.493 \\ 2.562 & 2.872 & 3.471 \end{bmatrix}$$

$$FS = \lambda_{\min}(\hat{\boldsymbol{K}}) = 1.573$$

Since the factor of safety is greater than one, the EP at the origin is asymptotically stable, and one can proceed with the determination of the limits of its associated DoA. For this, the potential energy function of the system is obtained using Eq. (6.6), and its local extrema are found and given in Table 6.5. As can be seen, all saddle-type EPs are at or outside the physical limits set by the lateral sub-system (there is at least one component in each EP that is larger than l_s = 12 in.). The x_1-component of EP # 7 is considered to be at the limit since $|x_1|$ = 11.92 in. ≈ 12 in., thus, the design may be considered satisfactory from the system restoration point of view.

The elasticity of the structure is considered to be maintained if the interstory drift ratios do not exceed the $(DR)_y$ values of the lateral sub-system's springs multiplied by their assigned reduction factors. To check on the fulfillment of the continuous elasticity requirement, the interstory-drift-ratio-response time-histories of the lateral sub-system are obtained and given in Fig. 6.13. The figure displays peak values that are equal or less than the allowable interstory drift-ratios given in the problem statement for each story.

Pushover analyses of the lateral sub-system's springs are then carried out to verify that the $(DR)_y$ assumptions are safe and their results are given in Fig. 6.14. The $(DR)_y$ assumptions are validated. Fig. 6.15 shows that pounding is avoided.

Table 6.5. Equilibrium points of the design example SDMI system

EP #	x_1 *(in.)*	x_2 *(in.)*	x_3 *(in.)*	*Type*
1	0	0	0	Stable spiral
2	±22.81	∓21.95	±11.12	Stable spiral
3	±3.98	∓18.61	±3.99	Stable spiral
4	±11.85	∓21.03	±7.61	Saddle
5	±3.10	∓12.15	±2.43	Saddle
6	±12.04	∓4.17	±2.22	Saddle
7	±11.92	∓11.40	±3.63	Saddle

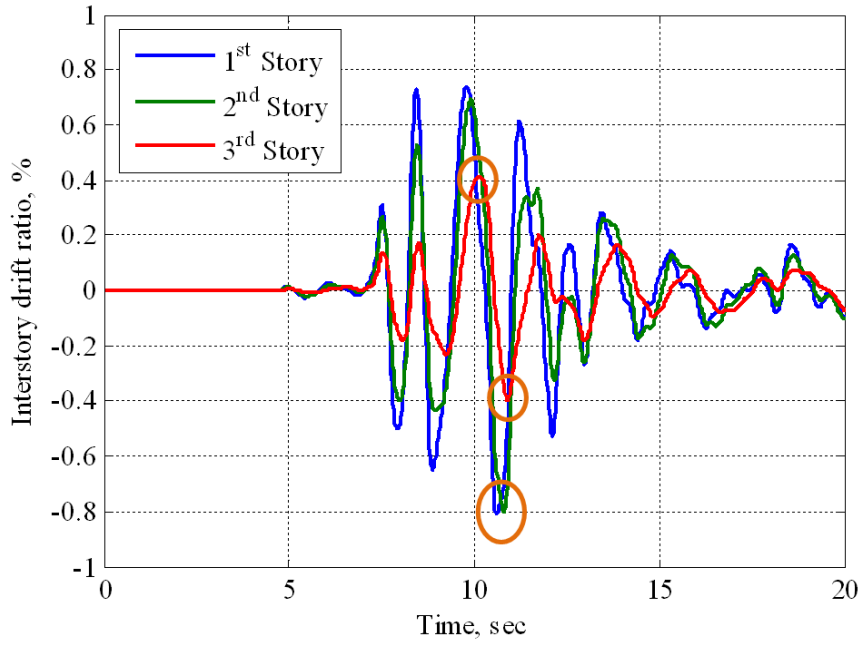

Fig. 6.13. Interstory drift ratios within the lateral sub-system

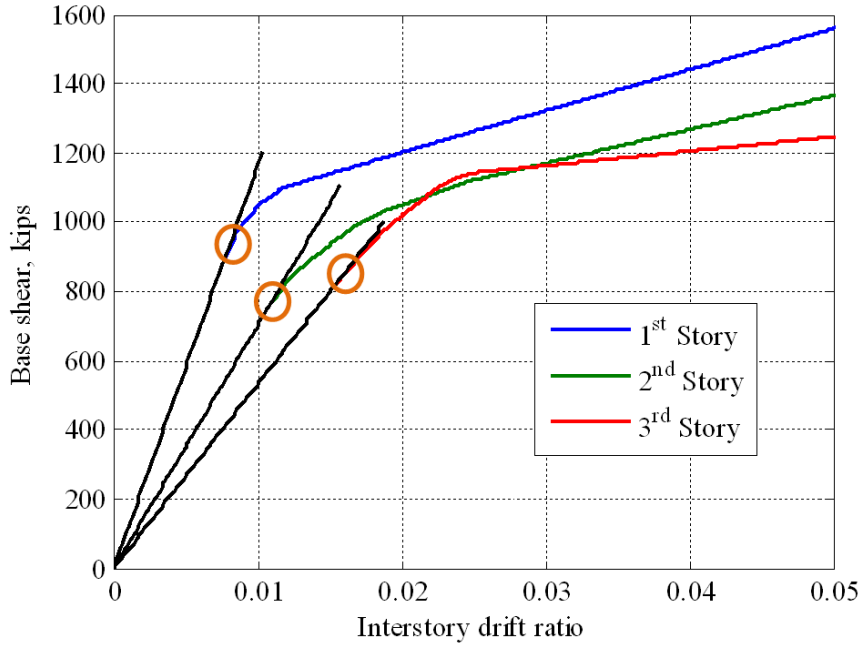

Fig. 6.14. Pushover curves of the SDMI design MRFs

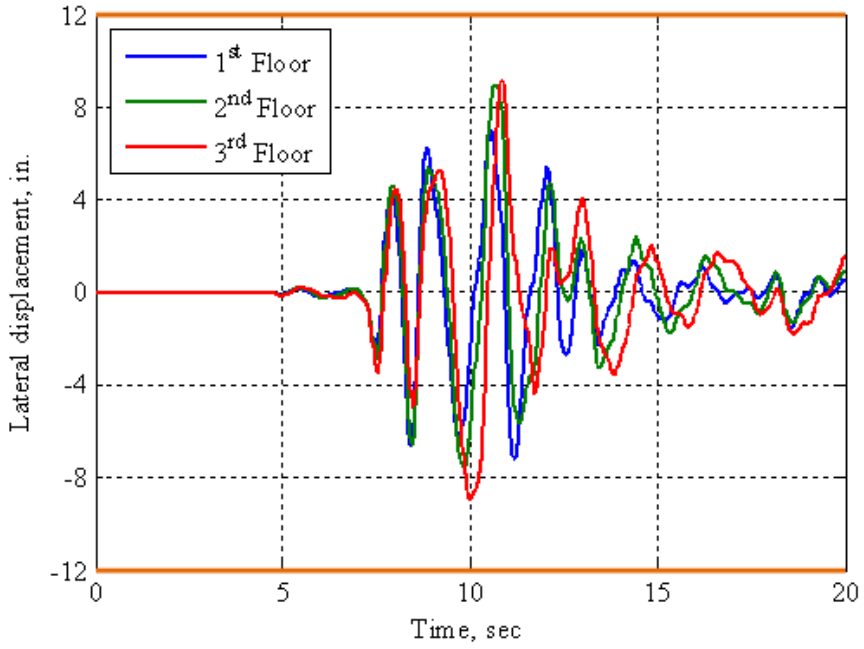

Fig. 6.15. Lateral displacements of the floor masses

7. PROTOTYPE ANALYTICAL SEISMIC PERFORMANCE ASSESSMENT

In this section, the SDMI method's effectiveness to control the seismic response of buildings is evaluated using analytical methods of analysis. For this, a series of analytical prototypes are subjected to a set of ground motions derived synthetically or from historical records. The results of these analyses as well as comments on the seismic performance of SDMI are given at the end of the section.

7.1 Prototype structure

For the purposes of this section, a three-story building structure is used. This structure has the geometric and mass properties of the three-story building of Ohtori et al. (2004) (Fig. 7.1 and Table 7.1), and is implemented with the SDMI concept. Because SDMI requires the lateral and stability springs to remain elastic, relatively stiff lateral subsystems might be required. The provision of lateral stiffness in the form of MRFs is heavy and expensive compared to lateral sub-systems based on braced frames or shear walls; therefore, in the SDMI prototypes, lateral-load resistance is provided in the form of braced frames.

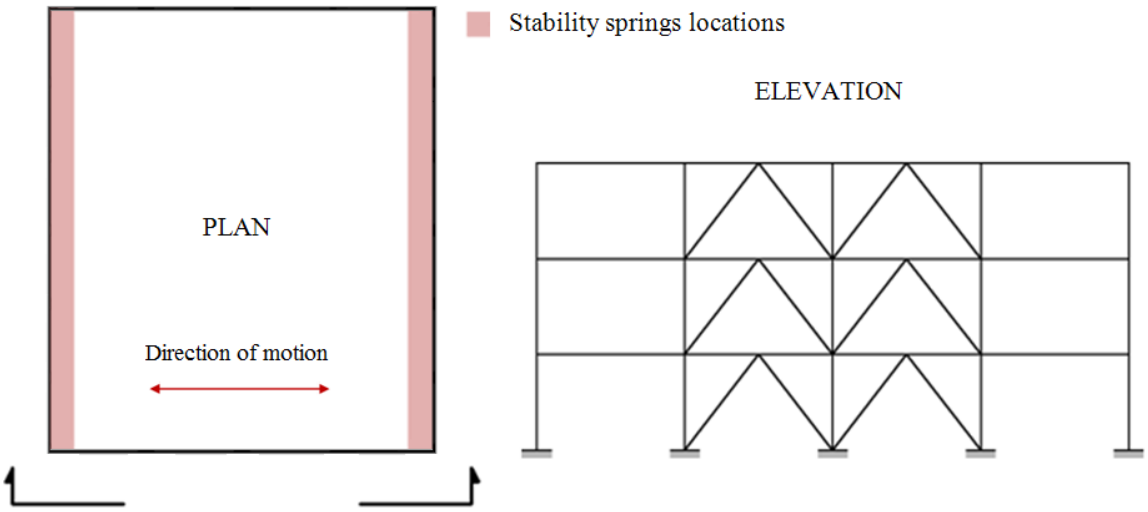

Fig. 7.1. SDMI building prototype used in the performance evaluation tests

Table 7.1. Geometric and mass properties

Dimensions	
Floor-to-floor heights	156 in.
Bay widths	360 in.
Undeformed stability springs length	50 in.
Weight	
1st level	1,055 kips
2nd level	1,055 kips
3rd level	1,142 kips
Material: steel (elastic, isotropic)	
Modulus of elasticity	29,000 ksi
Poisson's ratio	0.3

The beam-column connections in the braced-frame, those linking the frame to the ground, and the brace connections are considered pinned. Once the prototype is condensed for analysis, the lateral and stability springs take the form of "generic" equivalent springs that account for the lateral sub-system's springs as well as the stability springs. The performance evaluation analyses and optimization algorithm consider that the interstory drift ratio at the onset of yield $(DR)_y$ for braced frames occurs at 0.5%. This value constitutes a general round approximation that is consistent with the results provided by pushover analyses. Inherent damping of 2% is assigned to the SDMI models as an assumption for system damping, while 5% is assigned to the control structures to account for the damping that is due to the hysteretic behavior of the braces.

The use of energy dissipaters in the form of fluid viscous dampers is considered. Rather than allowing the general possibility of having dampers installed "everywhere" in the structure, three different damper configurations are considered in this study: 1. The dampers are located in the gravity sub-system (Fig. 7.2a), 2. The dampers are interconnecting the lateral and gravity sub-systems (Fig. 7.2b), and 3. The dampers are located in the lateral sub-system (Fig. 7.2c). These configurations may adapt to different constructional and architectural conveniences and adhere to the fact that the determination of the actual damper locations and properties from a reduced model damping matrix requires particular constraints and may yield damper arrays that are not convenient in practice, since the latter configuration could result in having a building with dampers "everywhere". Typical building structures are used as control prototypes to make adequate as-

sessments of the seismic performance of SDMI. The "typical" structures correspond to the same braced frame of Fig. 7.1 only without the implementation of SDMI.

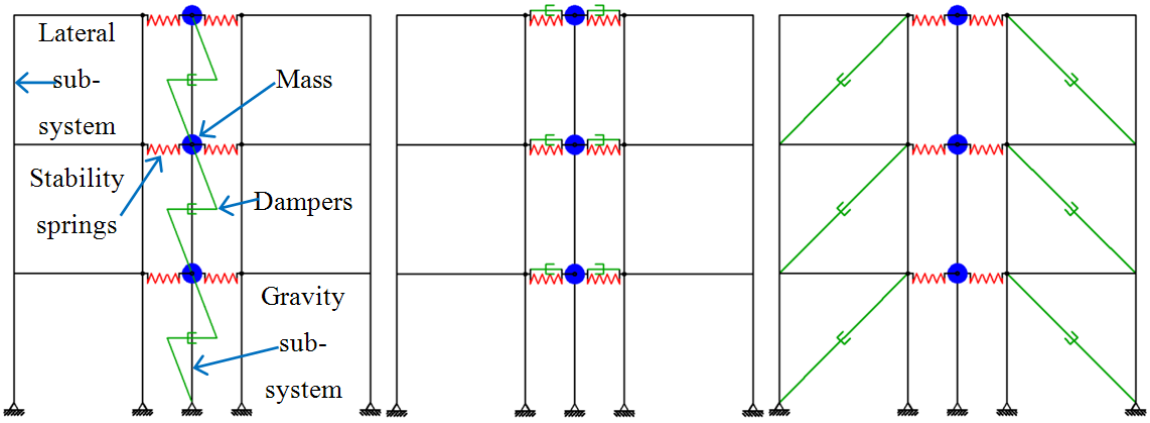

Fig. 7.2. SDMI building prototype with a) dampers in the gravity sub-system, b) dampers joining the gravity and lateral sub-systems, and c) dampers in the lateral sub-system

7.2 Determination of the structural properties of the analytical prototypes

To adequately study the technical advantages of SDMI and obtain response values that serve to compare the performance of this system with that of others, it is necessary to study SDMI prototypes that maximize the system's capabilities. These "ideal" prototypes have to be obtained through an optimization process.

A genetic algorithm (GA) is chosen to determine the analytical prototypes that minimize the response quantity of interest. The GA is chosen for the following reasons (Haupt and Haupt 2004):

- It can optimize continuous variables such as the spring stiffnessess, damping coefficients, and undeformed stability spring lengths,

- It optimizes variables with extremely complex cost surfaces, such as a response surface mapped by a SDMI system, which due to the stability, restoration, pounding, elasticity constraints, and the inherent nonlinearity of the system, is of a complex and discontinuous nature, and
- It works with numerically generated data, which makes it suitable to the SDMI problem, given the numerical nature of the time-history analyses that are needed to evaluate the performance of the system.

In GAs, the variable values may be represented by continuous or binary quantities. Here, continuous variables were chosen over binary variables following the recommendations given by Haupt and Haupt (2004) and Michalewicz (1992), whose experiences with GAs indicate that the use of continuous variables leads to faster, more consistent, and precise results.

A general GA follows the steps outlined in Fig. 7.3, which were adapted to the prototype optimization problem as follows:

Cost function: The cost function in the optimization process is the lateral acceleration-response of the floor masses. Since the continuous elasticity of the system is a fundamental requirement in SDMI, any design has to guarantee it. If the system is designed to remain elastic, then the magnitude of the springs' deformations (the interstory drift ratios within the lateral sub-system and the elongations and contractions of the stability springs) do not constitute a concern from a damage point of view, since, at least theoretically, they will not suffer the damage that results from plastic deformations.

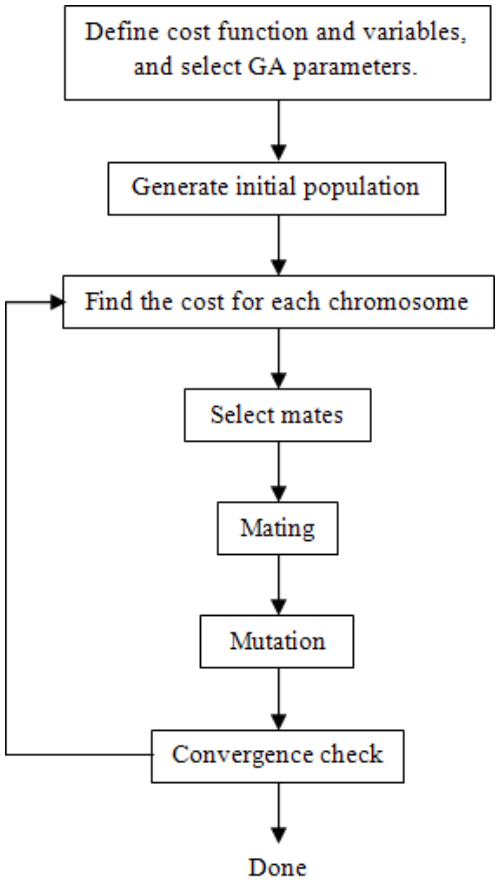

Fig. 7.3. Flowchart of the GA used in the optimization process (Haupt and Haupt 2004)

The recognition of the theoretical absence of damage in the springs leaves the interstory drift ratios within the gravity sub-system and the floor accelerations as the only response parameters that correspond to performance indicators. These two response quantities are related primarily to non-structural damage, which needs to be minimized to maximize the safety of the structure's users and the economy of the building. However, the gravity sub-system's interstory drifts cannot be subject to minimization because this would lead to the design of a typical building structure where there is no isolating interface between the lateral and gravity sub-systems; therefore, this option is discarded.

However, a proper SDMI design should limit these drifts so that unacceptable levels of non-structural damage are avoided.

By discarding the interstory drifts within the gravity sub-system as optimization variable, unanimously, the only response parameter that deserves minimization is the accelerations of the floor slabs; plus, the reduction of the floor accelerations results in increased safety for the building's occupants as was said in the introduction. Moreover, minimized floor accelerations result in reduced demands on the lateral springs, facilitating the continuous elasticity requirement and the possibility of lighter and more economic structural designs.

Variables: If a "full" analytical model of a building is considered in the optimization process, the structural variables that are involved in the dynamics of the SDMI system are the stiffnesses of the lateral and stability springs, the stability springs' undeformed lengths, and the damping coefficients of the energy dissipaters. Otherwise, if a condensed model is used, the structural variables are the equivalent springs and dampers' properties and the undeformed lengths of the stability springs.

In general, the use of "full" models leads to less optimization variables and more efficient optimization processes. Moreover, because in this optimization process the locations of the dampers have been determined a priori, the structural properties in a "full" analytical model are used as the optimization variables. This fact does not affect the practicality of having a condensed set of structural properties, since the actual values can easily be converted into equivalent values and back to different full-model value combi-

nations that represent the same reduced model with the schemes provided in past sections.

GA parameters: The chromosome natural selection rate is set to 50%, i.e., the fittest half of the population is kept and used to produce the other 50% of the next generation. The mutation rate is set to 20%; however, the chromosome yielding the best solution is not included in the mutation process in order to protect the possibility that it corresponds to the cost function's global minimum.

Initial population: An initial set of two hundred random chromosomes are generated using a uniform probability distribution for all the variables. The damping coefficients for the energy dissipaters are chosen to range from 0 to 10 kips-sec/in. in order to keep the norm of the reduced damping matrix small compared to that of the reduced stiffness matrix so that the dynamic condensation method introduced before can be appropriately used. This constraint is not of importance, since previous experience showed that small damping coefficients were sufficient to significantly reduce the response of the structure, (especially the displacements and interstory drift-ratios in the gravity sub-system) and sometimes required to maximize the isolation of the gravity sub-system.

The lateral spring stiffness is set to range from 300 to 7,500 kips/in., while the stiffness range for the stability springs is 0 to 300 kips/in. Finally, the undeformed length of the stability springs is given a range of 0 to 55 in.

Mating: The fittest chromosomes form the mating pool (50% of the population in this case). The father and mother chromosomes are paired in a random fashion using uniform probability; however, the pairing is carried out with a system of rank weighting that en-

sures that the fitter chromosomes in the mating pool produce most of the members of the new population.

The crossover of the parent chromosomes is performed using a single crossover point and the blend crossover *BLX-α* method (Haupt and Haupt 2004). The crossover point α and the blending parameter β are obtained randomly using uniform probability.

Mutation: The variables to be mutated are randomly selected according to uniform probability and the percentage specified above (20%).

7.2.1 Earthquake records used in the optimization process

The process that is carried out to determine optimal SDMI building structures involves the analysis of many different sub-optimal designs subjected to a specific ground motion. This implies that the result of the optimization process is a set of structural properties that minimizes the seismic response parameter of interest (the peak absolute floor acceleration in this case) when the associated building is subjected to the particular earthquake that generated the set. However, that particular set does not minimize the response of the building when subjected to other earthquake records. In reality, a design that minimizes some overall measure of the response due to a series of potential ground motions is more useful. In an ideal case, this series of motions would be the one that the structure would be subjected to during its service life, but these cannot be predicted. Building codes must be used to determine the characteristics and number of earthquake motions that the structure has to be designed to withstand.

In order to obtain a good approximation to a design that minimizes the overall response of the building when subjected to a series of earthquakes, twelve (sub-) optimal SDMI designs are first determined. These constitute three basic SDMI structures having dampers at different locations determined by the optimization of their seismic performance when subjected to four different historical earthquake records. To perform the evaluation of the performance of the system, four control structures are also determined by the same process of optimization.

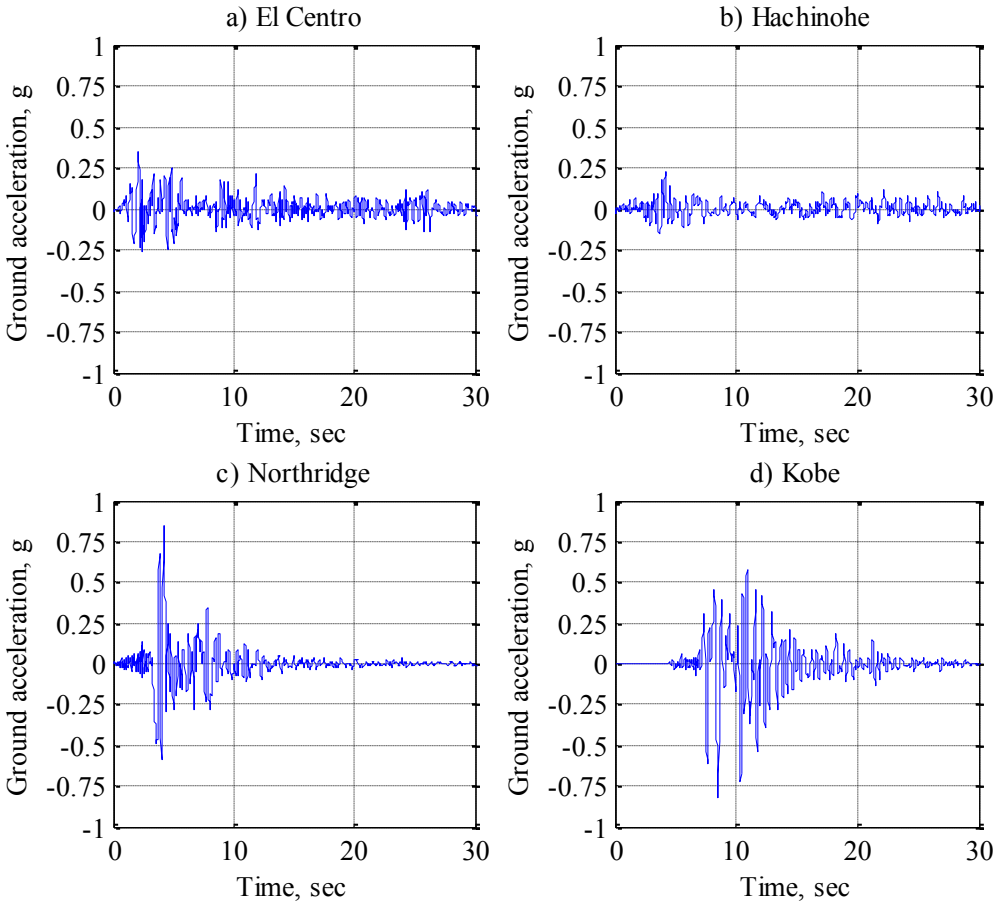

Fig. 7.4. Earthquake records selected to produce (sub-) optimal SDMI structures

The four historical records that are used to determine the prototype structures are given in Table 7.2 and Fig. 7.4. These consist of two near-field (El Centro and Tokachi-Oki) and two far-field (Northridge and Kobe) ground motions. Once the sixteen (sub-) optimal designs have been determined, their overall seismic performance is evaluated using a larger and more standardized series of earthquake records.

Table 7.2. Earthquake records used in the production of optimized analytical prototypes

Earthquake record	*Recording station*	*PGA (g)*	*Figure*
El Centro (1940) N-S component	Imperial Valley Irrigation District	0.3487	Fig. 7.4a
Tokachi-Oki (1968) N-S comp.	Hachinohe City	0.2294	Fig. 7.4b
Northridge (1994) N-S component	Sylmar County Hospital	0.8431	Fig. 7.4c
Kobe (1995) N-S component	Kobe Japanese Meteorological Agency	0.8213	Fig. 7.4d

7.3 Optimized structures

The optimization algorithm was implemented as described above to obtain the twelve reduced SDMI models and four control structures mentioned before. Each of these designs minimizes the absolute peak floor acceleration of the floor slabs when the building is subjected to the specific earthquake that produced it.

To translate the optimal reduced SDMI models into full models, the design provisions given in subsection 6.3 were used making sure that the continuous elasticity requirement was fulfilled under all of the records used for the prototype evaluation described later; i.e., the peak interstory drift-ratio within the lateral sub-system in all

twelve SDMI structures is less or equal to 0.005 under all evaluation records. In the case of the control braced-frame structures, the interstory drift ratios were limited to 0.015 for the El Centro and Hachinohe earthquakes and to 0.02 for the Kobe and Northridge records to comply with the life-safety and collapse-prevention performance limits, respectively (ASCE 2007). The structural properties of the optimized prototypes are given in Table 7.3. The first letter in the structure name corresponds to the first letter of the earthquake record that generated it (E for El Centro, H for Hachinohe, etc.), and the second letter corresponds to the place where energy dissipaters are located (G for the gravity sub-system, I for dampers interconnecting the gravity and lateral sub-systems, and L for the lateral sub-system). "T" is designated for the "typical" control structures.

Table 7.3. Structural properties of the optimized analytical models

Structure	$k_{l,1}$ (k/in.)	$k_{l,2}$ (k/in.)	$k_{l,3}$ (k/in.)	$k_{s,1}$ (k/in.)	$k_{s,2}$ (k/in.)	$k_{s,3}$ (k/in.)	$c_{x,1}$ (k*s/in.)	$c_{x,2}$ (k*s/in.)	$c_{x,3}$ (k*s/in.)
E-G	4,572	2,629	785	62.39	35.97	13.67	9.88	8.16	7.60
E-I	3,089	1,721	868	59.56	37.51	33.70	9.27	9.91	9.15
E-L	10,248	6,634	3,870	75.40	56.87	61.97	7.88	8.28	9.45
E-T	462	392	642	-	-	-	-	-	-
H-G	4,815	2,350	784	67.81	31.98	14.09	6.90	9.97	4.47
H-I	3,058	1,628	816	52.14	32.02	29.66	7.41	9.66	8.39
H-L	10,867	7,529	4,537	81.50	66.38	73.11	4.87	6.64	4.00
H-T	301	310	499	-	-	-	-	-	-
N-G	4,821	2,958	900	55.96	39.04	15.15	9.51	8.69	9.72
N-I	2,925	1,974	484	48.16	41.19	21.72	9.86	6.10	9.75
N-L	15,363	10,238	5,233	148.85	130.14	144.06	6.73	7.84	8.30
N-T	1,187	1,089	1,796	-	-	-	-	-	-
K-G	5,148	2,773	804	58.91	36.22	13.61	6.63	9.49	8.98
K-I	3,545	2,724	765	47.61	38.40	27.88	7.09	5.05	7.68
K-L	10,951	6,677	2,964	54.72	36.26	17.45	1.44	2.56	0.48
K-T	1,748	1,469	1,795	-	-	-	-	-	-

7.4 Analytical performance evaluation tests

7.4.1 Earthquake records used for the evaluation of seismic performance

The ground accelerations used for the performance evaluation of the prototype buildings consist of two suites of twenty earthquake records each, developed by Somerville (1997) from historical recordings and simulations of physical fault rupture processes for the FEMA project on steel MRFs (FEMA 1994) (Table 7.4). The records in each of the two suites correspond to the fault-parallel and fault-normal orientations of ten different ground motions that were later rotated forty-five degrees from these orientations to preclude biasing from excessive near-fault effects. The hazard levels associated with the records contained in each suite correspond to a 10% (records LA01-LA20) and 2% (records LA21-LA40) probability of exceedence in fifty years, respectively, according to the 1997 USGS maps for downtown Los Angeles, California. The records are also scaled so that their mean spectral acceleration matches the 1997 NEHRP design spectrum.

Table 7.4. Earthquake records used in the analytical performance evaluation of SDMI (FEMA 1994)

SAC name	*Record*	*Magnitude (Richter)*	*Distance (km)*	*Scale factor*	*Number of points*	*Δt (sec)*	*Duration (sec)*	*PGA (g)*
LA01	Imperial Valley, 1940, El Centro	6.9	10	2.01	2,674	0.02	39.38	0.461
LA02	Imperial Valley, 1940, El Centro	6.9	10	2.01	2,674	0.02	39.38	0.676
LA03	Imperial Valley, 1979, Array #05	6.5	4.1	1.01	3,939	0.01	39.38	0.394
LA04	Imperial Valley, 1979, Array #05	6.5	4.1	1.01	3,939	0.01	39.38	0.488
LA05	Imperial Valley, 1979, Array #06	6.5	1.2	0.84	3,909	0.01	39.08	0.302
LA06	Imperial Valley, 1979, Array #06	6.5	1.2	0.84	3,909	0.01	39.08	0.235
LA07	Landers, 1992, Barstow	7.3	36	3.2	4,000	0.02	79.98	0.421
LA08	Landers, 1992, Barstow	7.3	36	3.2	4,000	0.02	79.98	0.426
LA09	Landers, 1992, Yermo	7.3	25	2.17	4,000	0.02	79.98	0.52
LA10	Landers, 1992, Yermo	7.3	25	2.17	4,000	0.02	79.98	0.36

Table 7.4. Continued

SAC name	*Record*	*Magnitude (Richter)*	*Distance (km)*	*Scale factor*	*Number of points*	*Δt (sec)*	*Duration (sec)*	*PGA (g)*
LA11	Loma Prieta, 1989, Gilroy	7	12	1.79	2,000	0.02	39.98	0.665
LA12	Loma Prieta, 1989, Gilroy	7	12	1.79	2,000	0.02	39.98	0.97
LA13	Northridge, 1994, Newhall	6.7	6.7	1.03	3,000	0.02	59.98	0.678
LA14	Northridge, 1994, Newhall	6.7	6.7	1.03	3,000	0.02	59.98	0.657
LA15	Northridge, 1994, Rinaldi RS	6.7	7.5	0.79	2,990	0.01	14.945	0.534
LA16	Northridge, 1994, Rinaldi RS	6.7	7.5	0.79	2,990	0.01	14.945	0.58
LA17	Northridge, 1994, Sylmar	6.7	6.4	0.99	3,000	0.02	59.98	0.569
LA18	Northridge, 1994, Sylmar	6.7	6.4	0.99	3,000	0.02	59.98	0.817
LA19	North Palm Springs, 1986	6	6.7	2.97	3,000	0.02	59.98	1.019
LA20	North Palm Springs, 1986	6	6.7	2.97	3,000	0.02	59.98	0.987
LA21	1995 Kobe	6.9	3.4	1.15	3,000	0.02	59.98	1.283
LA22	1995 Kobe	6.9	3.4	1.15	3,000	0.02	59.98	0.921
LA23	1989 Loma Prieta	7	3.5	0.82	2,500	0.01	24.99	0.418
LA24	1989 Loma Prieta	7	3.5	0.82	2,500	0.01	24.99	0.473
LA25	1994 Northridge	6.7	7.5	1.29	2,990	0.01	14.945	0.868
LA26	1994 Northridge	6.7	7.5	1.29	2,990	0.01	14.945	0.944
LA27	1994 Northridge	6.7	6.4	1.61	3,000	0.02	59.98	0.927
LA28	1994 Northridge	6.7	6.4	1.61	3,000	0.02	59.98	1.33
LA29	1974 Tabas	7.4	1.2	1.08	2,500	0.02	49.98	0.809
LA30	1974 Tabas	7.4	1.2	1.08	2,500	0.02	49.98	0.992
LA31	Elysian Park (simulated)	7.1	17.5	1.43	3,000	0.01	29.99	1.296
LA32	Elysian Park (simulated)	7.1	17.5	1.43	3,000	0.01	29.99	1.186
LA33	Elysian Park (simulated)	7.1	10.7	0.97	3,000	0.01	29.99	0.782
LA34	Elysian Park (simulated)	7.1	10.7	0.97	3,000	0.01	29.99	0.681
LA35	Elysian Park (simulated)	7.1	11.2	1.1	3,000	0.01	29.99	0.992
LA36	Elysian Park (simulated)	7.1	11.2	1.1	3,000	0.01	29.99	1.101
LA37	Palos Verdes (simulated)	7.1	1.5	0.9	3,000	0.02	59.98	0.712
LA38	Palos Verdes (simulated)	7.1	1.5	0.9	3,000	0.02	59.98	0.776
LA39	Palos Verdes (simulated)	7.1	1.5	0.88	3,000	0.02	59.98	0.5
LA40	Palos Verdes (simulated)	7.1	1.5	0.88	3,000	0.02	59.98	0.625

7.4.2 Results

All sixteen optimized structures were subjected to the forty Los Angeles earthquake records that were described previously. The peak (absolute) values of the time-history analyses for the response parameters of lateral displacements, lateral accelerations, and interstory drift-ratios in the gravity sub-system are presented in Fig. 7.5 to Fig. 7.16; however, no values are displayed whenever the structure in question failed according to one or more of the criteria below.

For the SDMI structures (those ending in G, I, or L), whenever:

1. Any of the floor slabs pounded against the lateral sub-system; i.e., the peak lateral displacement exceeded 50 in., or
2. The interstory drift-ratios in the gravity sub-system exceeded 0.15.

For the “typical” control structures (those ending in T)

i. The interstory drift-ratios exceeded the collapse-prevention performance level limit for steel braced frames; i.e., 0.02.

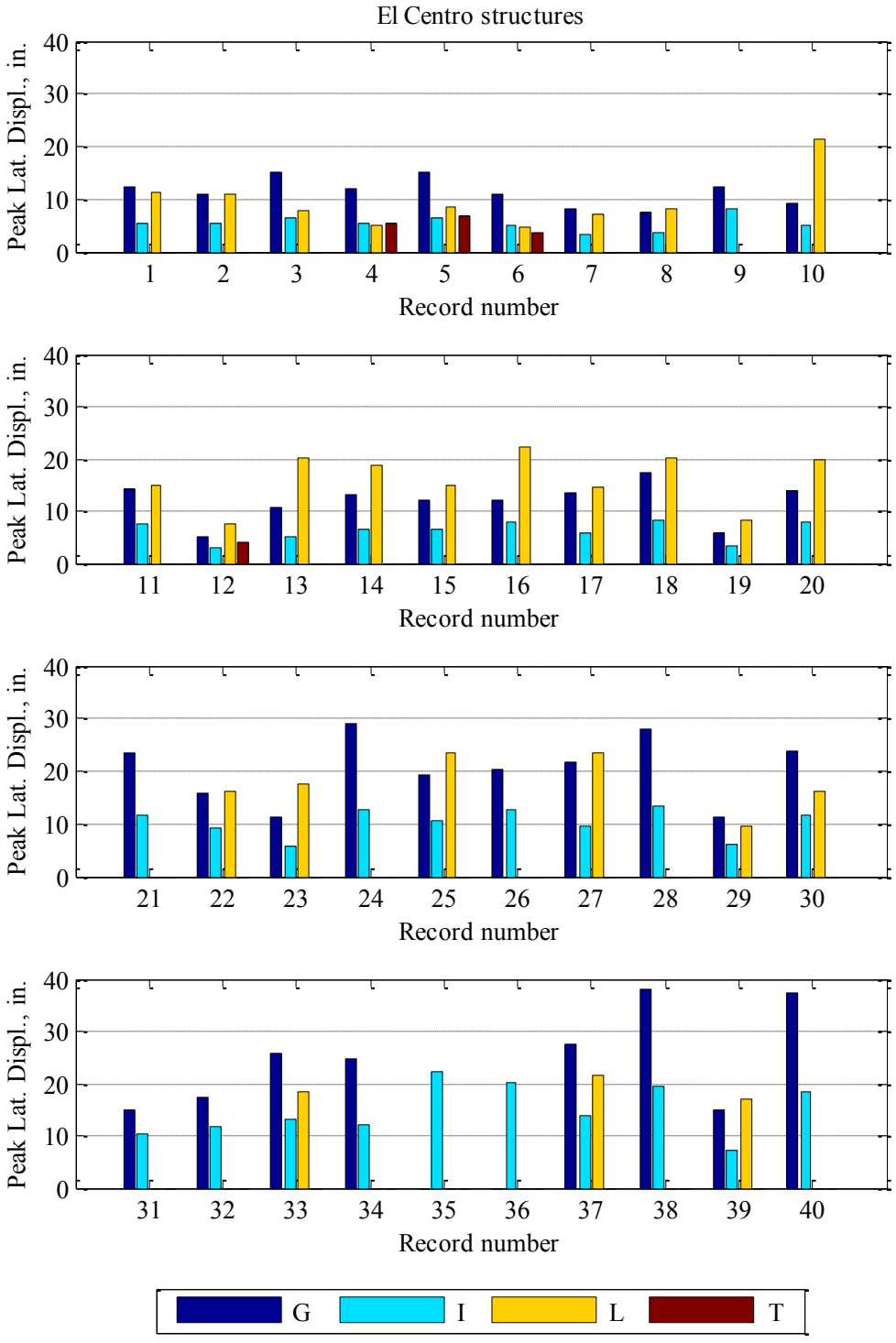

Fig. 7.5. Peak absolute lateral displacements of the El Centro structures

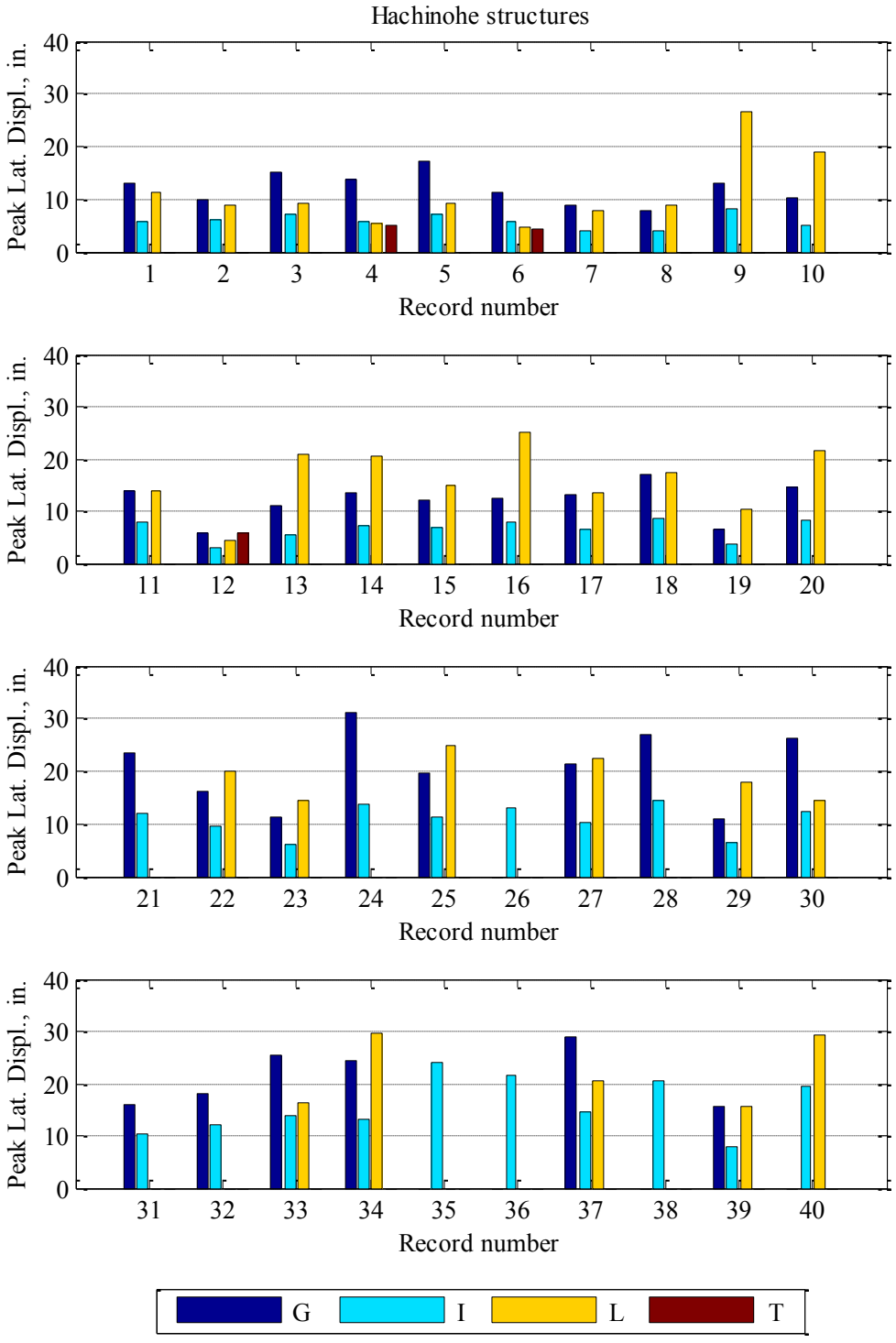

Fig. 7.6. Peak absolute lateral displacements of the Hachinohe structures

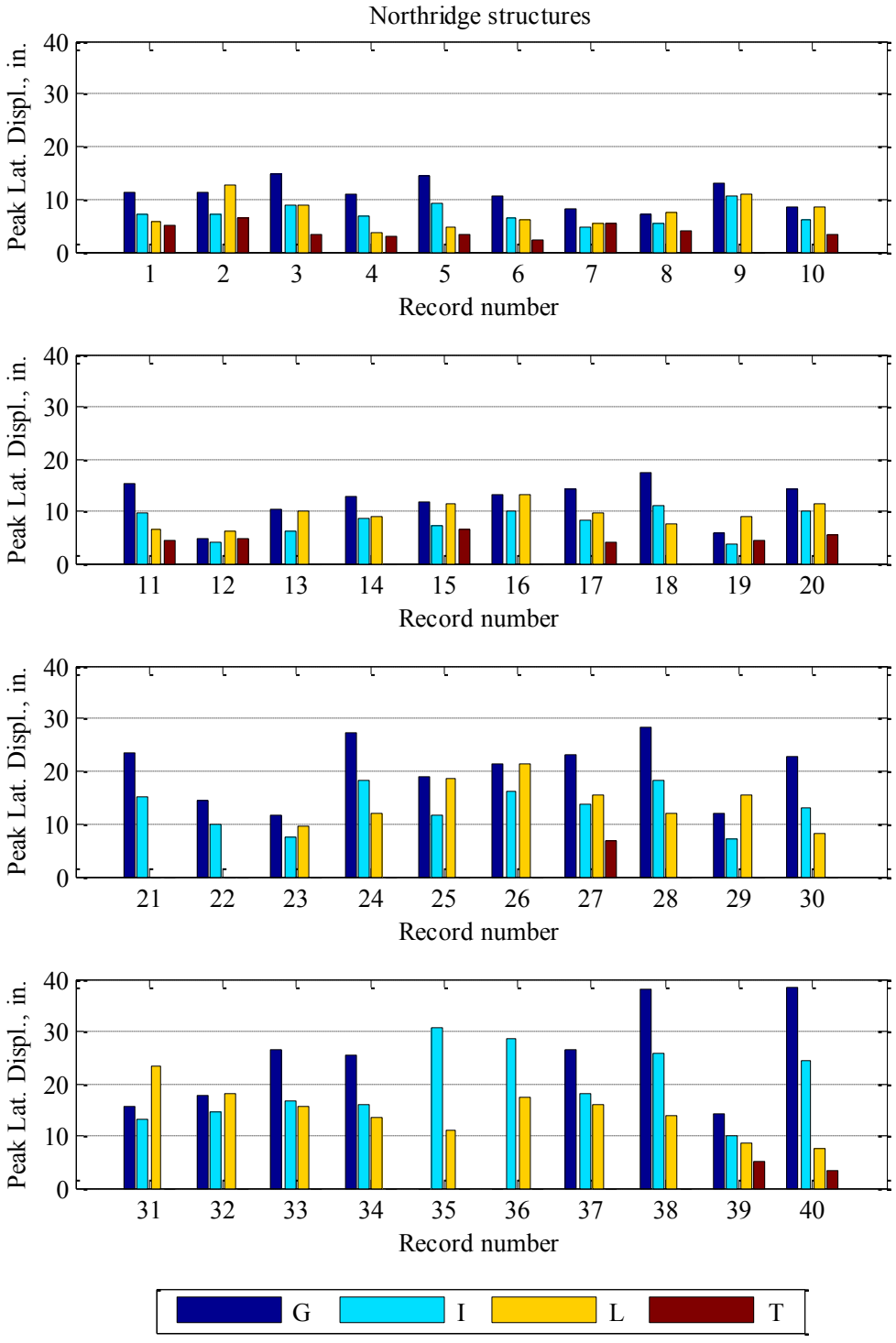

Fig. 7.7. Peak absolute lateral displacements of the Northridge structures

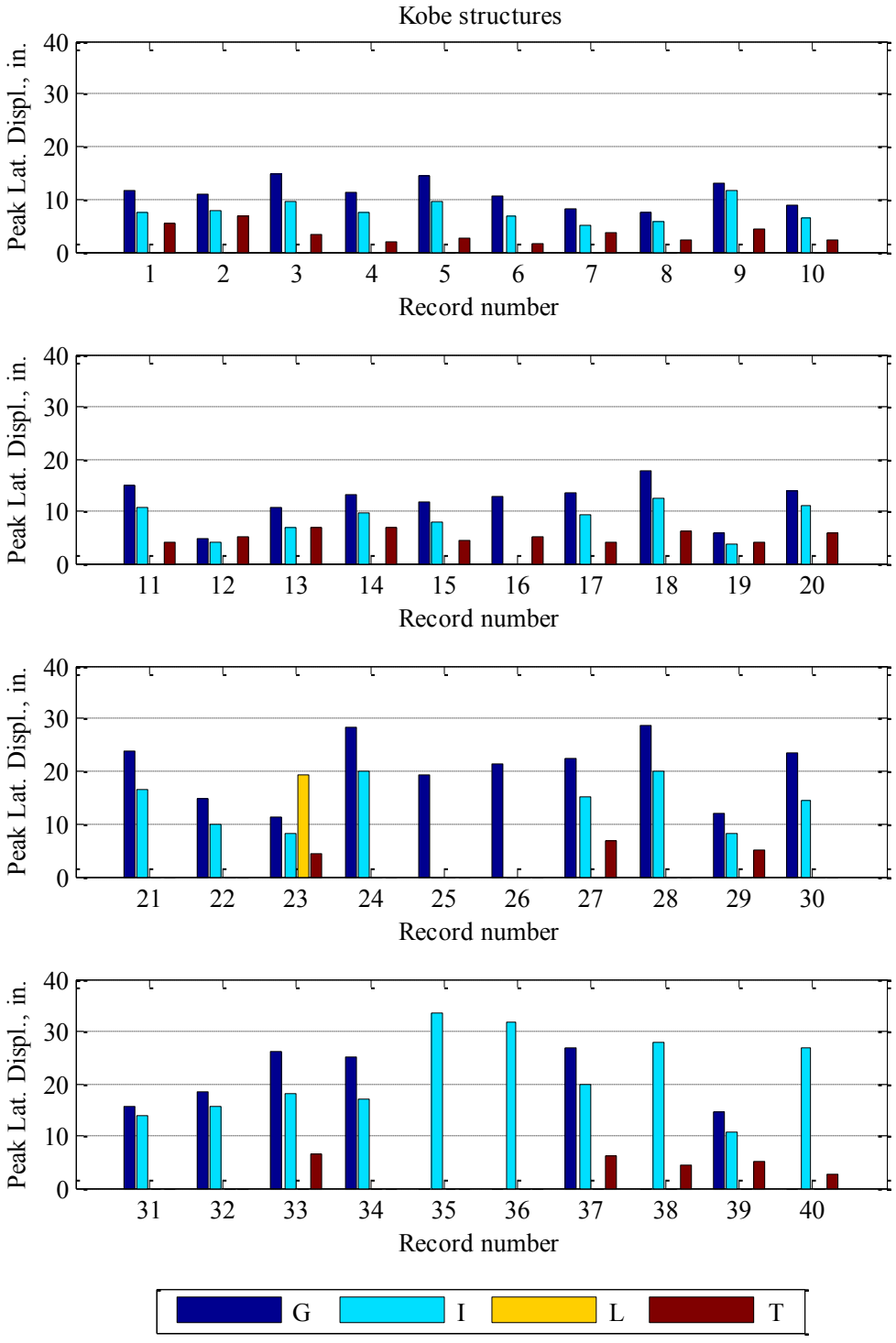

Fig. 7.8. Peak absolute lateral displacements of the Kobe structures

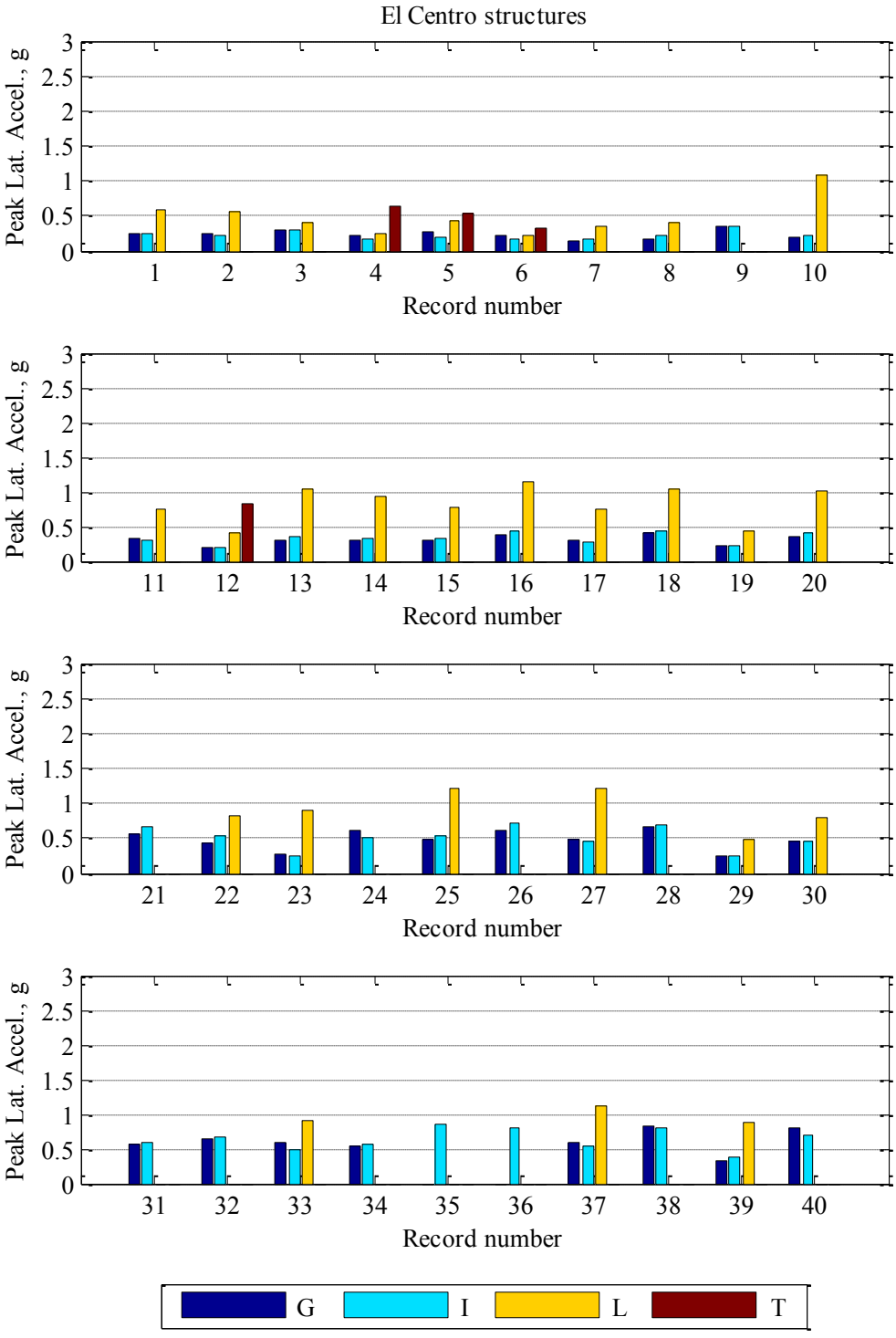

Fig. 7.9. Peak absolute lateral accelerations of the El Centro structures

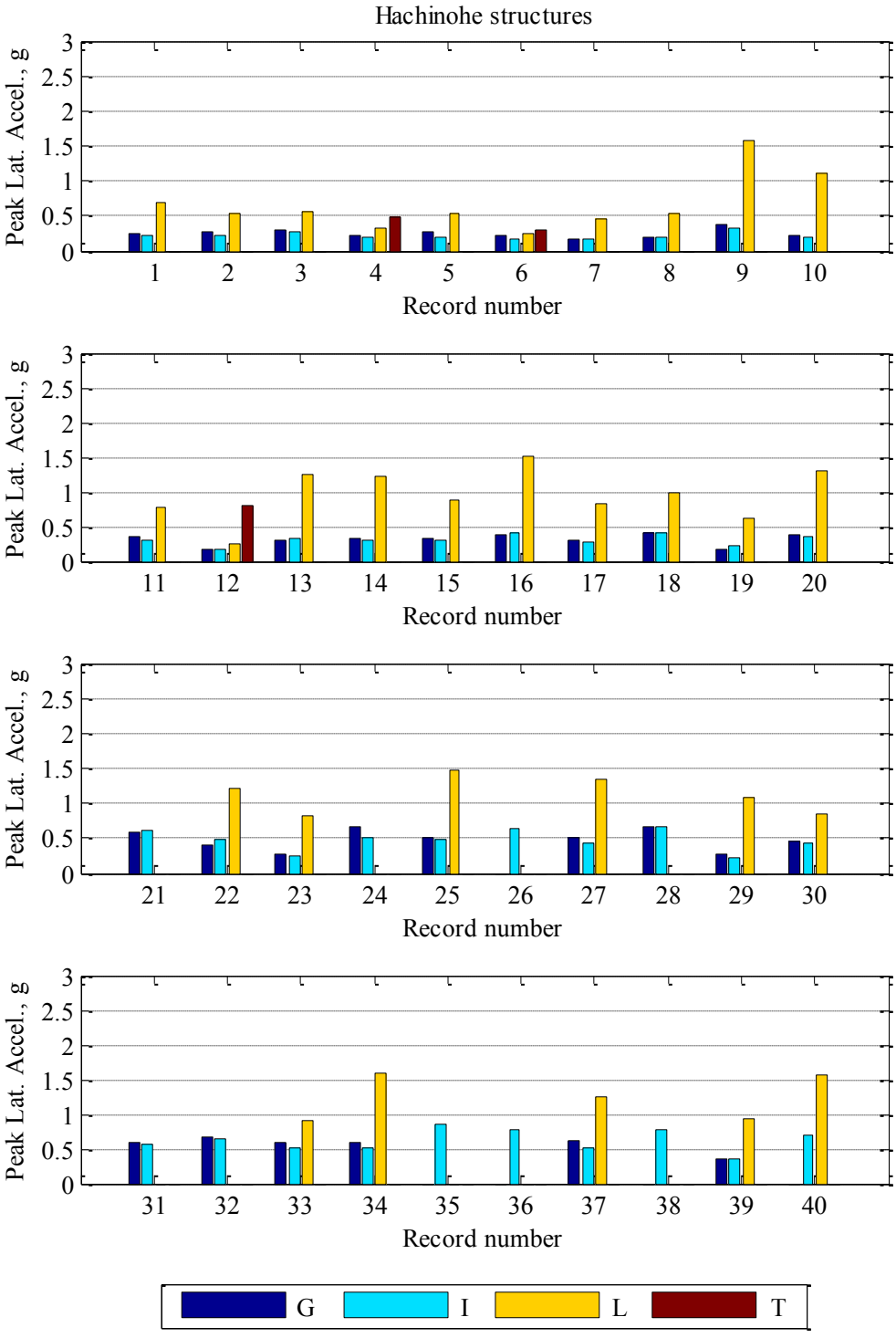

Fig. 7.10. Peak absolute lateral accelerations of the Hachinohe structures

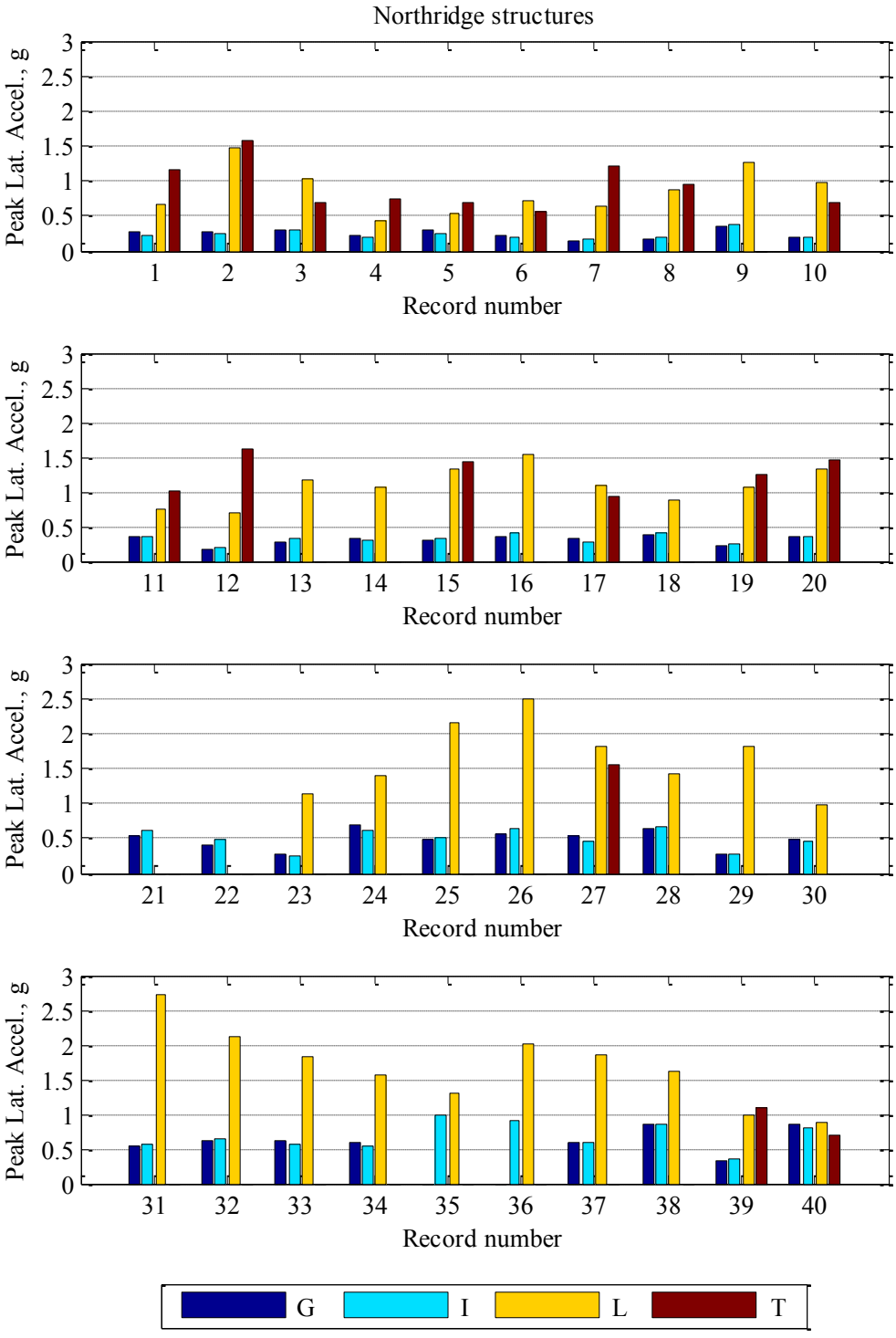

Fig. 7.11. Peak absolute lateral accelerations of the Northridge structures

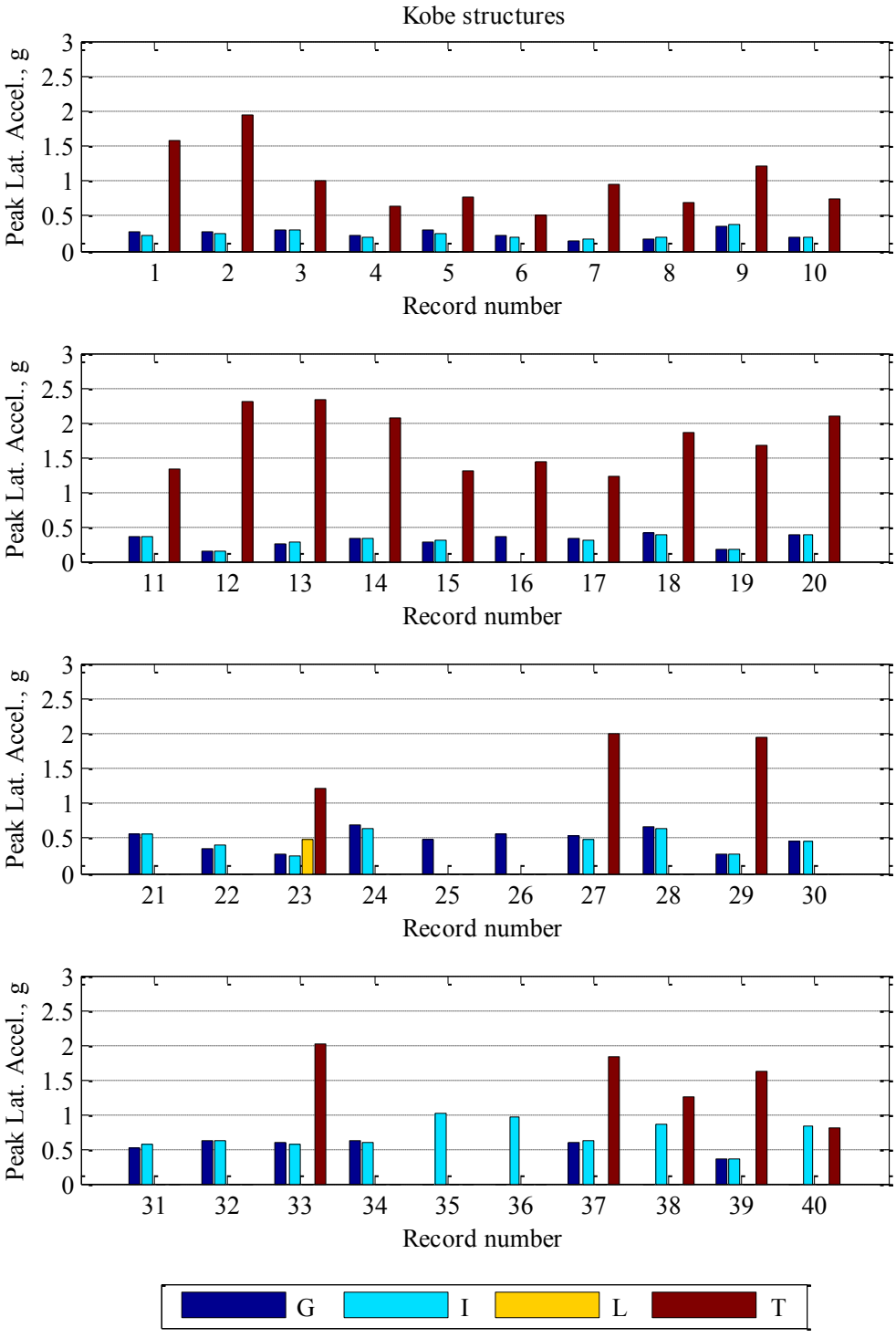

Fig. 7.12. Peak absolute lateral accelerations of the Kobe structures

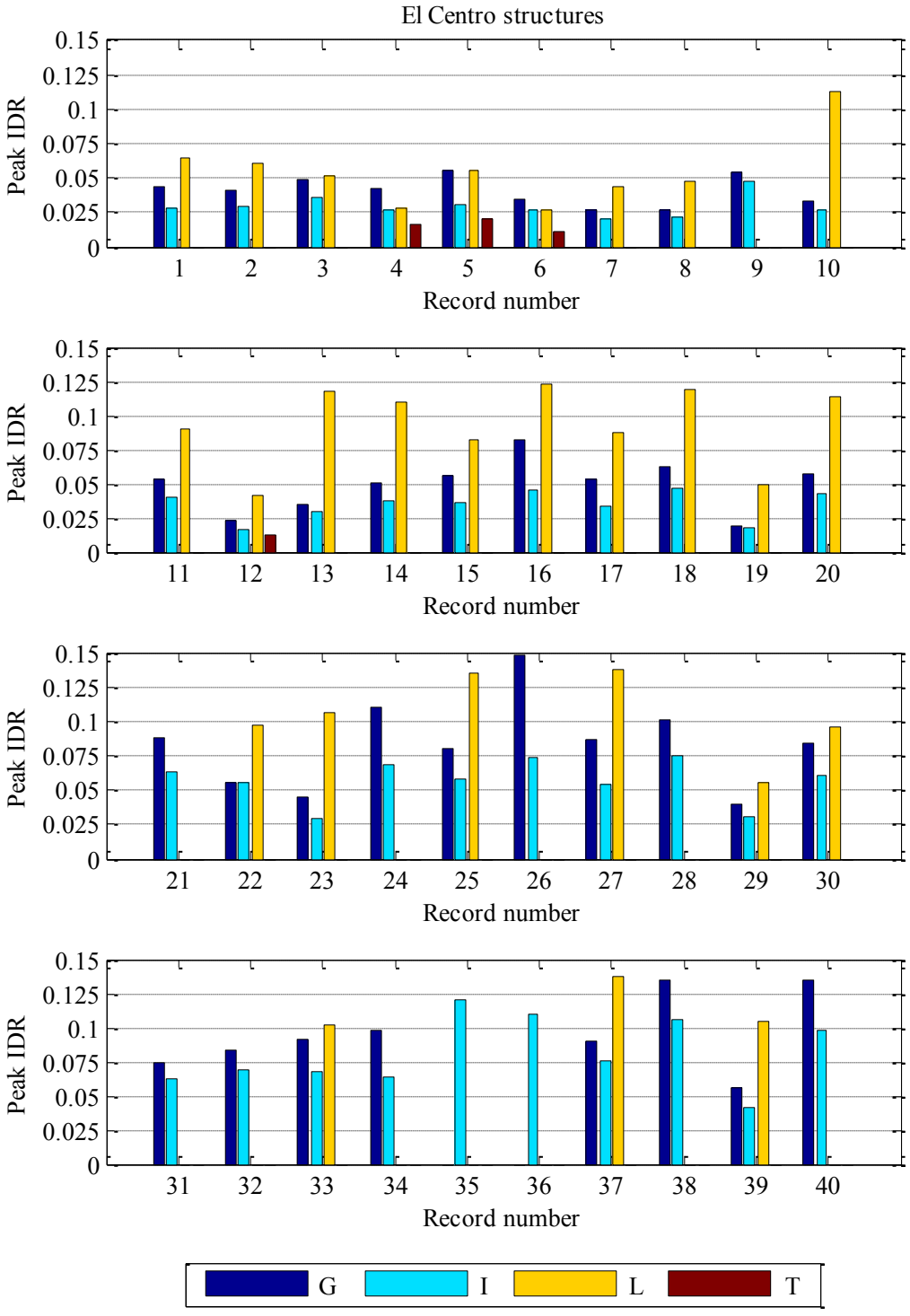

Fig. 7.13. Peak absolute interstory drift-ratios of the El Centro structures

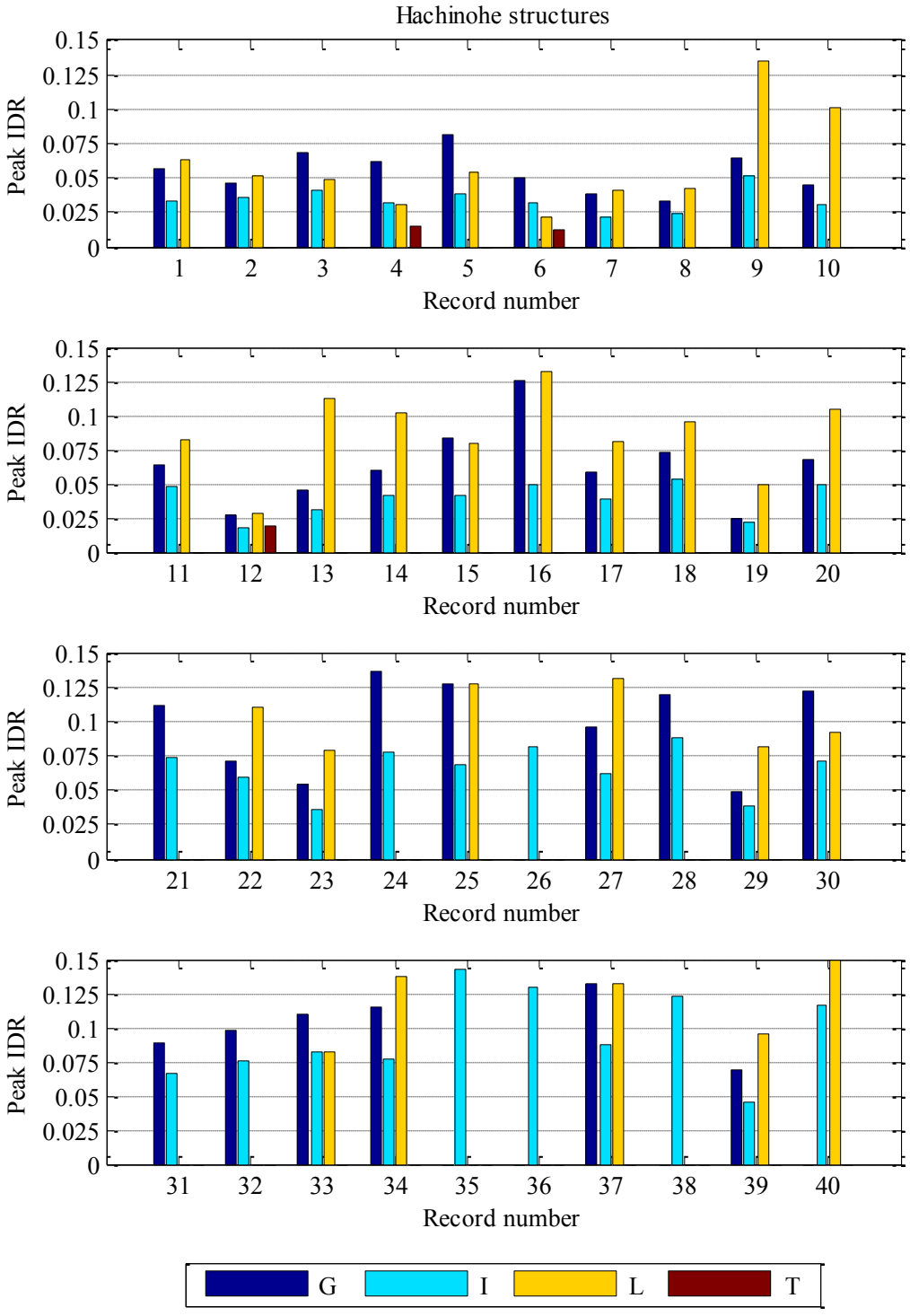

Fig. 7.14. Peak absolute interstory drift-ratios of the Hachinohe structures

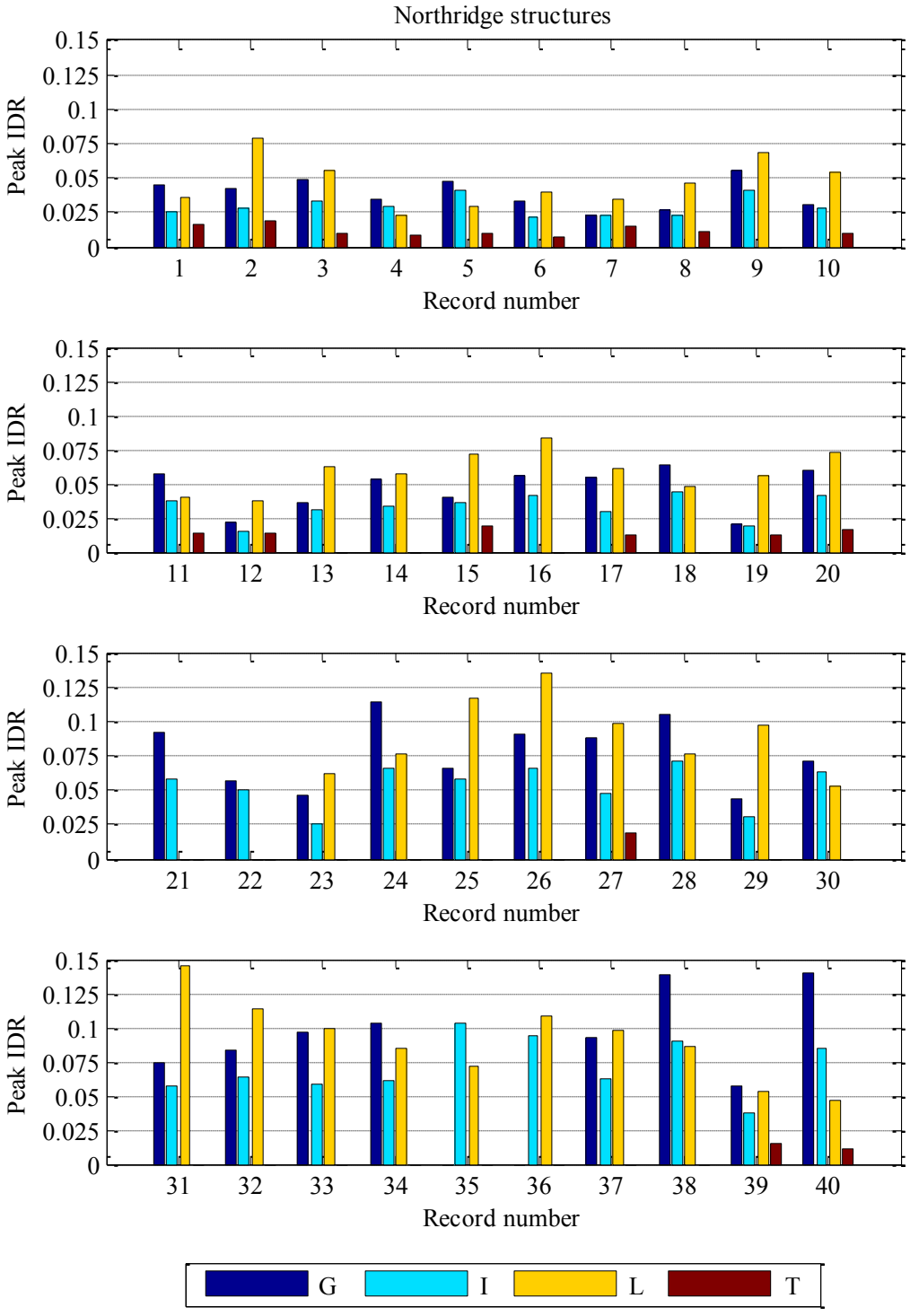

Fig. 7.15. Peak absolute interstory drift-ratios of the Northridge structures

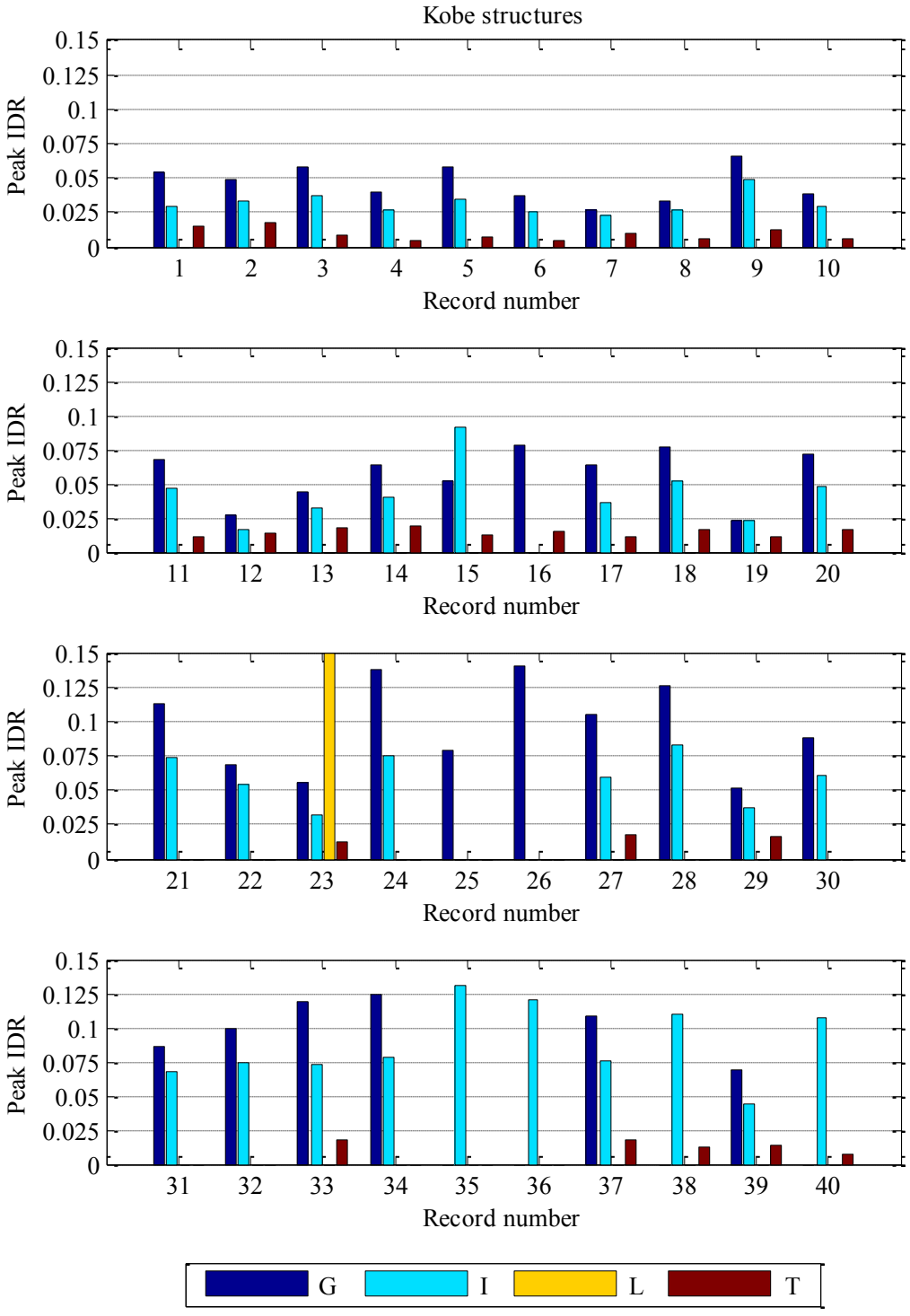

Fig. 7.16. Peak absolute interstory drift-ratios of the Kobe structures

Table 7.5. Average seismic performance of the optimized analytical models

Structure	*No. of successes*	*Avg. peak displacement (in.)*	*Avg. peak acceleration (g)*	*Avg. peak IDR**
E-G	38	16.74	0.401	0.0657
E-I	40	9.19	0.425	0.0506
E-L	28	14.67	0.749	0.0856
E-T	4	4.99	0.586	0.0149
H-G	35	15.88	0.382	0.0765
H-I	40	9.76	0.403	0.0584
H-L	31	16.11	0.945	0.0862
H-T	3	5.06	0.525	0.0157
N-G	38	16.70	0.404	0.0635
N-I	40	11.98	0.433	0.0468
N-L	38	11.19	1.306	0.0705
N-T	18	4.49	1.075	0.0132
K-G	36	15.65	0.377	0.0722
K-I	37	12.99	0.425	0.0555
K-L	1	19.44	0.477	0.1490
K-T	28	4.57	1.439	0.0125

*Interstory drift-ratio

7.5 System evaluation

7.5.1 Configuration

The results given in Table 7.5 demonstrate that the best places to install the energy dissipating devices are interconnecting the lateral and the gravity sub-systems or in the gravity sub-system. When the dampers were placed in the lateral sub-system, the SDMI structures did not perform well, but the L-structures were more successful than the "typical" ones according to the failure criteria set before.

Pounding was the primary reason for failures in the L-structures. Were it not for the physical limit set by the lateral sub-system, some peak displacements of the floor slabs would have exceeded 100 in. in the case of the K-L prototype. The lack of effec-

tive damping combined with the flexibility of the stability springs was responsible for the high displacements in these structures. The ineffectiveness of the dampers is the result of their location, since they cannot act directly on the floor slabs. Also, the total amount of energy that they dissipated was little, since the dissipation is directly proportional to the amplitude of the displacements, which are minimal in the lateral subsystem. Fig. 7.17 shows the compliances of the linearized N-L-structure compared to the linearized Northridge N-I and N-G configurations; as can be seen, the G- and I-structures use the floor velocities more efficiently to control the displacements, accelerations, and interstory drift-ratios.

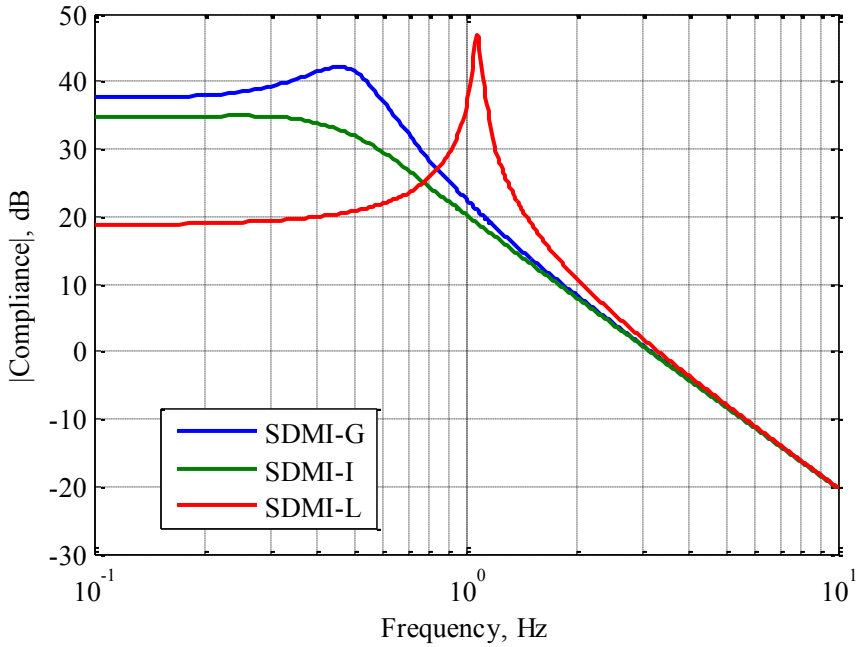

Fig. 7.17. Compliance of the third floor for the three types of SDMI structures studied

Although the lowest average peak acceleration was achieved when the dampers were located in the gravity sub-system, the G-structures did not achieve the same level of success as the I-structures, and success should be the main evaluation parameter. Besides, the I-structures yielded the second lowest average peak accelerations, which were barely above those achieved by the G-structures. The failures of the G-structures were due to excessive interstory drift-ratios.

7.5.2 Economy

The L-structures required the largest amount of stiffness in the lateral sub-system, which signifies a larger material necessity. The increased cost (and weight) of the lateral sub-system in L-models is related to the larger accelerance of these models (Fig. 7.18), which, at its time, is related to the ineffectiveness of the damping devices to control the motion of the floor slabs (when they are located in the lateral sub-system). In contrast, the G- and I-models achieved significant reductions in the floor accelerations by the use of relatively low damping coefficients. The lightest lateral sub-systems (smallest stiffnesses) corresponded to the I-models.

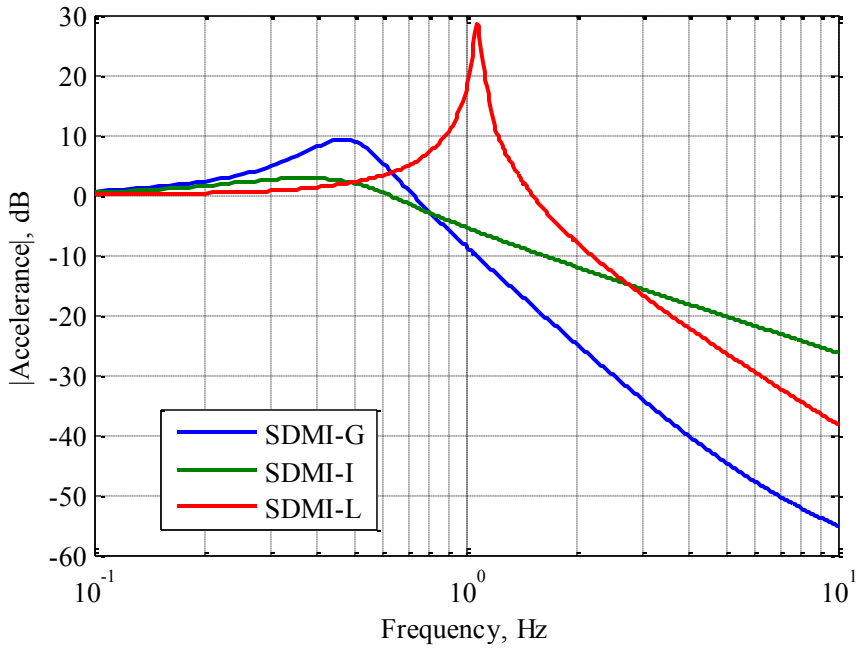

Fig. 7.18. Accelerance of the third floor for the three types of SDMI structures studied

7.5.3 Response

In order to make an appropriate evaluation of SDMI, it is necessary to pick a prototype that best represents the capacities of the concept. To choose a representative model, certain criteria are taken into account. The number of successes is the first criterion, meaning that the structure did not fail when subjected to a specific earthquake according to the failure criteria set before. Table 7.5 shows that structures E-I, H-I, and N-I achieved a 100% rate of success; therefore, these are separated from the rest.

The second criterion is more difficult to select. The peak displacement magnitude does not need to be considered, since it is not the best indicator of performance or of a failure state as long as it does not correspond to pounding, but the pounding cases have already been ruled out at this stage because structures E-I, H-I, and N-I are 100% suc-

cessful and pounding is considered as failure cause. Floor accelerations and interstory drift-ratios within the gravity sub-system are better indicators of the level of (non-structural) damage or the risk to the occupants or property inside the building. SDMI performs well at reducing the floor accelerations so that accelerations do not constitute a primary concern; on the other hand, the magnitudes of the interstory drift-ratios in the gravity sub-system are of consideration and are therefore used as the second criterion.

Of the three previously selected structures, the one that performs best according to the interstory drift-ratio criterion is model N-I. Hence, this prototype is used to assess the performance of the SDMI method. To select a representative control prototype, the number-of-successes criterion is applied to the "typical" structures, and, as a result, the K-T model is chosen as the representative control ("typical") prototype. After determining these SDMI and control models, a more direct comparison of their responses is given in Fig. 7.19, Fig. 7.20, and Fig. 7.21, where the N-I structure becomes the SDMI structure and the K-T structure becomes the control/"typical" structure.

For a quantitative comparison of the seismic performance between the SDMI and control structures, similar criteria, as those applied in the selection of the representative structures, are used; i.e., since displacements do not directly correspond to safety concerns, they are ruled out. On the other hand, it is assumed that in a SDMI building, architectural provisions need to and will be taken to handle the relatively large interstory drift-ratios in the gravity sub-system in order to protect non-structural elements. If this is the case, then the accelerations of the floor slabs become the only relevant dynamic re-

sponse parameter remaining for the evaluation of the performance of SDMI compared to a typical braced-frame structure.

According to Fig. 7.19, Fig. 7.20, Fig. 7.21, and Table 7.5, SDMI achieves a significant reduction of 70% in the average peak lateral acceleration response to the evaluation records. To better understand this effect, a comparison between the linearized accelerances of the SDMI and typical structures is given in Fig. 7.22. This graph shows a clear difference between the magnitudes of the two functions, especially in the frequency range that commonly includes the dominant frequencies of earthquakes.

A more significant comparison parameter than the difference in acceleration response is, however, the rate of collapse avoidance. While the SDMI structure performed successfully under all of the forty evaluation records, the typical braced frame failed when subjected to twelve of them. Furthermore, SDMI is 100% successful without experiencing structural damage, at least theoretically speaking. The absence of damage results in lower structural maintenance costs and in the availability of the structure for immediate occupancy, even after (MCE) earthquakes having a 2% probability of exceedence in 50 years. It is worth mentioning that this overall level of performance was achieved by the sole minimization of the floor accelerations.

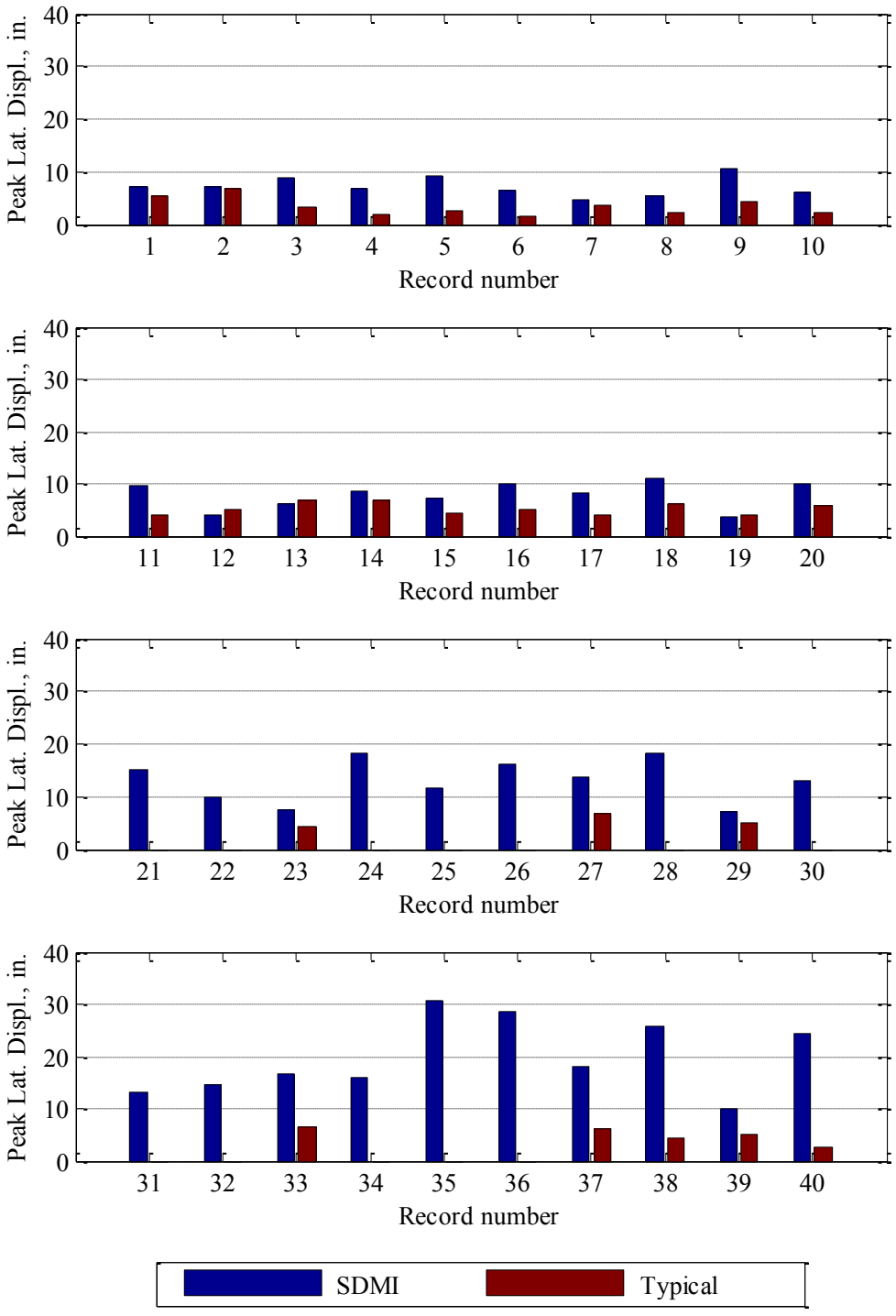

Fig. 7.19. Displacement-response comparison between SDMI and typical structures

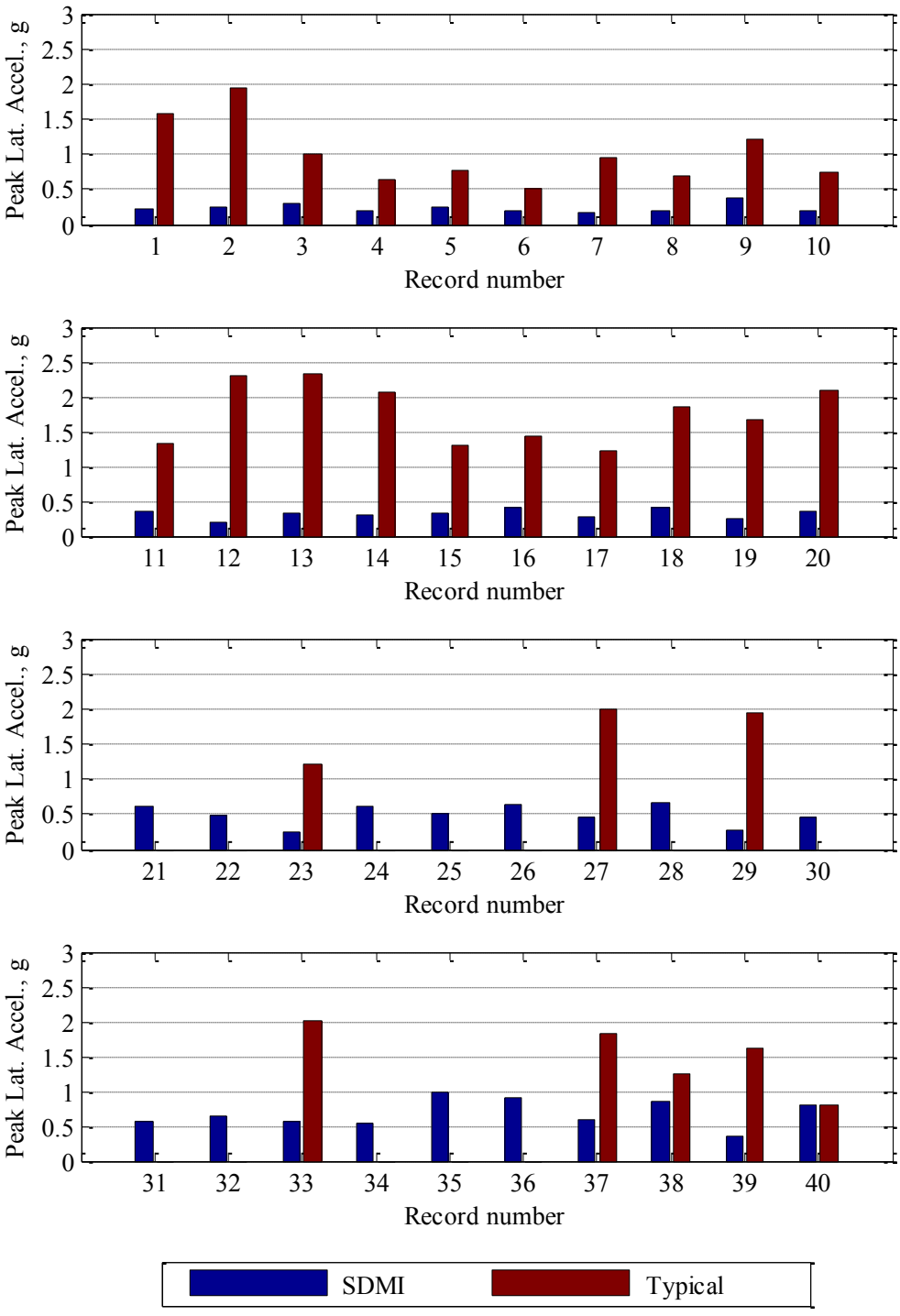

Fig. 7.20. Acceleration-response comparison between SDMI and typical structures

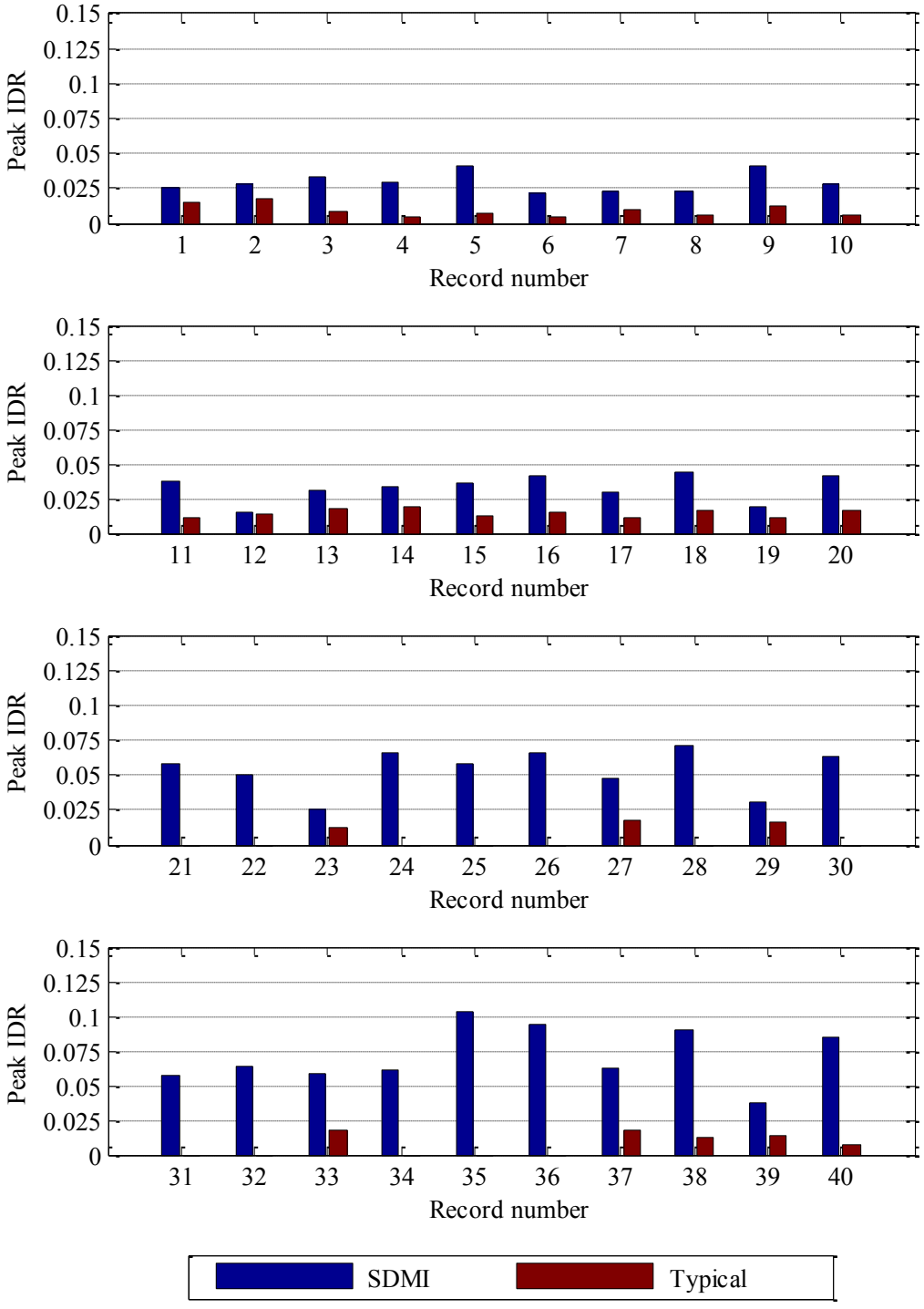

Fig. 7.21. IDR-response comparison between SDMI and typical structures

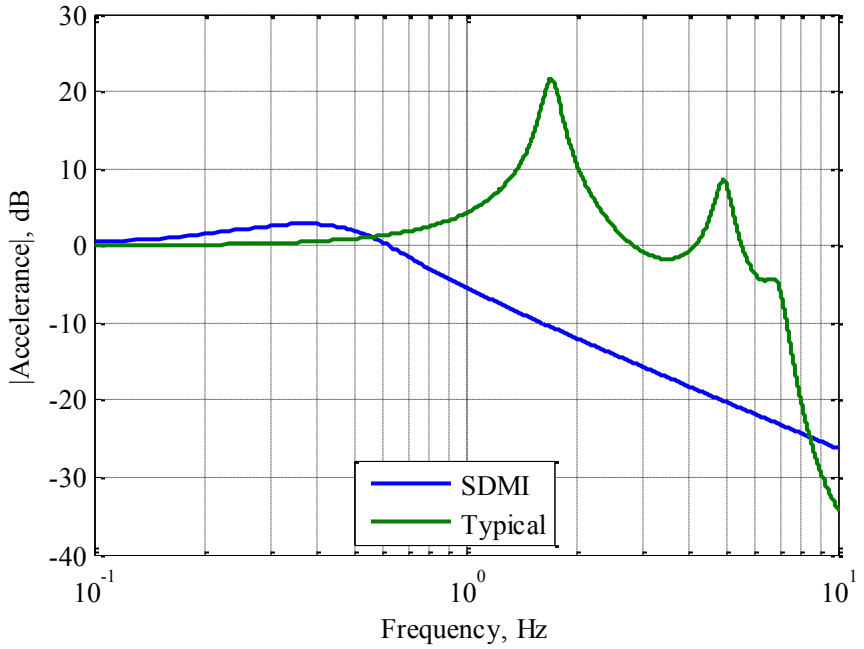

Fig. 7.22. Accelerances of the optimal SDMI and typical structures

8. CONCLUSIONS AND FUTURE WORK

8.1 Conclusions

A novel and alternative earthquake-resisting system based on the principle of mass isolation has been introduced. SDMI is capable of performing without causing structural damage to the lateral sub-system, even under MCE-level earthquakes. Besides reducing the structural life-cycle cost through its damage-less performance, it is able to reduce the peak acceleration-response in an average of more than 70% when compared to the response displayed by typical braced frames. Zero structural degradation of the lateral subsystem and the just mentioned level of reduction in the acceleration-response of the floors result in increased safety for the occupants of the building during earthquakes.

Due to the nature of the system, its stability and restoration during and after earthquakes has to be assessed carefully. In fact, these are primary constraints in the design of an SDMI system. For this purpose, simple design guidelines have been given to guarantee that the undistorted configuration of the system is always and safely restored. Despite the relative simplicity of the design guidelines and associated equations, these have been obtained through a strict mathematical treatment and analysis of the system by the use of Lyapunov's second theorem for the stability of dynamic systems. It is proven that the stability of the system can be achieved using a form of nodal bracing with stiffnesses that are well below the AISC requirements. This allows for the effective isolation of the building's floor masses.

The reduced accelerations of the floors result in the transmission of smaller seismic forces to the lateral sub-system. Thanks to this reduction, the lateral sub-system in an SDMI system can be made lighter than in a typical building. The same happens in the gravity sub-system where, because the columns need to only resist axial forces, they can be made of lighter elements than in a conventional building. Both, a lighter structure and structural-degradation-free performance contribute to the sustainability of the building.

The mechanism of SDMI solves two major technical drawbacks of Base Isolation; first, the lateral displacements of the floor slabs are limited since the gravity sub-system vibrates inside the containing lateral sub-system; second, since SDMI is not vertically supported by isolating devices, it can be applied to heavy structures without concerns for isolator load- and p-delta capacities.

The achievements in terms of acceleration-response result in increased interstory drift-ratios of the floor slabs; however, by an intelligent use of fluid viscous dampers in terms of their location and selection of their properties, the interstory drift-ratios can be kept within acceptable levels, provided special architectural provisions are made to safeguard non-structural elements. The provisions and acceptable interstory drifts will have to be determined through future Architectural (Engineering) studies that consider the mechanisms and kinematics of SDMI.

Given its potential for seismic response control, SDMI could become a widespread strategy for improving the seismic performance of buildings. Its introduction could also inspire and motivate the development of other hybrid seismic control strategies.

8.2 Future work

The present document constitutes a starting point in the development of SDMI. Although the dynamics, performance, technical advantages, and design for stability and restoration of the system have already been addressed, there are still several aspects that need to be studied to consider the practical implementation of SDMI.

Among the items that are pending study, there is the experimental verification and calibration of the analytical models that have been given. At the component level, there are different elements that are still subject to development, like the columns' pin connection assembly and the stability springs. In the case of the pinned connections, the requirements are the same as those for the stability spring and damper connections, i.e., the connection assembly has to maximize the free and isolated three-dimensional translations of the floor slabs. The development of the pin connection would also have to consider the required rotation capacities, its different possible forms of degradation, required force capacities, etc.

The stability spring concept also needs to be materialized. As said before, the use of industrial coil springs is an option, especially because of their large deformation capacities and their ability to be mounted around telescopic guides that permit them to deform in the intended way. The use of continuous elastic interfaces is another possibility, which should make use of high-deformation-capacity materials. An appropriate mechanism would have to be developed so that these interfaces behave the way they have been idealized in the analytical models. Otherwise, the latter would have to be modified to incorporate any changes in the material and/or kinematic behavior of the springs.

The properties (linear or nonlinear) of the fluid viscous dampers do not change any of the design guidelines or equations that have been given because the developed stability and restoration criteria are based on the locations of the EPs of the system, which always lie along the displacement-axis on the phase plane where the velocities are zero. Once all the special components have been developed, they will also have to be tested experimentally as part of the whole SDMI system.

From the safety point of view, apart from guaranteeing the stability and restoration of the system, it would be important to study the potential consequences of pounding. Although the chances of pounding can be made minimal by design, and its eventual occurrence would not necessarily mean a safety hazard, the system's condition of bare stability demands a study that considers the possibility of material yielding that could result from pounding. This study should contemplate any changes in the energy functions, EPs, DoAs, etc. that would follow the yielding of structural elements. If necessary, the findings of such study should be reflected in the system's design equations and/or provisions that were, until now, determined in this Dissertation.

Studies on the architecture of the building are also required. The architectural design of the building will have to be able to accommodate the relatively large interstory drifts that take place during earthquakes in exchange for the low accelerations. This affects the mechanical and electrical equipment as well as non-structural elements such as walls, windows, etc. (e.g., in earthquakes, floors in SDMI buildings come down more than in typical ones).

REFERENCES

AISC. (2011). *Steel construction manual*, American Institute of Steel Construction, Chicago, IL.

ASCE. (2003). "Seismic evaluation of existing buildings." *ASCE-31*, American Society of Civil Engineers, Reston, VA.

ASCE. (2004). *Primer on seismic isolation*, American Society of Civil Engineers, Reston, VA.

ASCE. (2007). "Seismic rehabilitation of existing buildings." *ASCE-41*, American Society of Civil Engineers, Reston, VA.

ASCE. (2010). "Minimum design loads for buildings and other structures." *ASCE-7*, American Society of Civil Engineers, Reston, VA.

ATC. (1999). *ATC TechBrief 2: earthquake aftershocks - entering damaged buildings*, Applied Technology Council, Redwood City, CA.

Chen, G., and Chen, C. (2004). "Semiactive control of the 20-story benchmark building with piezoelectric friction dampers." *Journal of Engineering Mechanics*, 130(4), 393-400.

CSI. (2010). "SAP2000 Advanced 14.2.3." Computer and Structures, Inc., Berkeley, CA.

Earl, C. L., and Ryan, K. L. (2006). "Effectiveness and feasibility of inter-story isolation systems." Proc. 8th U.S. National Conference on Earthquake Engineering, San Francisco, CA.

Eatherton, M., Hajjar, J., Ma, X., Krawinkler, H., and Deierlein, G. (2010). "Seismic design and behavior of steel frames with controlled rocking - part I: concepts and quasi-static subassembly testing." *Proc. of the 2010 Structures Congress*, Orlando, FL, 1523-1533.

FEMA. (1994). *SAC Steel Project*, <http://www.sacsteel.org> (Aug. 4, 2011).

FEMA. (2006). "Earthquake preparedness - what every child care provider needs to know." *FEMA-240*, Federal Emergency Management Agency, Washington, DC.

Ferreira, E. D., and Krogh, B. H. (1997). "Using neural networks to estimate regions of stability." *Proc. of 1997 American Control Conference*, Albuquerque, NM, 1989-1993.

Genesio, R., Tartaglia, M., and Vicino, A. (1985). "On the estimation of asymptotic stability regions: state of the art and new proposals." *IEEE Transactions on Automatic Control*, 30(8), 747-755.

Gent, A. N. (1964). "Elastic stability of rubber compression springs." *Journal of Mechanical Engineering*, 6(4), 318–326.

Gent, A. N., and Lindley, P. B. (1959). "Internal rupture of bonded rubber cylinders in tension." Proc. of the Royal Society of London. Series A., 195-205.

Haringx, J. A. (1948). "On highly compressive helical springs and rubber rods and their applications to free mountings - part III." *Philips Research Reports*, 4, 206-220.

Haupt, R. L., and Haupt, S. E. (2004). *Practical genetic algorithms*, Wiley Interscience, Hoboken, NJ.

Jordan, D. W., and Smith, P. (2007). *Nonlinear ordinary differential equations*, Oxford University Press Inc., New York.

Kelly, J. M. (1999). "The role of damping in seismic isolation." *Earthquake Engineering & Structural Dynamics*, 28(1), 3-20.

Kircher, C. A., Delfosse, G. C., Schoof, C. C., Khemici, O., and Shah, H. C. (1979). "Performance of a 230 KV ATB 7 power circuit breaker mounted on GAPEC seismic isolators." *Rep. No. 40*, The John A. Blume Earthquake Engineering Center, Stanford University, Stanford, CA.

Komodromos, P., Polycarpou, P. C., Papaloizou, L., and Phocas, M. C. (2007). "Response of seismically isolated buildings considering poundings." *Earthquake Engineering & Structural Dynamics*, 36(12), 1605-1622.

LaSalle, J. P. (1976). *The stability of dynamical systems*, Hamilton Press, Berlin, NJ.

Ma, X., Eatherton, M., Hajjar, J., Krawinkler, H., and Deierlein, G. (2010). "Seismic design and behavior of steel frames with controlled rocking - part II: large scale shake table testing and system collapse analysis." *Proc. of the 2010 Structures Congress*, Orlando, FL, 1534-1543.

McCormick, J., DesRoches, R., Fugazza, D., and Auricchio, F. (2007). "Seismic assessment of concentrically braced steel frames with shape memory alloy braces." *Journal of Structural Engineering*, 133(6), 862-870.

Michalewicz, Z. (1992). *Genetic algorithms + data structures = evolution programs*, Springer-Verlag, New York.

Naeim, F., and Kelly, J. M. (1999). *Design of seismic isolated structures - From theory to practice*, John Wiley and Sons, New York.

Niiya, T., Ishimaru, S., Yamaguchi, N., and Hayashida, T. (1992). "Seismic response control by 'mode(s)-isolation' method - Part II: Control of a tall building by tuned multi-masses damper system." Proc. 10th World Conference on Earthquake Engineering, Balkema, Rotterdam, 2337-2337.

NIST. (2008). "Strategic plan for the National Earthquake Hazards Reduction Program FY 2009-2013." DHS, ed., NIST, Gaithersburg, MD.

Noldus, E., and Loccufier, M. (1995). "A new trajectory reversing method for the estimation of asymptotic stability regions." *International Journal of Control*, 61(4), 917-932.

NPA. (2012). "Damage situation and police countermeasures associated with 2011 Tohoku district - off the Pacific ocean earthquake." National Police Agency of Japan, Tokyo, Japan.

Ohtori, Y., Spencer Jr, B. F., and Dyke, S. J. (2004). "Benchmark control problems for seismically excited nonlinear buildings." *Journal of Engineering Mechanics*, 130(4), 366-385.

Pan, T. C., and Cui, W. (1998). "Response of segmental buildings to random seismic motions." *ISET Journal of Engineering Technology*, 35(4), 105-112.

Pan, T. C., Ling, S. F., and Cui, W. (1995). "Seismic response of segmental buildings." *Earthquake Engineering & Structural Dynamics*, 24(7), 1039-1048.

PDL. (2009). *Pall Dynamics Limited*, <http://www.palldynamics.com> (May 30, 2012).

Pourmohammad, H., Ashtiany, M. G., and Ziyaeifar, M. (2006). "Buildings with local isolation system: Performance and simplified method of dynamic analysis." *Asian Journal of Civil Engineering (Building and Housing)*, 7(5), 501-516.

Qu, Z. Q. (2004). *Model order reduction techniques with applications in finite element analysis*, Springer, New York.

Ricles, J. M., Sause, R., Garlock, M. M., and Zhao, C. (2001). "Posttensioned seismic-resistant connections for steel frames." *Journal of Structural Engineering*, 127(2), 113-121.

Sabelli, R., Mahin, S., and Chang, C. (2003). "Seismic demands on steel braced frame buildings with buckling-restrained braces." *Engineering Structures*, 25(5), 655-666.

Sakamoto, M., Koshika, N., and Kobori, T. (2000). "Development and applications of structural control systems - Active-passive composite tuned mass damper." *Der Stahlbau*, 69(6), 455-463.

Singh, M. P., and Matheu, E. E. (1997). "Active and semi-active control of structures under seismic excitation." *Earthquake Engineering & Structural Dynamics*, 26(2), 193-213.

Somerville, P. G. (1997). "Development of ground motion time-histories for phase 2 of the FEMA/SAC steel project." *Rep. No. SAC/BD-97/04*, Sacramento, CA.

Spencer, B. F., Dyke, S. J., and Deoskar, H. S. (1998a). "Benchmark problems in structural control: part I - active mass driver system." *Earthquake Engineering & Structural Dynamics*, 27(11), 1127-1139.

Spencer, B. F., Dyke, S. J., and Deoskar, H. S. (1998b). "Benchmark problems in structural control: part II - active tendon system." *Earthquake Engineering & Structural Dynamics*, 27(11), 1141-1147.

TheMathWorks. (2009). "MATLAB." The MathWorks, Natick, MA.

Topcu, U., Packard, A. K., Seiler, P., and Balas, G. J. (2010). "Robust region-of-attraction estimation." *IEEE Transactions on Automatic Control*, 55(1), 137-142.

USGS. (2009). "U.S. Geological Survey Earthquake Hazards Program." Reston, VA.

Vidyasagar, M. (2002). *Nonlinear systems analysis*, SIAM, Philadelphia, PA.

Villaverde, R. (1998). "Roof isolation system to reduce the seismic response of buildings: A preliminary assessment." *Earthquake spectra*, 14(3), 521-532.

Villaverde, R., Aguirre, M., and Hamilton, C. (2005). "Aseismic roof isolation system built with steel oval elements: exploratory study." *Earthquake Spectra*, 21(1), 225-241.

Villaverde, R., and Mosqueda, G. (1999). "Aseismic roof isolation system: Analytic and shake table studies." *Earthquake Engineering & Structural Dynamics*, 28(3), 217-234.

Yaghoubian, N. F. (1988). "Earthquake isolating support." U.S. Patent 4,726,161, February 23, 1988.

Yang, C., Leon, R. T., and DesRoches, R. (2008). "Design and behavior of zipper-braced frames." *Engineering Structures*, 30(4), 1092-1100.

Yang, C., Leon, R. T., and DesRoches, R. (2010). "Cyclic behavior of zipper-braced frames." *Earthquake Spectra*, 26(2), 561-582.

Ziyaeifar, M. (2000). "Method of mass isolation in seismic design of structures." Proc. 12th World Conference on Earthquake Engineering, Pergamon, Auckland, New Zealand, 1411-1411.

Ziyaeifar, M. (2002). "Mass isolation, concept and techniques." *European Earthquake Engineering*, 16(2), 43-55.

Ziyaeifar, M., and Noguchi, H. (1998). "Partial mass isolation in tall buildings." *Earthquake Engineering & Structural Dynamics*, 27(1), 49-65.

APPENDIX: THEOREMS FOR DETERMINING THE STABILITY OF THE ZERO SOLUTION

The following pages include the mathematical theorems that are needed to analyze and understand the stability of the SDMI system both in its single-story and multi-story versions. The following theorems are found in (Jordan and Smith 2007) and are stated here without proof.

Definition 1: In some connected neighborhood N of the origin, let $V(x,y)$ satisfy:

i. $V(x,y)$ is continuous; $\partial V/\partial x$, $\partial V/\partial y$ are continuous except possibly at the origin.

ii. $V(0,0) = 0$ and $V(x,y) > 0$ elsewhere in N.

iii. A value of $\mu > 0$ exists such that, for every value of the parameter α in the interval $0 < \alpha < \mu$, the Eq. $V(x,y) = \alpha$ for (x,y) in N defines, uniquely, a simple closed curve T_α in N which surrounds the origin. Then the family of curves $V(x,y) = \alpha$, $0 < \alpha < \mu$ is called a topographic system on N_μ where N_μ is a connected neighborhood of the origin defined by $V(x,y) < \mu$, where $N\mu \subseteq N$.

Theorem 1: The topographic system of Definition 1 has the following properties:

i. $V(x,y) < \alpha$ in the interior of the topographic curve T_α, $0 < \alpha < \mu$.

ii. There is a topographic curve through every point interior to T_α, $0 < \alpha < \mu$.

iii. If $0 < \alpha_1 < \alpha_2 < \mu$, then $T_{\alpha 1}$ is interior to $T_{\alpha 2}$, and conversely.

iv. As $\alpha \rightarrow 0$ monotonically, the topographic curves T_α close on to the origin.

Theorem 2: In some neighborhood N of the origin let $V(x,y)$ be continuous, and $\partial V/\partial x$, $\partial V/\partial y$ be continuous except possibly at the origin. Suppose that in N, $V(x,y)$ takes the polar coordinate form $V(x,y) = r^q f(\theta) + E(r,\theta)$,

where

i. $V(0,0) = 0$;

ii. $q > 0$

iii. $f(\theta)$ and $f'(\theta)$ are continuous for all values of θ;

iv. $f(\theta) > 0$, and has a period 2π;

v. $\lim_{r\to 0} r^{-q+1}(\partial E/\partial r) = 0$ for all θ.

Then there exists $\mu > 0$ such that $V(x,y) = \alpha$, $0 < \alpha < \mu$ defines a topographic system covering a neighborhood of the origin N_μ, where N_μ lies in N.

Theorem 3: Let N be a closed, bounded region in the (x,y) plane on which the system $\dot{x} = X(x,y)$, $\dot{y} = Y(x,y)$ is regular. If a positive half-path H lies entirely on N, then either

i. H consists of a closed phase path on N;

ii. H approaches a closed phase path on N;

iii. H approaches an equilibrium point on N.

Theorem 4: Let T_α be a topographic curve in N_μ, defined by $V(x,y) = \alpha < \mu$, and suppose that $\dot{V}(x,y) \le 0$ in N_μ. Let H be any half-path that starts at a point P on, or in the interior of T_α. Then H can never escape from this region.

Theorem 5: Let $V(x,y)$ satisfy the conditions of Definition 1, and let the system $\dot{x} = X(x, y)$, $\dot{y} = Y(x, y)$ be regular in N_μ and have an equilibrium point at the origin. Suppose that $\dot{V}(x, y) \leq 0$ in N_μ with the origin excluded. Then the zero solution is uniformly stable in the Lyapunov sense.

Theorem 6: Let $V(x,y)$ satisfy the conditions of Definition 1 for a topographic system in N_μ and let the system $\dot{x} = X(x, y)$, $\dot{y} = Y(x, y)$ be regular in N_μ. Suppose also that $\dot{V}(x, y) < 0$ in N_μ with the origin excluded. Then (a) there are no equilibrium points in N_μ; (b) N_μ does not contain any closed phase paths.

Theorem 7: Let $V(x,y)$ satisfy the conditions of Definition 1 for a topographic system in N_μ and let the system $\dot{x} = X(x, y)$, $\dot{y} = Y(x, y)$ be regular in N_μ. Suppose also that $\dot{V}(x, y) < 0$ in N_μ with the origin excluded. Then the zero solution is (a) uniformly and (b) asymptotically stable.

Theorem 8: Let $V(x,y)$ satisfy the conditions of Definition 1 for a topographic system in N_μ and let the system $\dot{x} = X(x, y)$, $\dot{y} = Y(x, y)$ be regular in N_μ. Suppose that

i. $\dot{V}(x, y) \leq 0$ in the region consisting of N_μ with the origin excluded;

ii. None of the topographic curves in N_μ is also a phase path.

Then N_μ does not contain a closed phase path.

Theorem 9: Let $V(x,y)$ satisfy the conditions of Definition 1 for a topographic system in N_μ and let the system $\dot{x} = X(x, y)$, $\dot{y} = Y(x, y)$ be regular in N_μ with a single equilibrium point at the origin. Suppose also that

i. $\dot{V}(x, y) \leq 0$ in the region consisting of N_μ with the origin excluded;

ii. No curve of the topographic system is also a phase path.

Then the zero solution is uniformly and asymptotically stable.

Theorem 10: Let C be any curve along which $\dot{V}(x, y) = 0$, under the conditions of Theorem 9. If either (a) C is not closed in N_μ, or (b) C is closed, but is not a topographic curve, or (c) C is not a phase path of the system, then C is not a curve that needs to be considered under condition (b) of Theorem 7.

Theorem 11: Suppose that in a neighborhood N of the origin

i. $\dot{\boldsymbol{x}} = \boldsymbol{X}(\boldsymbol{x})$ is a regular system and $\boldsymbol{X}(\boldsymbol{0}) = 0$;

ii. $V(\mathbf{x})$ is continuous and positive definite;

iii. $\dot{V}(\boldsymbol{x})$ is continuous and negative semi definite.

Then the zero solution of the system is uniformly stable.

Theorem 12: Suppose that in a Neighborhood N of the origin

i. $\dot{\boldsymbol{x}} = \boldsymbol{X}(\boldsymbol{x})$ is a regular system and $\boldsymbol{X}(\boldsymbol{0}) = 0$;

ii. $V(\boldsymbol{x})$ is continuous and positive definite;

iii. $\dot{V}(\boldsymbol{x})$ is continuous and negative definite.

Then the zero solution of the system is asymptotically stable.

Theorem 13: If the n-dimensional system $\dot{\boldsymbol{x}} = \boldsymbol{A}\boldsymbol{x} + \boldsymbol{h}(\boldsymbol{x})$ with $\boldsymbol{A}$ constant, is regular, and

i. The zero solution of $\dot{\boldsymbol{x}} = \boldsymbol{A}\boldsymbol{x}$ is asymptotically stable;

ii. $\boldsymbol{h}(\boldsymbol{0}) = 0$, and $\lim_{\|x\| \to 0} \|\boldsymbol{h}(\boldsymbol{x})\| / \|\boldsymbol{x}\| = 0$,

Then $\boldsymbol{x}(\mathrm{t}) = 0$, $t \geq t_0$, for any t_0 is an asymptotically stable solution of $\dot{\boldsymbol{x}} = \boldsymbol{A}\boldsymbol{x} + \boldsymbol{h}(\boldsymbol{x})$.